Modeling Membrane Active Peptides with Implicit Membrane models

by

Yi He

A dissertation submitted to the Graduate Faculty in Biochemistry in partial fulfillment of the requirements

for the degree of Doctor of Philosophy, The City University of New York

2013

This manuscript has been read and accepted for the

Graduate Faculty in Biochemistry in satisfaction of the

dissertation requirements for the degree of Doctor in Philosophy.

Dr. Themis Lazaridis

_____	_____
Date	Chair of Examining Committee

Dr. Edward J. Kennelly

_____	_____
Date	Executive Officer

Dr. Chwen-Yang Shew

_____

Dr. Marco Ceruso

_____

Dr. Mark Kobrak

_____

Dr. Michael E. Green

_____

Supervisory Committe

THE CITY UNIVERSITY OF NEW YORK

Abstract

Modeling Membrane Active Peptides with Implicit Membrane models

by

Yi He

Advisor: Professor Themis Lazaridis

Membranes are the natural barriers of all cellular organisms. They separate the inner environment from the outer environment. They also divide cell contents into different functional compartments. Many membrane active peptides, however, challenge the function of membranes. They translocate through, form pores inside, or even break down the membranes. Understanding their mechanisms will help us design better drugs.

Molecular dynamics (MD) provides a unique way to study these peptides at small time scales. A lot of useful information can therefore be determined: such as, peptide orientation, structure adjustment, insertion into the membrane, and binding energy. Implicit membrane models are particularly useful because their low computational cost allows us to study peptides at longer time scales or larger numbers.

The object of the thesis is to study the membrane active peptides using implicit membrane models. The study is focused on three areas:

1) We first examined the transmembrane peptide orientation in both implicit and explicit MD simulations. Using theoretical methods, we tried to explain the gap between the tilt angles predicted by hydrophobic mismatching theory and the ones determined by ^{2}H NMR experiments.

2) To study the interaction between cationic peptides and anionic pores, we extended the current implicit pore model to anionic membranes. This model was applied to two typical antimicrobial peptides — magainin and melittin — and was used to explain their different preferences for anionic lipid fractions. We also evaluated the stability of three protegrin octameric pore models using this model.

3) We then tried to determine the link between binding affinity to membrane surface and biological activities of antimicrobial peptides. We found that both the experimental binding free energy and the theoretical transfer energy correlate with the biological activities, although the correlation is weak. Many other factors may also affect the biological activities of antimicrobial peptides. Moreover, based on a critical evaluation of "carpet" model, we found that most peptides would show higher activity than the prediction of the "carpet" model. The deviation of their biological activities from the "carpet" model correlates with their transfer energies to pores. The knowledge we gained from this study can help us establish quantitative models for predicting antimicrobial peptide activities.

Acknowledgements

I first would like to express my gratitude to my supervisor Themis Lazaridis for the comments, remarks and engagement through the learning process of this PhD thesis. He brought me into this exciting area of Computational Chemstry. Without his kind guidance and endless support, this dissertation would not have been possible. His influence will still be a great treasure for my furture professional life.

I am also indebted to my committee members, Doctor Marco Ceruso, Professor Mark Kobrak, Professor Michael E. Green and Professor Chwen-Yang Shew, for their patience and dedication. Their professional knowledge and unconditioned help let me procede through all these difficulties.

I would like to thank my parents for their support and understanding, especially for that I cannot stay with them during the years of my study. I thank Duo Yang for the scintillating company all the time through the hard times of my graduate research.

Also I would like to thank my brothers: Rodney Versace for constant encouragement, Zhou Shi for all the kindness. Without them, the graduate student life would have been a tough and lonely journey I have to fight against.

I also would like to thank my lab mates, especially Maja Mihajlovic, Lidia Prieto, Huan Zhan and Jingmin Zhang, for the warm help they gave me through the years in our lab.

At the end, I would like to thank the CUNY High Performance Computing Center. Without their resources, many of the work I presented here would have been impossible.

Contents

List of Tables

List of Figures

1. Introduction

1.1. Membrane active peptides

Membranes function as barriers that separate the cellular contents into different compartments or from the outside solutions. However, many cellular activities require the barriers to be broken down, to allow material exchange between compartments and extracellular environments. The structure and function of the membrane can be modified by many small peptides. In general, these membrane active peptides can be classified into the following categories in terms of their function and orientation:

Antimicrobial peptides (AMPs) They are a group of peptides that have antibacterial activity [1]. Many of them are naturally produced by organisms as a host-defense mechanism. It is generally believed that these peptides kill bacteria by creating apoptosis. These peptides are normally cationic amphipathic molecules. To be used as anti-infective drugs in mammals and to be transported through the blood, it is quite important that they have low toxicity against mammalian cells, especially erythrocytes.

Toxins As their names indicate, toxin peptides are toxic to cells [2, 3]. They produced not to kill pathogens but to kill or paralyze their prey, predators, or competitors, even though in general most toxins also have antimicrobial activity. They have hardly any selectivity and thus are not therapeutically useful. They are good starting points for designing potent antimicrobial peptides. Many successful antimicrobial peptides are derived from toxins by enhancing their selectivity.

Cell penetrating peptides (CPPs) They are peptides that can cross the membrane by themselves [4]. They are not cell-specific because their entrance into the cell does not require receptors. They are small and often positively charged peptides. These peptides have the potential to help deliver drugs into the cells. They have many common features with the antimicrobial peptides.

Fusion peptides The fusion peptide [5] segment at the N-terminal end of viral fusion glycoproteins is often found to be hydrophobic, rich in Glycine residues. They destabilize bilayers and promote lipid-mixing between liposomes. They are required for the viruses to fuse their lipid envelopes to the host cell membranes and transfer their DNA/RNA into the host cells. Many of these peptides are found to be α-helical and insert in the membrane at an oblique angle. They can lower the transition temperature of phosphatidylethanolamine from bilayers to hexagonal phase, which indicates that they promote negative curvatures. They can also lower the critical tension required to rapture the membrane.

Transmembrane peptides They are hydrophobic segments of transmembrane proteins or their designed analogues [6, 7]. The transmembrane proteins constitute a large percentage of the membrane proteins. However, although they present a challenge to the traditional methods due to their large size and the complicated surrounding membrane environment, their components (transmembrane peptide) are relatively easier to study. These peptides are mainly composed of hydrophobic residues. Besides, they can modify the membrane thickness or promote lipid segregation.

The boundary between these peptides is quite vague. One example is melittin, which can be considered either as an antimicrobial peptide or toxin because of its profound antibacterial and toxic effects. It can also be considered fusogenic [8] because it can induce vesicle fusion in anionic lipids. The difference between antimicrobial peptides and cell penetrating peptides is also unclear: many antimicrobial peptides can induce lipid flip-flop and transfer themselves to another side of the membrane. One example is buforin[9]. Alamethecin can be considered as a transmembrane peptide because it can adopt both transmembrane and surface orientation. There is also no simple criterion to distinguish them based on their composition and structure. Cationic residues and hinge domains are commonly found in all these peptides.

1.2. Transmembrane peptide orientation.

The position and orientation of a peptide in the membrane are crucial for determining the peptide function [10, 11] or mechanism [12].

The relative location of a peptide can be determined as the insertion depth. The orientation of a peptide can be defined by two kinds of angles: the angle by which the peptide tilts away from the membrane normal("tilt" angle τ) and the angle by which the peptide rotates around the main axis("azimuthal angle" ρ).

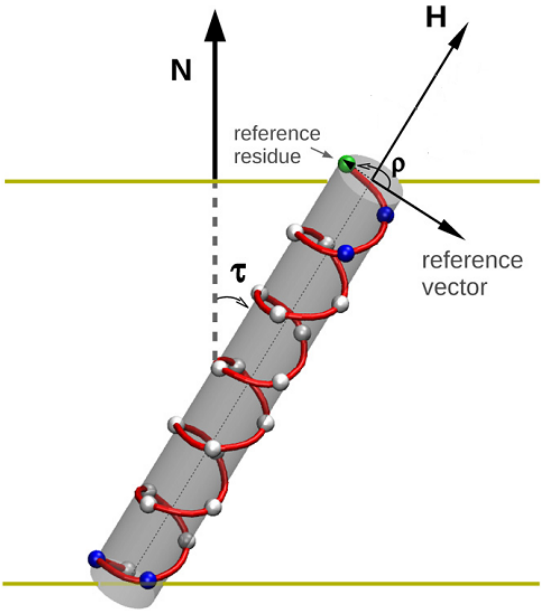

Figure 1.1.: Relative placement of a helical peptide in lipid bilayers. The peptide position is defined by its depth of insertion, d, and a pair of orientational angles, tilt (τ) and the azimuthal rotation (ρ). With the membrane normal (N) aligned with the z-axis, the distance d is the z coordinate of the peptide center of mass, with a z = 0 set arbitrarily at the center of the lipid bilayer. τ is the angle formed between the molecular long helix axis (**H**, from the C-terminus to the N-terminus) and the membrane normal. ρ is the angle between the direction of the peptide tilt and a vector perpendicular to H pointing to the C_α carbon of a reference residue (Glycine in most studies of WALP/KALP peptides). The figure is adapted from Strandberg et al. [13].

1.2.1. Hydrophobic mismatch theory.

The peptide orientation can be explained by the concept of the hydrophobic mistmach theory. This theory is based on the "mattress" model that assumes the membrane is a elastic medium ("mat-

tress") that has a single spring constant [14]. The difference between the peptide hydrophobic length and the membrane hydrophobic thickness is called mismatch. If the peptide hydrophobic length is longer than the membrane hydrophobic thickness, it is called positive mismatch. Otherwise, it is called negative mismatch. Membrane and peptide both have their own ways to respond to the mismatch. Under positive mismatch, a clear response by the peptide is that it can increase its tilt angle to fit with the membrane. The peptide can also oligomerize with other peptides to minimize the exposed polar/nonpolar surface. Although energetically expensive, conformation changes like kinking may also be possible. The membrane can respond either by adjusting its local thickness or changing its phase properties or undergoing lateral phase segregation (i.e. lipid rafts). Among these adaptations, the tilting should be a primary response of small peptides. First, the membrane thickening is not quite significant in X-ray diffraction experiments [15]. Second, peptide tilting is more energetically favorable than lateral sorting or oligomerization [16].

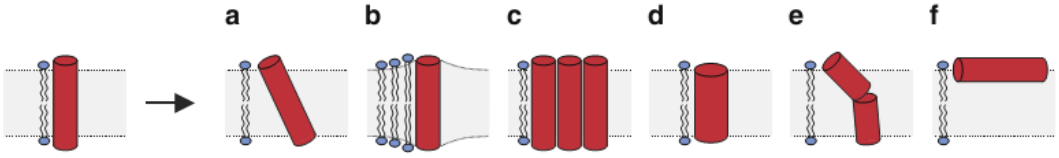

Figure 1.2.: Possible responses to positive hydrophobic mismatch. a) helix tilting; b) acyl chain stretching; c) oligomerization; d) backbone deformation/distortion; e) backbone kinking/flexing; f) switching to a non-transmembrane state, i.e., binding to the membrane interface. The figure is obtained from Holt and Killian [7].

1.2.2. Model peptides for studying peptide orientation.

Designed peptides provide a more desirable way to understand hydrophobic mismatch. The hydrophobic segment can be constructed by repeats of hydrophobic residues. Leucine, alanine, or their combination are normally used to create segments with different hydrophobicity. In some cases, several flanking residues are added at the termini of the hydrophobic segment to restrict the tilt angle and to enhance the solubility of the peptide. Tryptophan, a residue that highly prefers membrane interface, is normally used as flanking residue. Polar residues, such as lysine, are also occasionally used. The flexible side chain of lysine is able to "snorkel" into the water, allowing the backbone of lysine residue to be buried in the membrane and thus to have a smaller peptide tilt.

1.2.3. Peptide orientation determined from solid state NMR.

Solid state NMR is a unique technique for determining the structure and dynamics of membrane proteins. Because molecules do not tumble in the solid state, solid state NMR provides much broader transitions than that of solution NMR. As a result, the anisotropic information can be obtained. Such information is extremely useful for us to understand the overall orientation of molecules in anisotropic systems.

There are several ways to determine peptide orientation from solid state NMR. Depending on the probe used, different fitting methods can be applied to extract the peptide orientation from the angular information of individual probes. Two major methods are used: PISEMA[17, 18] and GALA[19, 20]. For both methods, theoretical spectra can be calculated from the ideal geometry of the peptide. The peptide orientation can be obtained by fitting theoretical spectra with experiments.

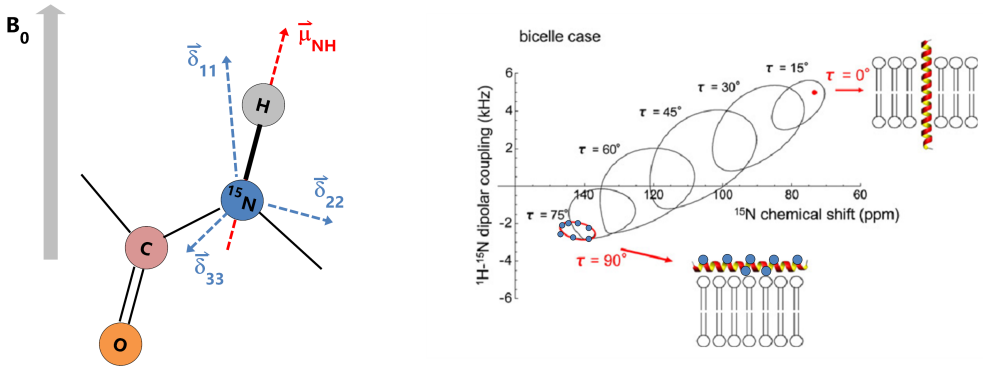

Figure 1.3.: Illustration of the orientation of NMR tensors and examples of "PISA wheel". Left panel shows the location of NMR probe (^{15}N) and the orientation of the NMR tensors. Right panel shows the example spectrum of a helical peptide with different tilt angles. The blue dots on the figure showed the location of peaks of different ^{15}N label. The lines are the theoretical lines resulting from rotating a helix around its axis at different tilts. The figure is adapted from Dürr et al. [21].

PISEMA is an abbreviation for Polarization Inversion Spin Exchange at the Magic Angle. In this method, the amide nitrogen atoms on the backbone are labeled with ^{15}N . Two tensors can be measured: the ^{15}N chemical shift and the ^{1}H–^{15}N dipolar coupling. The chemical shift tensor $\overrightarrow{\sigma}$ is asymmetric. Its principal axis frame is denoted $(\overrightarrow{\sigma_{11}}, \overrightarrow{\sigma_{22}}, \overrightarrow{\sigma_{33}})$ and the corresponding principal

values are denoted σ_{11},σ_{22},σ_{33}. The value of σ is given by:

$$\sigma = \sigma_{11}(\vec{B_0} \cdot \vec{\sigma}_{22})^2 + \sigma_{22}(\vec{B_0} \cdot \vec{\sigma}_{22})^2 + \sigma_{33}(\vec{B_0} \cdot \vec{\sigma}_{22})^2 \tag{1.1}$$

where $\vec{B_0}$ is the direction of NMR magnetic field.

The dipolar tensor $\overrightarrow{\gamma}$ is traceless and axially symmetric with unique rotation axis $\vec{\mu}_{NH}$ in the direction of covalent bond between ^{15}N and H atoms. If $\gamma_{||}$ is the value of γ when the direction of$\vec{B_0}$ is the same as $\vec{\mu}_{NH}$, then:

$$\gamma = \frac{\gamma_{||}}{2}(3(\vec{B_0} \cdot \vec{\mu}_{NH})^2 - 1) \tag{1.2}$$

The orientation of $\vec{\mu}_{NH}$ and $\overrightarrow{\sigma_{11}}$, $\overrightarrow{\sigma_{22}}$, $\overrightarrow{\sigma_{33}}$ are related with the peptide orientation. The value of σ and γ of residues on the helical wheel of a ideal helix will fall onto a ellipse (so-called "PISA wheel") whose location and shape are affected by the orientation of the helix.

Another method is called "Geometric Analysis of Labeled Alanines" ("GALA"). The alanine residues on the peptides are labeled with deuterium (^2H). The quadrupole splitting of deuterium is related to the orientation of C-^2H covalent bond:

$$\Delta v_Q = \frac{3e^2qQ}{4h}(3cos^2\beta - 1) \tag{1.3}$$

$\frac{e^2qQ}{h}$ is the quadrupole coupling constant (QCC), β is the angle between the applied magnetic field (B_0) and the C-^2H bond. Without any molecular motion, the quadrupole coupling constant for aliphatic carbon-hydrogen bond is 168 kHz [22]. However, due to the rapid rotation of alanine methyl groups, the QCC for alanines is reduced to 1/3 of its original values[23]. Also, β should be the angle between B_0 and the average vector of the three C-^2H bounds (the same direction as the $C_\alpha - C_\beta$ bond of the alanine). The angle β can be evaluated from the geometry of an ideal helix.

For WALP peptides, QCC values between 47 and 56 kHz give similar tilt angles[19].

With several alanine labels, the theoretical splitting can best fit with the experimental measurements (Figure 1.4). With the correct tilt/rotation angle, the theoretical splittings should have minimal deviation with the experimental values:

$$rmsd = \frac{1}{N}\sqrt{\sum_{i}^{N}(v_i^{theoretical} - v_i^{experimental})^2} \tag{1.4}$$

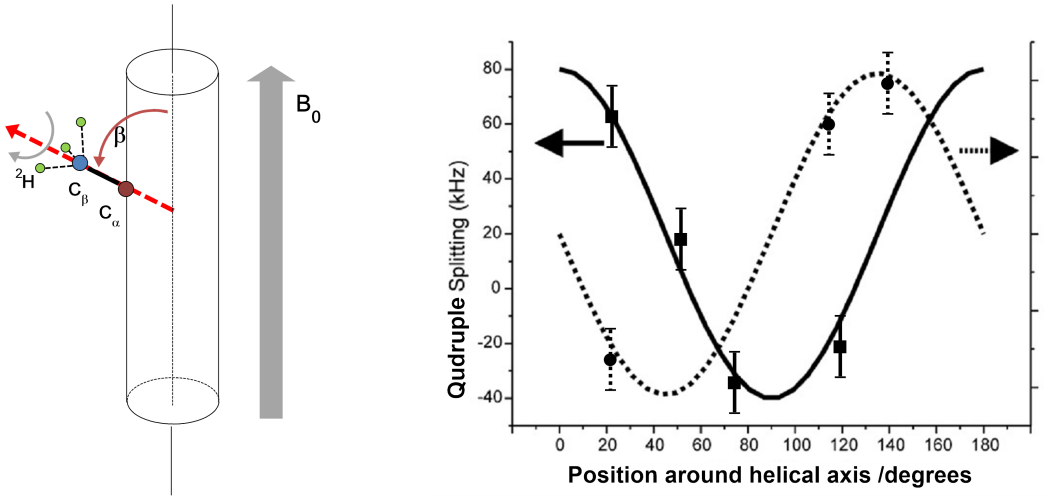

Figure 1.4.: Illustration of relationship of peptide orientation and NMR probes with the ^2H-NMR spectrum. Left, the C_β atom of the alanine residues is labeled with deuterium (^{2}H). The fast rotation of the deuterium atoms makes the average vector of the three C_β–^{2}H bonds to be equivalent to the vector of $C_\alpha - C_\beta$ bond. Right, example quadrupole splittings for labels on an helix wheel. The lines are the the theoretical curves resulting from rotating the helix around its helix at different tilts. The figure is adapted from Bechinger et al. [24].

1.2.4. Discrepancy between theory and solid state NMR result from ^2H NMR

The tilt angles of transmembrane peptides should be determined mainly by the extent of hydrophobic mismatch. This idea is supported by MD simulations in coarse-grained [25] and all-atom models [26]. The remarkable correlations between tilt angle and hydrophobic mismatch were observed for several natural peptides and protein fragments, such as the TM helix of the M13 major coat protein (determined by fluorescence spectroscopy)[27], the pore-lining segment of influenza A virus

M2 protein (by EPR)[28], the cell-signaling peptides containing nuclear localization sequences [29], and the channel-forming domain of Vpu from HIV-1[30](by PISEMA ^{15}N NMR).

The tilt angles of WALP and KALP determined from $^{2}H\ NMR$ studies are, however, much smaller, which disagrees with the hydrophobic mismatch theory [31]. It was proposed that rapid motion of peptides would reduce the measurement of ^{2}H NMR splittings and lead to an underestimation of tilt angles[32]. The PISEMA method is expected to be less sensitive to peptide motion than the "GALA method", because the average $C_\alpha - C_\beta$ bond directions with respect to the helix axis is close to the magic angle, whereas the average N-H direction is far from the magic angle. In recent studies, WALP is first found to have small tilt angles by $^{15}N\ NMR$[33] but subsequent researches using $^{15}N\ NMR$[34, 35, 36] and fluorescence spectroscopy[37] indicate larger tilt angles. The large tilt angle predicted by hydrophobic mismatch theory is also supported by MD simulations [38, 39].

Furthermore, it is reported that $^{2}H\ NMR$ data can indeed be better interpreted by introducing peptide dynamics in the form of Gaussian fluctuations of the orientation angles [40, 34]. Incorporating the anisotropic information into molecular dynamics also is reported to lead to moderate tilt angles[41, 42] .

1.3. Antimicrobial peptides

1.3.1. General Aspects

1.3.1.1. Therapeutic uses of antimicrobial peptides and their advantages and disadvantages.

The spectrum of antimicrobial peptides is broader than that of traditional antibiotics. They can act effectively against gram-positive/negative bacterium, fungus, tumor cells, parasites, and even virus. The antimicrobial peptides can thus be of great therapeutic importance.

Table 1.1.: List of Cationic Antimicrobial Peptide Drugs, Company Responsible for Commercialization, Testing Status, and the Disease it is Designed to Treat. The table is obtained from Mcphee and Hancock [43].

Compund	Company	Testing status	Disease drug designed to treat
Pexiganan	Magainin Pharmaceuticals	Phase III completed	Infection of diabetic foot ulcers
Iseganan	IntraBiotics Corporation	Phase III halted prematurely	Ventilator-associated pncumonia
rBPI21	Xoma Ltd.	Phase III completed	Severe bacterial meningitis
Omiganan	Migenix (formerly Micrologix)	Phase III completed	Infrection at site of in-dewelling catheter insertion
IMXC001	Inimex Pharmaceuticals	Preclinical	Sepsis

The killing induced by AMP is usually quite fast, and their minimum lysis concentrations are the same as or at least not much higher than their minimum inhibitory concentrations. Even though some cases have been reported, it is quite difficult to develop a resistance to AMP, because they could have multiple targets and the main target is the membrane itself; reconstructing the membrane completely is nearly impossible for biological organisms and will affect the normal functions of the cells. Compared to conventional antibiotics, the loss of peptide activity due to resistance is trivial: only two- to four- fold increment in effective concentrations is observed [44].

There are also some disadvantages which might limit their usages: 1) many of these peptides aggregate in water solutions, which can easily percipitate and lose their activities. 2) the activities of many peptides are highly sensitive to salt concentration (such as LL-37). In some environments with high salt concentration (such as in lungs), they will become quite ineffective. 3) compared to the conventional antibiotics, their potency is lower while their cost is critically higher. Therefore, currently these peptides might not be an economical alternative to the conventional antibiotics. 4) some peptides such as melittin, even though they are highly potent, have high cell toxicity. However, antimicrobial peptides will likely show more potentials in therapeutic applications with the improvement of our understanding of them.

1.3.1.2. Sources of AMPs

In general, almost all living organisms can produce a certain amount of AMPs. Arthropods have far more diverse species than any other classes in the plant and animal kingdoms. They are frequently exposed to potential pathogens but rarely be infected. It is not surprising that the currently well-studied antimicrobial peptides have been mainly characterized in anthopods, including melittin,

mastorparans, cecropins, and so on. Most of these peptides are actually toxins, only part of which are produced by the innate immune system.

Amphibian skin is another amazing source of AMPs because enormous quantities and diversity of antimicrobial peptides can be easily isolated from it and studied. The first such peptide, bombinin, was identified more than 30 years ago [45]. Subsequently, magainins were isolated from xenopus skin in 1980s and have been extensively studied ever since[46, 47, 48, 49, 50]. Until very recently, amphibian peptides remained one of the largest and best studied group of antimicrobial peptides.

The innate immune system of most organisms also produces a large variety of antimicrobial peptides as a response to pathogenic invasion. These homologous peptides comprise two major families, defensins and cathelicidins. Mammalian defensins are β-sheet peptides with 29-40 amino acid residues and intramolecular cysteine-disulfide bonds [51]. They are a large family of cationic and relatively arginine-rich antimicrobial peptides. The cathelicidins comprise a large amount of cathelin-containing precursors of antimicrobial peptides. Cathelin is an inhibitor of cathepsin L. It is a highly conserved domain at the carboxyl terminus of a 15–18 kDa precursor [52]. In response to pathogenic invasion, cathelicidins are cleaved to release the active antimicrobial peptides located on their carboxyl terminus.

1.3.1.3. Structure of AMPs

The antimicrobial peptides have various structures. Although there are also other possibilities, the structures of most antimicrobial peptides are generally divided into four groups:

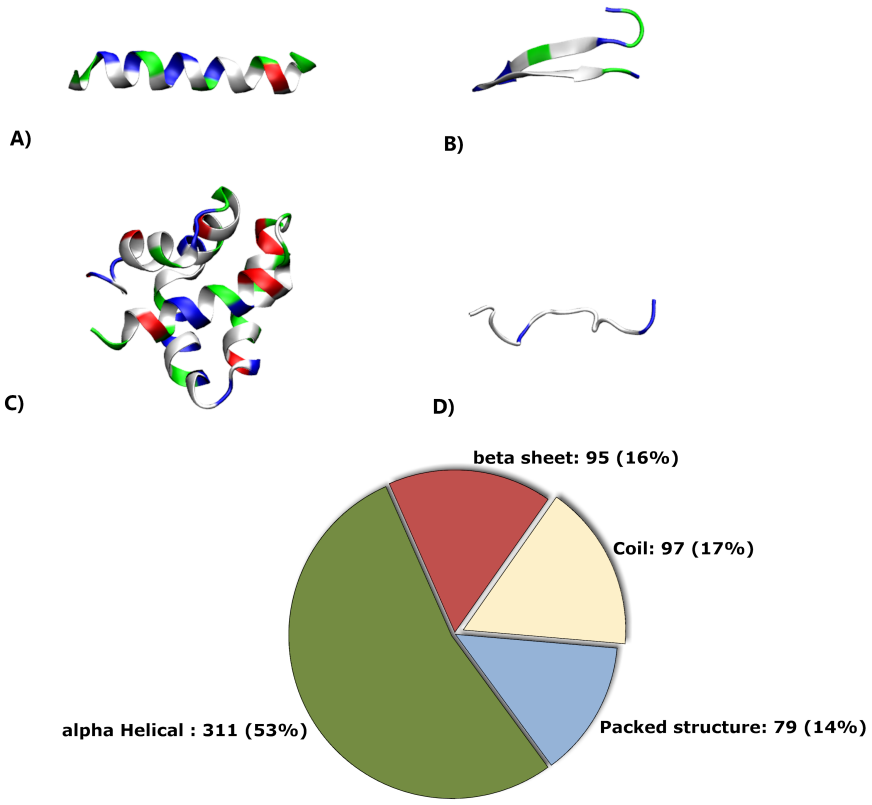

Figure 1.5.: A)-D) Examples of antimicrobial structures: A) Magainin 2 (α helix) B) Protegrin-1 (β hairpin) C) NK-lysin (helical bundle) D) Indolicidin (random coil). E) Number of peptides for each structure category in APD2 database[53]. Percentages were calculated based on peptides that have known structure.

Amphipathic α-helical peptides are perhaps the most well studied group. Most peptides from this group are unfolded or have part β-sheet structure in aqueous solution but fold into α-helices on membranes. Flexible hinges are also commonly found in these peptides.

β structured peptides are another large structural group. To form an amphipathic structure, the β peptides have to bend to allow anti-parallel hairpins to form. However, this is quite difficult for small peptides because of the entropy loss of forming such structures. Either disulfide bonds or a cyclic backbone is generally observed in many β antimicrobial peptides because they help stablize the hairpin structure by lowering the enthalpy.

Some antimicrobial peptides have multiple secondary structure segments and packed tertiary structures. Defensin is one of such peptide groups that are composed of multiple β-sheet structures. The NK-lysin is a 78 residue protein, containing 4 α helical segments that are connected with disulfide bonds [54, 55].

Some antimicrobial peptides have random coiled structures. These peptides are often rich in certain amino acids. This group includes the bactenecins and PR-39, both of which are rich in proline (33–49%) and arginine (13–33%) residues; prophenin, which is rich in proline (57%) and phenylalanine (19%) residues; indolicidin, which is rich in tryptophan residues; and histatin, which is rich in histidine.

1.3.2. Mechanism

There have been many techniques used to determine the mechanism of antimicrobial activity. However, different views are provided by different methods. There are still quite a lot of debates on how these peptides act. Many models have been suggested. They are not completely in conflict with each other, but only concentrate on different aspsects of antimicrobial peptide actions.

1.3.2.1. Modes of peptide actions

Membrane disruption or metabolism? It has been generally accepted that the membrane permeabilization/disruption is central in the killing of microorganisms. This idea has recently been challenged by the increasing evidence of antimicrobial activity in the absence of membrane disruption. TWF, an analog of tritrpticin, showed very low membrane disrupting activity but had strong bactericidal activity [57]. Another example is buforin[58], which translocates into cell and inibits cellular functions. There are many possible mechanisms that do not require membrane permeabilization or disruption, such as inhibition of DNA and protein synthesis, chaperone-assisted protein folding, enzymatic activity, cytoplasmic membrane septum formation, and cell wall synthesis. Most of them require a specific intracellular target. Table 1.2 lists these peptides that have intracellular targets [59]. Even though the antimicrobial peptides can kill the cells through intracellular mechanisms, such examples are rather rare and many of them may be more effective

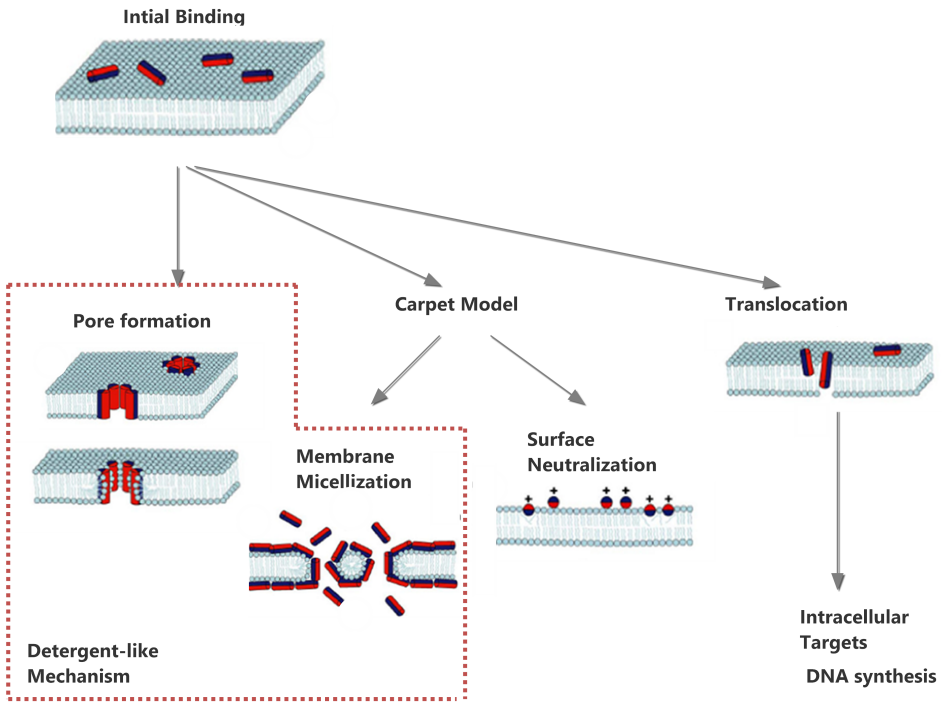

Figure 1.6.: Possible mechanisms for antimicrobial peptides. The figure is adapted from Teixeira et al. [56].

through membrane-related mechanisms. Moreover, since the peptides have to cross the cell membrane to reach their intracellular targets, formation of transient pores is mostly likely to happen in the uptake process, considering evidence of membrane receptor assistance is quite rare. Indeed, for typical antimicrobial peptides, translocation is completely coupled to pore formation and lipid flip-flop [60, 61, 62].

Pore formation One possible mechanism of membrane permeabilization is through formation of pores inside the membrane. Two types of pores can be generally induced by the antimicrobial peptides: "barrel-stave" pore and "toroidal" pore. More details about pore formation mechanism will be discussed later in the section "pore formation induced by membrane active peptides".

Carpet Model The "carpet" model was first proposed to describe the mode of action of dermaseptin S [63], but it has subsequently been used to describe the mode of action of other antimicrobial peptides, such as dermaseptin natural analogues [64, 65], cecropins [66], the human antimicrobial peptide LL-37 [67], caerin 1.1 [68], Trichogin GA IV [69], and diastereomers of lytic

Table 1.2.: Antimicrobial peptides that are suggested to have intracellular mechanisms. Membrane-bound structure, suggested internalization mechanism and effect on microbial functions of intracellular-targeting antimicrobial peptides are listed. The table is adapted from Nicolas [59].

Name	Membrane-bound Structure	Uptake Mechanism	Intracellular targets
Pyrrhocoricin	Reverse turns at the termini bridged by an extended segment	Receptor/ docking component on inner membrane	Dnak; DNA and protein synthesis
Apidaecin		Receptor/ docking component	Dnak; DNA and protein synthesis
Drosocin		Receptor/ docking component	Dnak; DNA and protein synthesis
Histatin-5	Amphipathic α-helix	> MIC: membrane permeabilization/ disruption < MIC: receptor-mediated endocytosis (heat shock protein 70, permease); MIC: transient membrane leakage (membrane potential-dependent)	DNA? Vacuole (nonlethal) Mitochondrial F_1F_0-ATPase
Buforin-2	Amphipathic α-helix	Transient toroidal pores	DNA?
Indolicidin	Extended boat-shaped amphipathic structure	No uptake	DNA synthesis?
Tachyplesin I	β-Hairpin with two disulfide bonds	Transient pores	DNA?

peptides [70, 71]. These peptides are found to have in-plane orientation at the lysis concentration. They are suggested to partition on the surface of membrane and accumulate to an extremely high local concentration. They will act as "carpets" so that they can break down the membrane barrier when a critical surface coverage is reached. However, it is not clear how the membrane breaks down under a high peptide concentration.

One possibility is that peptides induce positive curvature in the membrane because they generate void spaces between acyl-chains. When the positive strain is large enough, this certainly leads to toroidal pore formation or even micellization. Another possibility is that accumulation of positively charged peptide on one side will create a transmembrane voltage to such an extent that electroporation will be induced. Because AMPs are highly cationic and bind strongly to the membrane, neutralization of bacterial surface charge would be also likely at high P:L ratios. This phenomenon would be expected to critically affect membrane function as well as integrity. In fact, taking into account the peptide and membrane charges, an analysis of published data reveals that neutralization does occur along threshold events displayed by several AMPs [72, 73, 74, 75]. As such, membrane charge neutralization coupled with saturation of the bacterial membrane is a likely killing mechanism, at least for some peptides.Recently, it has been suggested that the surface coverage itself may induce membrane curvature even when membrane insertion is absent [76].

Clearly, this mode is not a universal mechanism for antimicrobial activity, but instead is an extreme case [77]. Although high peptide densities have been observed on the surface of bacterial cells [76],

most of them may bind to cell wall or outer membrane. The actual concentration on the cell membrane may not be quite high. In most cases, membrane activities have been demonstrated at reduced peptide-to-lipid ratios [49] .

1.3.2.2. Models of peptide-lipid interaction

The previous models focus mainly on the exact events that lead to membrane lysis and cell death. There are several models focused on why and how the membrane defects are formed under the influence of antimicrobial peptides.

Detergent-like activity An frequently referred mechanism is “detergent-like mechanism”. This mechanism suggests that all antimicrobial peptides, since they are amphipathic molecules, can disintegrate the membrane in a way similar to detergents.

The detergents affect membrane structure in different ways based on the level of their concentrations: at very low detergent-to-lipid ratios they can have a neutral effect on model membranes or even stabilize them [78, 79]; at moderate concentration, opening can form temporarily; at high detergent/lipid ratio, detergents can micellize the membrane and create a huge opening in the membrane.

Take melittin for example, it has pronounced effects on the phase behavior of DPPC at rather low peptide concentrations (lipid-to-peptide molar ratio of 1000/1)[80, 81]. The same phenomenon also occurs to the detergent cetyltrimethylammonium chloride [79]. However, at high melittin concentrations (lipid-to-peptide molar ratio of 15/1), disk-shaped particles were found in the DMPC/melittin mixture [82, 83], suggesting a detergent-like solubilization of the membrane under these experimental conditions. Below the gel to fluid phase transition temperatures of the pure lipid, the presence of intermediate amounts of melittin (< 5mol%) results in the reversible disintegration of the bilayers into disks [82, 84].

This model does not conflict with either the ”carpet” model or the pore model that were mentioned previously. The latter two models actually are different results of the detergent-like activities of antimicrobial peptides.

Positive Curvature induced by peptides Another hypothesis is that antimicrobial peptides will affect the curvature stress of the membrane. The spontaneous curvature of membrane is suggested to be affected by the geometric shape of the lipids. That is, only if the sizes (cross section areas) of head group and acyl chain are balanced, planar membranes can form. Otherwise, if the head groups have a larger cross section area than acyl chains, the lipids tend to form micelles and tubes(hexagonal lipid phase H_I) that has high positive curvature ; if the head groups have a smaller cross section area than acyl chains, the lipids tend to form inverted micelles and inverted hexagonal lipid phase H_{II}.

As amphipathic molecules, antimicrobial peptides favors partition into the head group region and thus make the overall head group area larger than the acyl chains. As a result, a positive curvature stress is generated. To release this stress, the planar membrane will be reorganized into structures such as toroidal pores or micelles that have high positive curvatures (Figure 1.7g)-i)). The positive stress accompanied with peptide insertion is indirectly measurable by the phase transition temperature from fluid lamellar phase to hexagonal phase [85] and is evidential for several peptides [50, 86, 87].

Electroporation induced by unbalanced distribution of cationic peptide This model has been proposed to interpret membrane pore formation by annexin V [89]. The fundamental idea of this model is that the accumulation of cationic peptides on one side of the membrane will create a transmembrane voltage. For highly cationic peptides, the transmembrane voltage can reach 0.2 volts [54], which is large enough to induce electroporation [90].

Peptide-induced lipid segregation Cationic peptides have been shown to induce lateral phase segregation of zwitterionic lipid from anionic phospholipids. Formation of such lipid-peptide domain itself does not lead to toxicity. However, the boundary between lipid domains is prone to the formation of defects [91, 92, 93, 94]. Such phase boundary defects have been suggested to be responsible for the increased leakage of liposomes at the phase transition temperature, where gel and liquid crystalline domains coexist [95]. The importance of induced lateral phase separation has been

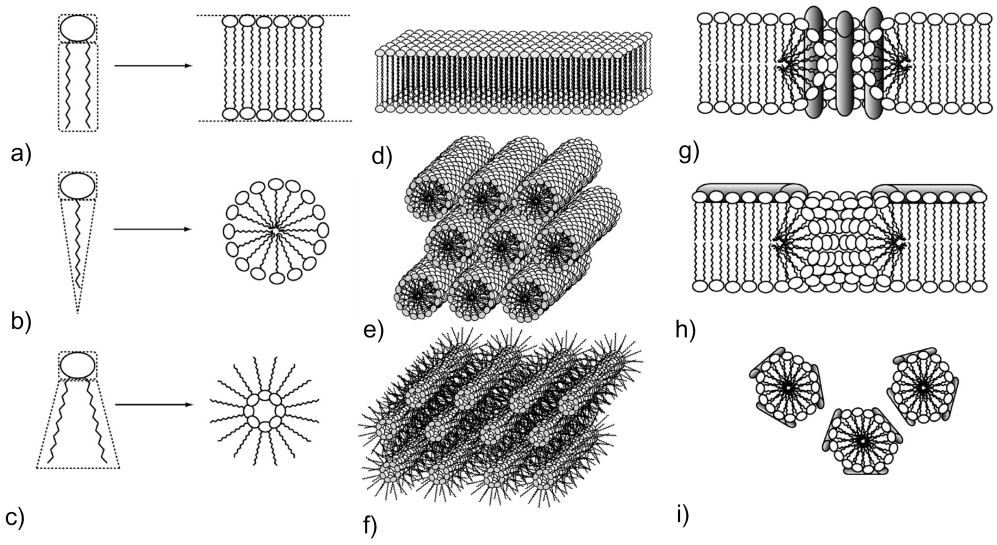

Figure 1.7.: Relationship between lipid shape and preferred lipid phase and possible results of the positive curvature induced by antimicrobial peptides. a)-c) the three types of lipid shapes: a) cylinder (for example, PC lipids). b) cone (for example, PG lipids). c) inverted cone (for example, PE lipids). d)-f) the three lipid phase of these lipids: d) L_αLaminar phase. e) H_I phase. f) H_{II} phase. g)- i) possible results of peptides that induce positive curvature stress. g) toroidal pore with peptide inserted to the pore. h) toroidal pore without requirement of peptide insert. i) completely break up the membrane into micelles. The figure is adapted from Haney et al. [88].

specifically proposed as a mechanism contributing to the antimicrobial activity of a designed α/β-peptide [91], flexible sequence-random polymer [93], cateslytin [94], and oligo-acyl-lysine (OAK) [92].

1.3.3. Origin of the selectivity

1.3.3.1. The difference in membranes.

The elementary component of all biomembranes is the phospholipid bilayer. However, in terms of composition and cell energetics, biomembranes of prokaryotic and eukaryotic cells differ significantly. Table 1.3 listed the lipid components of several organisms.

The major neutral component of prokaryotic cell membrane is phosphatidylethanolamine (PE), but eukaryotic cell membranes contain three diffferent lipids: phosphatidylcholine (PC), sphingomyelin

(SM), and phosphatidylethanolamine (PE). PC and SM are bilayer forming lipids which favors formation of a planar membrane. PE has a tendency to induce negative curvature. Prokaryotic and eukaryotic membranes thus have significantly different mechanical properties.

Both prokaryotic and eukaryotic cell membranes contain anionic components. Hydroxylated phospholipids phosphatidylglycerol (PG), cardiolipin (CL; effectively a dimer of PG), and phosphatidylserine (PS) all sustain a net negative charge and are normally found in both membranes. However, the distribution is not the same. The anionic lipids in eukaryotic cell membranes are mainly comprised of PS. They concentrate primarily in the inner leaflets of the membranes that are not exposed to antimicrobial peptides. However, the major anionic lipids of prokaryotic cell membrane are PG and CL, which are found in both leaflets of the membrane. The anionic lipid of a typical Gram-negative bacteria is around 20-30% of the total lipids . The anionic lipid of typical Gram-positive bacteria is much higher, at a range between 60-100% of the total lipids. The difference in the distribution of the anionic lipids is traditionally considered to be the major cause of the selectivity of cationic antimicrobial peptides because these peptides are easily attracted to the anionic surface of bacterial membranes.

However, human erythrocytes, for example, contain also a large number of highly negatively charged sialic acid-containing carbohydrate moieties in the form of glycoproteins and glycosphingolipids, which form their outer glycocalix barriers. Therefore, cationic antimicrobial peptides need first to cross this layer in order to reach the cytoplasmic PC membrane.

Unlike prokaryotic cell membranes, another important difference is the presence of sterols, such as cholesterol and ergosterol. The cholesterol has been demonstrated to have an influence on the activity of several antimicrobial peptides [96, 97, 98].

The membranes of HIV viruses are also significantly different from their host cell membranes [104]. The content of cholesterol is about 2 times higher than that of the host cell membranes.

Cancer cell membranes typically carry a net negative charge due to a higher than normal expression of anionic molecules, such as PS (about 9% of the total phospholipids of membranes) [105, 106] and O-glycosylated mucins [107, 108]. In addition, the negative membrane potential of cancer cells may also contribute to the selective cytotoxic activity of anticancer peptides [48].

Table 1.3.: Lipid composition of Cell membranes of different organism. OM: outer membrane. CM: cell membrane.

Lipid (%)	Microorganism					
	Escherichia coli (Gram-)		*Staphylococcus aureus* (Gram+)	*Saccharomyces cerevisiae* (Fungi)	Erythrocyte	
	OM	CM			Outer Leaflet	Inner Leaflet
Cardiolipid(CL)	6	12	4.1	0.2	—	—
Phosphatidylglycerol(PG)	3	6	76.5	—	—	—
Lysylphosphatidylglycerol(LPG)			16.0	—	—	—
Phosphatidylserine(PS)	—		—	33.6	—	29.6
Phosphatidic acid (PA)	—	—	—	3.9	—	2.2
Phosphatidylinositol(PI)			—	17.7	—	1.2
Phosphatidylethanolamine(PE)	90	82	—	20.3	11.1	43.9
Phosphatidylcholine(PC)			—	16.8	44.8	14.0
Sphingomylin(SM)			—	—	42.1	9.1
Sterol			—	Ergosterol	Cholesterol	
Reference	Anisimova et al. [99], Lu et al. [100]		Joyce et al. [101]	Rest et al. [102]	Virtanen et al. [103]	

The difference between mammalian cell membrane and fungus cell membrane is much smaller. Many peptides act indiscriminately against those two type of organism [109].

1.3.3.2. Does selectivity really exist?

When it comes to the definition of "selectivity", it has generally been used in such a loose way that its strict definition has never been taken into account. The experimental assays for antibacterial activity and hemolytic activity are quite different from each other: 1) the minimum inhibitory concentrations are measured under bacterial cell concentration of $1 \times 10^5 - 1 \times 10^6$ colony-forming units/mL. The hemolysis assays are performed with hematocit values of 1-10%, which is about $1 \times 10^8 - 1 \times 10^9$ cell/ml; 2) the eukaryotic cells are much larger than the bacterium. The diameter of a typical erythrocyte is around 10 μm while the diameter of a typical bacterium is 0.1 μm. 3) the criteria are different in the two assays: the MIC is measured as the concentration without growth of bacterium but the hemolysis assays measured the cellular content leakage; Inhibiting cell growth is clearly easier than completely breaking down the cell membrane. 4) the time scale is also quite different. The bacterial growth is monitored for over 24 hours while the hemolytic activity is measured in 30 minutes to 1 hour.

Indeed, reducing the erythrocyte concentration to 6×10^5 cell/ml, only 10 μM of magainin is required for complete membranal lysis [110]. However, in the same study, different modes of action can be visualized in bacterial and mammalian membranes. In the vesicle experiments whose lipid

concentration can be easily controlled, it is frequently observed that many antimicrobial peptide causes more lysis on vesicles whose lipid components are similar to bacterial membranes than on those whose lipid components are similar to eukaryotic cell membranes. The term "selectivity" thus is more complicated than we previously assumed and therefore should be used in a more strict sense.

1.3.4. Linking mechanism to activity

To design novel peptides that possess maximum antibacterial activity and minimum hemolytic activity, we must establish a relation between the peptide properties and the biological activities, no matter qualitative or quantitative.

1.3.4.1. Biophysical factors that affect biological activities

Mutagenesis studies provided extensive information on how the biophysical properties of antimicrobial peptides would affect the activity of the peptides.

Peptide Charge One of the most important features of antimicrobial peptides is their net positive charge. Indeed, the α helical peptide can also be hydrophobic or even slightly anionic. Gramicidin A is a mostly hydrophobic peptide to form a helical transmembrane structure. Alamethicin is anionic and less selective against bacterium and eukaryotic cells. However, these cases are rare. The majority of these peptides have multiple cationic side chains, which make them very favorable to treat anionic membranes of bacteria and cancer cells. The positive net charge is suggested to be a main reason that these peptides exhibit selectivity over host cells.

Increase in the net charge of the peptide will inevitably result in increased antimicrobial activity, as has been demonstrated in a number of studies [111, 112, 113]. However, increment of charge will also have other side-effects on the peptide structure in which occasionally causes reversed relationship[111, 114]. Raising net charge beyond a certain threshold will no longer increase the antimicrobial activity [115].

Amphipathicity Amphipathicity reflects the balance of hydrophobic and hydrophilic domains within a protein. Amphipathicity is normally described quantitatively as hydrophobic moment [116]. It can be calculated from the structures of the peptides, which, in most of cases, are assumed to be an ideal α-helical structure. Hydrophobicity potential is the extension of the hydrophobic moment concept, depicting both the hydrophobicity gradient along a peptide sequence and the hydrophobicity contours around the helices [117].

Increased hydrophobic moment results in a significant increase in the permeabilization and hemolytic activity of model peptides against target membranes.

The amphipathicity is not limited to α-helical peptides, but also include the β-sheet antimicrobial peptides. This β-sheet amphipathicity is characterized by a variable number of β-strands, with relatively few or no helical domains, organized to create both polar and non-polar surfaces. These findings have demonstrated that residue-specific modifications in hydrophobicity enhance the selectivity among cationic peptides. For example, studies based on synthetic derivatives of gramicidin S have revealed that reductions in hydrophobicity will significantly increase selective toxicity against microorganisms, with an approximately 10,000-fold increase in the estimated therapeutic index of such peptides [118].

Hydrophobicity Hydrophobicity is a quite essential feature of antimicrobial peptide membrane interactions, as it governs the extent to which a peptide can partition into the lipid bilayers. Although hydrophobicity is required for the effective membrane permeabilization, increasing levels of hydrophobicity are strongly correlated with mammalian cell toxicity and the loss of antimicrobial specificity. Therefore, many antimicrobial peptides are moderately hydrophobic such that they optimize activity against microbial cell membranes.

Polar angle Polar angle is a measurement of the relative proportion of polar versus nonpolar facets of a peptide conformed to an amphipathic helix. For example, in a hypothetical α-helical peptide, in which one facet is exclusively composed of hydrophobic residues and the other is solely composed of charged residues, the polar angle would be 180°. If the peptide has larger hydrophobic domains, the polar angle will be reduced.

In numerous studies of native and synthetic peptides, a smaller polar angle is associated with increased capacity to permeabilize membranes [119, 120, 121]. Even in the context of reduced membrane affinity, peptides with smaller polar angles induced greater membrane permeabilization, translocation, and pore formation rates [121]. However, although the rate of pore formation was greater for peptides with smaller polar angles, the rate of pore collapse was also higher. These results suggest that peptides with smaller polar angles achieve less stable pore structures, compared with peptides having larger polar angles. Greater stability of pores formed by the latter peptides could result from larger charged surfaces, and/or more peptide molecules per channel. These concepts are consistent with those observed in native peptides, showing that peptide PGLa (100°) is more readily translocated than magainin 2 (180°; [50]).

Chain length The size of the peptides also correlates positively with their biological activity. In a research, a series of peptides containing simple sequence repeats, $(RW)_n$-NH_2 were tested [122]. The effective concentrations against bacterium and erythrocytes are found to have a linear relationship with the peptide length (n). Chemical cross linking that artificially increases the peptide size also increases the activity of the peptide [123].

Helicity Previous mutagenesis studies always lead to unclear conclusions on the role of helicity in the peptide activity because it is hard to maintain other peptide properties when modifying peptide helicity. Dathe used a series of design peptides named "KLAL" to study the effect of helicity on the peptide activity and concluded that helicity has a positive effect on antimicrobial activity [113].

Shai added D-amino acids into several typical antimicrobial peptides [71, 70, 124]. Introducing D-amino acid to the peptide will disrupt the helical structure. Changing two adjacent residues to their D-enantiomers will yield even greater reduction in helical content. Based on these studies, it is generally believed that reduced helicity will greatly decrease the permeabilizing activity against neutral and moderately negatively charged lipid vesicles whereas having low or even no effect on the permeabilizing activity against highly negatively charged membranes [71, 70, 124].

It is generally accepted that many membrane peptides will fold in the membrane [125]. The formation of α helix in the membrane exerts a negative influence on the total membrane binding

energy. It is therefore not quite surprising that the helicity plays an important role in the biological activity. In highly anionic membranes, the contribution of helix formation is overriden by the highly negative contribution of electrostatic interaction.

Oligomerization ability Many antimicrobial peptides are able to oligomerize in the solution and membrane. This ability is found to be associated with the hemolytic activity of these peptides. Melittin is one example of peptides that oligomerize in the aqueous solution. It is suggested that melittin contains a leucine zipper-like motif in its sequence that is responsible for the aggregation [126, 127]. Mutations on this motif will reduce the hemolytic activity of melittin but won't affect its antibacterial activity. Another example is pardaxin, whose C terminus is responsible for the aggregation in membrane. Without its C terminus, the peptide preserves antibacterial activity with their hemolytic activity significantly reduced. Other examples includes LL-37, which binds to zwitterionic membranes in oligomeric state and binds to anionic membranes in monomeric state[128]; and dermaseptin B, which has higher ability to self-associate and to permeate zwitterionic membranes[129].

The exact connection between oligomerization and hemolytic activity still remains unclear. One possibility is that the oligomerization state can act as an intermediate state of the pore formation. The existence of aggregates may also have an advantage *in vivo*: in human wounds and blister fluids, resistance to proteolytic digestion can influence the life span of the peptide and its efficacy.

Interfacial activity Wimley [130] suggested that the antimicrobial activity is correlated with its interfacial activity, which includes the ability to partition into membrane-water interface and the ability to affect lipid packing . The first is correlated with the amphipathicity while the latter is related with "imperfect amphipathicity". Several peptides have been designed to verify this theory [131].

1.3.4.2. Connection between partition energy and activity

No matter how complicated the mechanism of antimicrobial peptides is, the actions of most antimicrobial peptides can be divided into two steps: the first one is that the peptide binds to the

membrane surface; the second step is to accumulate to a critical concentration until the peptide starts to kill the cell.

The effective concentration (EC) of peptide is defined as the sum of moles of peptide(n_b) on membrane and in water(n_f) divided by the total volume (V_{total}).

$$EC = (n_b + n_f)/V_{total} \tag{1.5}$$

Because partition coefficient is defined as $K_c = \frac{n_b/V_L}{n_f/V_W}$ (V_L and V_w are the volume of lipid and water respectively), so $n_f = \frac{n_b}{K_c V_L} V_{water}$ and :

$$EC = \frac{n_b}{n_L}\frac{n_L}{V_{total}} + \frac{n_b}{K_c V_L}\frac{V_{water}}{V_{total}} \tag{1.6}$$

Because $V_w \approx V_{total}$ and $V_L = n_L v_L$ (moles of lipid times molar volume of the lipid), the above equation can be finally converted to:

$$EC = P^*/L(\frac{1}{K_c v_L} + [L]) \tag{1.7}$$

if P^*/L is the critical peptide to lipid ratio (n_b/n_L) that cell dies and [L] is the concentration of lipid. This equation (Equation 1.7) was used by Melo et al. [132] to predict the effective concentration of two peptides . v_L is about 0.68 L/mol for DOPC/DOPE lipids. [L] depends on the experimental condition and the size of the organism. In typical condition of MIC measurement (for CFU around 1×10^5), [L] is about 20-70 nM. In typical condition of hemolytic measurement (cell concentration of 5 % v/v), [L] is around 90 μM. Compared to the range of MIC and EC50 ($\geq 0.1\mu M$ and$\geq 100\mu M$), [L] is often negligible.

K_c in Equation 1.7 can be calculated from the partition energy of peptide in membrane:

$$-RTlnK_c = \Delta G_c^0 \tag{1.8}$$

However, for most antimicrobial peptides, K_c varies with the peptide concentration [133]. This is because there is an insertion of a peptide into membranes increases the cost of energy, considering the electrostatic repulsion between the free peptides and the membrane bound peptides or the elastic expansion of the membrane result by peptide insertion. The further binding of peptides will be significantly reduced. Therefore, we must take that energy cost into account:

$$-RTlnK_c = \Delta G_c^0 + E(P/L) \tag{1.9}$$

The energy cost of binding a peptide to membrane surface is a function of surface concentration(P/L) of the peptide. Huang suggested it to be the elastic energy of membrane expansion [134, 135], so that:

$$-RTlnK_c = \Delta G_c^0 + \frac{K_a}{2}\frac{A_P^2}{A_L}P/L \tag{1.10}$$

where A_P is the surface area occupation of a peptide, A_L is the area per lipid, K_a is the area compressibility modulus. The elastic energy does not only prevent peptides from binding to the membrane but also forces peptides to reorient to transmembrane orientation. In the second case, pore formation is observable. Huang further suggested that the critical peptide surface concentration to form pore can be calculated as[136]:

$$P^*/L = \frac{\Delta G_{p\to s}^0}{K_A(A_P^2/A_L)(1-\beta)} \tag{1.11}$$

where $\Delta G^0_{p\to s}$ is the energy difference between the surface binding state and the pore state, β is a parameter that can be either positive or negative. If β is positive, the pore formation tends to reduce the thickness of the membrane. If the β is negative, the pore formation will increase the thickness of the membrane.

1.3.4.3. QSAR models

To predict biological activities from peptide structures, one can establish quantitative Structure Activity Relationship (QSAR) models.

The first steps of establishing QSAR models is building a training set that contains peptides with measurable structure and activity descriptors. Statistical methods can be used to establish the mathematical relationship between structure descriptors and activity descriptors. The most simple method is the widely used multiple linear regression. Fractional factorial design (FFD) algorithm sometimes can be used to help pick up the descriptors that contribute more significantly to a linear model[137]. Machine learning methods may also be applied to the model building. Cherkasov and colleague used Artificial Neutron Network (ANN) to screen useful descriptors from hundreds of structure descriptors [138, 139, 140, 141].

For a group of peptides that have similar structures, one to four structure descriptors are enough to describe a biological activity. Pathak et al. [142] established a relationship between the minimal inhibitory concentration and three structure descriptors: hydrophobicity , amphipathicity, α helicity. For β peptides, the activities of cyclic analogs of protegrin-1 can also be fitted into equations of two variables: charge and lipophilicity of nonpolar surface[143]. Juretic focused on the antimicrobial peptides produced by frog skins. They found that a "D-descriptor" which describes the angle between the hydrophobic and hydrophillic residue clusters alone can effectively determine the therapeutic index of the peptide [144]. Other than these factors, in vitro/in vivo aggregation are also demonstrated to be important in determining the biological activity[145].

The descriptors that are normally used in ligand-protein studies[137, 146, 147] or the descriptors collected from MD simulations [148] can also be used to predict antimicrobial peptide activities. However, large numbers of descriptors are required in those cases because they are only loosely correlated with the activity descriptors so that each of them contribute little to the linear model.

Instead of finding the QSAR relationship, sometimes, the sequence patterns of active antimicrobial peptides can also be established [149, 140, 150]. These patterns cannot help us determine the activity of an antimicrobial peptide but can be used to discriminate non-antimicrobial peptides from antimicrobial peptides.

1.4. Pore formation induced by membrane active peptides

The formation of transient pores in lipid bilayers is a crucial step in many biological processes including the transport of molecules and ions across membranes, apoptosis, membrane fusion, and drug & gene delivery [151, 152]. Recent experiments[153, 154] and computer simulations [155, 156, 157, 158, 159, 160, 152] of protein-free bilayers in the fluid phase have provided new insights on the localized density perturbations of membranes and the formation of transmembrane pores.

1.4.1. Pore formation without peptide

Lipid bilayers separate the contents of all biological cells from the outside world. Their hydrophobic interiors turn them into very effective barriers for charged species. The spontaneous formation of pores in lipid bilayers is rare but can happen under electric [161, 162], and mechanical [163, 164] tensions or when the temperature is close to phase transition temperature[165, 166].

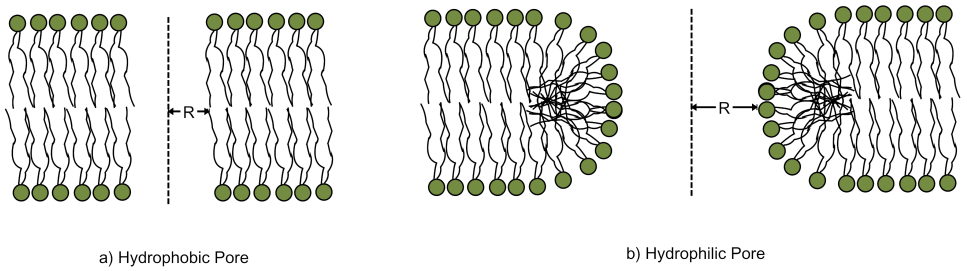

Figure 1.8.: Types of pores formed inside membrane.

Two types of pores can be formed in the membrane depended on the stages of poration (Figure 1.8). At the first stage, a so-called “hydrophobic pore” is formed under thermal fluctuation, ion penetration, or other external forces. At this stage, the pore is merely an opening in the membrane; there

is no separation between the water channel and acyl chains. As the pore enlarges, it becomes highly unfavorable because exposing the hydrophobic membrane interior to water is energy consuming. The energy of hydrophobic pore can be calculated as [167]:

$$E = 2\pi Rh\sigma_0(R) \tag{1.12}$$

where $\sigma_0(R)$ is the interface tension between hydrophobic lipid tails and water, R and h are the radius of the pore and the thickness of the membrane respectively. The interface tension is not a constant as one could intuitively assume. Instead, when the pore is small enough (Less than a length ρ, normally equal to 1 nm), the overlapping of water layers would significantly reduce σ_0 [168]. Hence, an empirical function had been suggested [ref]:

$$\sigma_0(R) = \sigma_0(\infty)I_1(R/\rho)/I_0(R/\rho) \tag{1.13}$$

where $I_n(x)$ is modified Bessel function of n-th order.

A more sophisticated model was suggested by assuming the water molecules exist in vapor form inside narrow hydrophobic pores[169]. If no external tension is added, the energy of a "vapor pore" is suggested to be [169]:

$$E = \frac{K_A}{2A_0}(A - A_0 - \pi R^2)^2 + 2\pi Rh\gamma_{tv} + 2\pi R^2\gamma_{wv} \tag{1.14}$$

where K_A is the compression modulus, A_0 and A are the initial and final areas of the membrane; γ_{tv} and γ_{wv} are the line tensions of the acyl chain and head groups respectively.

When the pore enlarges, it will fast evolve into "hydrophilic pores", in which the lipids around the pore region reorient to line the pore surface with head groups. The energy of hydrophilic pore is

proposed by “classic nucleation theory” [170]:

$$E = 2\pi\gamma R - \pi\sigma R^2 \tag{1.15}$$

where γ is the edge energy (“line tension”) of the pore wall and σ is the mechanical surface tension. In Equation 1.15, the γ also is not a constant when the pore radius is small. The packing of lipids along the wallside of a narrow pore leads to substantial deformation of molecular orders. The contribution of this deformation to pore energy steeply rises when R approaches the size of the lipid heads [165]. Unfortunately, the energetic of this deformation process is not well understood and the energy of “hydrophilic pores” with small radius can only be speculated.

Tolpekina et al. [157]and Notman et al. [169] extended the above equation to elastic membranes without external surface tension:

$$E = \frac{K_A}{2A_0}(A - A_0 - \pi R^2)^2 + 2\pi R\lambda \tag{1.16}$$

in which K_A, A_0, A , and γ are defined previously.

Based on the above theories, pore formation is unlikely under zero or negative surface tensions. Even a pore opens due to the thermo fluctuations, it would reseal quite quickly. If a surface tension is applied, the pores formed in the membrane still would not be stable. They would reseal if the pore size is too small or enlarge to infinity if the pore radius exceeded a certain threshold.

Such a phenomenon is indeed observed. In GUVs, under tensions driven by adhesion of the vesicle to appropriately treated surfaces, or by intense optical illumination in the presence of membrane embedded fluorescent probes, a small opening can lead to an extremely large pore(10 - 20 μm in radius) [171]. This pore is, however, transient. After several seconds, when the inner liquids leak out and the membrane tension is reduced, the membrane will reseal. The kinetic process of pore evolution can be well fitted into Equation 1.15 assuming the osmotic pressure changes with the percentage of leakage.

The free energy of pore formation can also be obtained from simulation methods [154, 160, 172]. The results also agreed witht the above models quite well.

1.4.2. Pores induced by the peptides

Based on the equations given above, the formation of a pore is possible only if : 1) there is an external surface tension that stretches the membrane. 2) there are some molecules that can reduce the energy of a lipidic pore. In the first case, the pores formed in the membranes are not stable: it will close immediately after the pore opens or enlarges until a large fraction of enclosed content leaked out. Peptides indeed can induce positive surface tension that lead to such cascade: magainin can induce transient pores in GUVs that open up to $100\mu m$ and reseal to pores with much smaller radii [173].

In more cases, stable pores were observed: Huang crystallized the pores and then visualized them with x-Ray and cryo-EM [174, 175, 176]. LL-37 could increase the area of a GUV and create stable pores on the membrane after a critical point [177]. Although the hydrophobic pores are quite energetically unfavorable in their nature, formation of such pores is much easier with the assistance of transmembrane peptides because the amphipathic peptide can separate the hydrophobic acyl chains from water. Such type of pores are also called barrel-stave pores because peptides have to form a well-defined bundle surrounding the water channel.

Forming hydrophilic pores is also likely to be accelerated by the antimicrobial peptides. Such types of pores are often termed as “worm-holes” or “toroidal pores”. Well organized structure is not necessary [178]. The reason peptides can facilitate and stabilize the formation of hydrophilic pores is not quite clear right now. Antimicrobial peptides are generally considered to be able to reduce the line tension of the membrane[179]. This can reduce the energy barrier for pore formation but is not enough for pores to be metastable. To create a stable pore, the peptide must contribute a negative free energy to create a local energy minimum at certain radius.

1.4.3. Peptides inducing pores

1.4.3.1. alamethicin

Alamethicin is a peptaibol peptide which contains the non-proteinogenic amino acid residue Aib. It is produced by the fungus *Trichoderma viride*. It can induce multiple level conductances under transmembrane voltage [180, 181] and membrane tension [182]. The conductance levels are reproducible by different experiments. Each discrete level can be explained by a corresponding oligomerization state. Neutron in-plane scattering also suggested that the pores formed by alamethicin in DLPC have an inner radius of 9 Å and an outer radius of 20 Å[183]. The thickness of the pore wall (11 Å) agrees with the diameter of an alamethicin helix [184]. The requirement of a well organized structure suggests that the pore formation mechanism of alamethicin complies with "barrel stave" model.

The structure of alamethicin pore was solved later by X-ray diffraction analysis[185]. The electron density distribution map clearly indicates that the head groups are not present on the pore wall, which further supports the "barrel-stave" model. High-resolution EC-STM images also showed that the alamethicin form well-defined 2D nanocrystals in which pore to pore distance is about 19 Å [186].

Native alamethicin channels exhibit either cation selectivity or anion selectivity depending on which end of the channel is at the low salt side of the membrane [187]. When the glutamine residue at position 18 in the sequence is replaced by a lysine residue, an anion-selective channel can be obtained no matter which end of the channel was at the low salt side of the membrane [187].

Even though alamethicin has a net charge of -1, its activitiy is not quite sensitive to the presence of anionic lipids [188].

1.4.3.2. magainin

Magainin, a peptide in *Xenopus laevis* skin, was found to be active against bacteria, fungi, and viruses but it has low toxicity against normal cells. More recently, magainin was reported to selectively lyse tumor cells without killing healthy vertebrate cells [189]. Interestingly, PGLa, another peptide that is found in frog skin, can synergistically enhance the activity of magainin [50].

The structure of magainin is mainly helical, with a long α-helix at the N terminus and a short $\pi-$helix at the C terminus. However, at peptide-to-lipid molar ratios of 1:10 a mixture of α-helical and β-sheet conformations are detected by means of FTIR and rotational echo solid-state NMR spectroscopy in the gel state DPPG and DPPC/DPPG 1:1 membranes[190] .

Determined from solid state $^{15}N-NMR$, magainin orients parallel to the membrane surface when the concentration of magainin 2 is between 0.8 and 3 mole% [191]. Half of the peptides were found to change to perpendicular orientation in DMPC:PG(3:1) when P/L is increased to 1/10 [192]. Similar orientation change is observed by ATR-FTIR, from which a tilt angle of 20° is determined [193]. This change to transmembrane orientation suggests a pore formation mechanism for the magainin. Besides, magainin can also induce lipid "flip-flop" [61]. Such action also is accompanied by pore formation [61]. Leakage kinetics showed that the magainin pore could be tetrameric [194] or pentameric [195].

In contrast to pores formed by alamethicin, a large range of conductivities of the pores, starting at 1.8 pS, has been detected[196]. The size of pores can be determined directly from Neutron diffraction [197, 192], X-Ray diffraction [198], Cryo-EM [199] or indirectly from osmoprotection [200, 173]. With all these methods, the pore size was found to vary with the concentration of magainin. The "Worm-hole" model (or later called "toroidal pore") was proposed for magainin to explain the pore size of magainin determined by neutron diffraction experiment [192]. The inner radius determined by this experiment is 15 - 25 Å with corresponding outer radius of 35 - 42 Å. The difference between the inner and outer radius of magainin pores cannot be explained by the thickness of a helix. The toroidal pore model was also supported by its selectivity for cations [49], because, without reorientation of anionic lipids, the magainin bundle will create a positive potential in the pore, which favors anions over cations.

"Detergent-like" and "Carpet" model could also be plausible explanations for magainin's lytic activities. $^{31}P-$NMR showed that magainin causes the formation of disk-like micelles in POPC bilayers but not in anionic ones [201]. Spontaneous buckling of membrane was observed in μs level simulations [202]. Studies on the kinetics of pore formation in GUV indicated that the pore formation induced by magainin has two successive stages: a transient but huge pore is first formed and then this pore reduces its size and stabilizes to several pores with much smaller size ($<$ 35 Å)

[173].

The molecular mechanisms for magainin are quite different on eukaryotic and bacterial membranes [110]. The peptide forms pores with a diameter of $\backsim$2.8 nm in *B. megaterium*, and translocates into the cytosol. In contrast, it significantly perturbs the membrane of CHO-K1 cells, allows large molecules (diameter >23 nm) enter into the cytosol, induces membrane budding and lipid flip-flop, and accumulates in mitochondria and nuclei. Under the same surface bound peptide concentration, the leakage induced by magainin is slightly higher in lipid vesicles with higher anionic lipid fractions [203, 204].

1.4.3.3. melittin

Melittin, the major component of the honey bee venom, is a 26-residue hemolytic and membrane active peptide [205].

In aqueous solutions, melittins aggregate into tetramers, which is further promoted by high salt, melittin concentration, and pH. The three-dimensional structure of melittin tetramer has been determined by X-ray crystallography at high resolution [206, 207] . A leucine zipper motif was found in the melittin sequence, which is responsible for the high tendency of aggregation[208, 127, 209]. The ability to aggregate is crucial for melittin's hemolytic activity. Mutations that destroy the leucine zipper motifs will greatly reduce the hemolytic activity without affecting the antibacterial activity [208, 127, 209].

Compared to magainin, melittin can easily adopt transmembrane orientation. Like alamethicin, transmembrane potential can easily affect the orientation of melittin in membranes [210, 211]. The energy cost of transferring a melittin molecule to transmembrane orientation is so little that transmembrane orientation is also observed in MD simulations [212].

In earlier studies, melittin was suggested to form barrel-stave pores. But the peptide concentration required for poration is much higher than real channel forming peptides which can form pore at a peptide/lipid ratio as low as 1/10000 [213].

Pores formed by melittin have discrete multilevel conductances [214, 215]. However, these levels are not that well-defined and vary in different experiments. Like magainin, the pore size increases

with rising peptide/lipid ratio [216, 112, 217]. In zwitterionic lipid vesicles, the inner radius of a melittin pore is about 17.5–22.5 Å while the outer radius is about 35–40 Å[218, 219]. These results are consistent with the studies by osmotic protection for erythrocytes that showed an estimated inner pore radius of ~12.5–15 Å at high melittin concentrations [220, 217]. Like the pores formed by magainin, the difference between the inner radius and outer radius is also too wide for a helix.

The activity of the pore formation of melittin is also suggested to be related with the spontaneous curvature radius [221], which further supports the toroidal pore model. In this study, higher and faster leakages are observed in membrane with positive spontaneous curvature. However, in contrast with magainin, melittin pores showed selectivity for anions over cations [210], which is hard to be explained by the toroidal pore model.

Presence of negatively charged lipids in the membrane had been shown to inhibit membrane lysis by melittin and this inhibition is enhanced at increased surface charge density [83, 222, 223]. Dual-color fluorescence-burst experiments also indicated that melittin induced leakage through different mechanisms in neutral and anionic lipids: in neutral lipids, melittin induces pore formation; in anionic lipids, melittin induces vesicle fusion [224].

1.4.3.4. protegrin

Protegrin-1 (PG-1) is an 18 residue peptide, isolated from porcine leukocytes with antimicrobial activity. The structure of protegrin is a β-hairpin stabilized by disulfide bonds [225, 226].

PG-1 was reported to form anion-selective channels in planar phospholipid bilayers, even in anionic ones [227]. The conductances of protegrin pores are in well separated discrete levels, indicating that the pores have orderly structures[227].

The PG-1 peptides aggregate into NCCN antiparallel dimers in DPC micelles [228]. However, in neutral POPC bilayers, NCCN parallel structure seemed more consistent with solid state NMR experiments [229] . In simulations [230], both parallel and antiparallel dimers can be organized into octamer pores that are stable for at least 30 ns. We later found that NCNC parallel structures might make more stable octarmeric pores[231].

At low levels of hydration or temperatures, the protegrin pores can be crystallized[175]. The X-ray

diffraction pattern for protegrin pore is similar to that of magainin instead that of alamethicin. Atomic Force Microscopy (AFM) can also be used to visualize the protegrin pore structure. In dioleoylphosphatidylserine (DOPS)/palmitoyloleoyl phosphatidylethanolamine (POPE) bilayers, a pore is composed of 3-5 subunits, where each subunit can be a protegrin dimmer [232]. The inner and outer radii of the pore are 6.5-7 Å and 26.5-27.5 Å respectively [232]. Based on this evidence, the pores formed by protegrin should be toroidal pores.

As a cationic peptide, protegrin binds to anionic membranes with high affinity [233]. The interactions of protegrin to zwitterionic and anionic lipids are, however, different. Revealed by ^{2}H NMR and ^{31}P NMR, the head groups of phosphatidylcholine (PC) lipids show significant orientation disorder when protegrin is added while those of phosphatidylglycerol (PG) lipids stay in an isotropic phase [234]. Wi and Kim [234] later tried to fit the spectra into theoretical models. They found that the solid state NMR spectrum of PC lipids agrees with an elliptic toroidal pore model, although the spectrum of PG lipids does not. Considering the factor that protegrin can induce pores with even higher stability in anionic membranes [227], such pores must have been formed without the requirement of reorienting the lipid head groups. Explicit simulation of an octameric pore in POPE/POPG(3:1) membranes also confirmed that the pore structure resembles partially toroidal and partially barrel-stave pore [235].

2. Methodology

2.1. Implicit membrane model

In the EEF1 [236] and IMM1 [237] implicit solvation models, the effective energy (W_{eff}) of a solute is the sum of the intra-molecular energy of the solute (E) and its solvation free energy (ΔG^{slv}):

$$W_{eff} = E + \Delta G^{slv} \tag{2.1}$$

E is calculated from the CHARMM19 force field, and ΔG^{slv} is obtained as the sum of atomic contributions, each calculated from a Gaussian solvent exclusion model:

$$\Delta G^{slv} = \sum_i \Delta G_i^{slv} = \sum_i \Delta G_i^{ref} - \sum_i \sum_j \frac{2\Delta G_i^{free}}{4\pi\sqrt{\pi}\lambda_i r_{ij}^2} V_j exp(-\frac{(r_{ij} - R_i)^2}{\lambda_i^2}) \tag{2.2}$$

where, the first term is the sum over all atoms whose solvation free energy is ΔG_i^{ref} when it is fully accessible to solvents, and the second term is the solvation free energy loss due to the shielding of the atoms by their neighboring atoms: ΔG_i^{free} is a value close to but not identical to ΔG_i^{ref}, so that the deeply buried atoms have zero solvation free energy; R_i is the van der Waals radius of the atom i; r_{ij} is the distance between atom i and a neighboring atom j; V_j is the volume of atom j; and $\lambda_i$is a correlation length describing how fast the solvation free energy density diminishes with distance. The transition of ΔG_i^{ref} from water to hydrophobic core of the membrane is described

as a linear combination of the values for water and cyclohexane (mimicking hydrocarbon core):

$$\Delta G_i^{ref}(z) = f(z)\Delta G_i^{ref,water} + (1 - f(z))\Delta G_i^{ref,chex} \tag{2.3}$$

where $f(z)$ is a transition function that describes the transition of solvent from water to membrane hydrophobic core (represented by cyclohexane), which is defined as a function of the the z coordinate(z axis is assumed to be membrane normal in the model):

$$f(z') = z'^n/(1 + z'^n),\ z' = \frac{|z|}{(T/2)} \tag{2.4}$$

The electrostatic interaction between two solute atoms was estimated by the distance dependent dielectric model [238]. In this model, the dielectric constant $\epsilon_{i,j}$ that used to calculate the electrostatic interaction between two partial charges i and j relies on the distance $r_{i,j}$ between the two charges:

$$\epsilon_{i,j} = r_{i,j} \tag{2.5}$$

Because the dielectric constant in membrane is much lower than that in water, the Equation 2.5 was modified to an empirical equation:

$$\epsilon_{i,j} = r_{i,j}^{f_{i,j}} \tag{2.6}$$

where $f_{i,j} = a + (1 - a)\sqrt{f(z_i')f(z_j')}$, and a is an adjustable parameter that we chose to be 0.85. At this value, we found that the model gives membrane insertion or adsoption energies in correct magnitude [237]. This model gives reasonable result with low computational cost.

2.2. Implicit membrane model for planar anionic membrane

In the model presented in the previous section, the membrane is assumed to be neutral. To describe the effect of anionic lipids on peptide binding, the electrostatic interaction energy between solute atom i and the membrane is calculated as the sum over all atoms of the product of the electrostatic potential at that point, with the partial charge of the atom [239]:

$$W_{GC} = \sum_i q_i * \phi(\vec{r}_i) \tag{2.7}$$

If the charges of anionic lipids distribute uniformly on an infinite planar surface, the electrostatic potential in the ionic solution adjacent to the membrane can be calculated from Gouy-Chapman theory [240], an analytic solution of the Poisson-Boltzmann equation:

$$\phi(d) = \frac{2k_bT}{zq} ln \frac{[1 + \alpha exp(-\kappa d)]}{[1 - \alpha exp(-\kappa d)]} \tag{2.8}$$

In this equation (Equation 2.8), k_b is the the Boltzmann constant, T is the Kelvin temperature, z is the valence of the counter ions, q is the unit charge,κ is the inverse Debye length, d is the distance to the charged plane, and α is defined as:

$$\alpha = \frac{exp(q\phi(0)/2k_bT) - 1}{exp(q\phi(0)/2k_bT) + 1} \tag{2.9}$$

κ can be calculated as $\kappa = \sqrt{\frac{2\rho z^2 q^2}{\epsilon_0 \epsilon_w k_b T}}$, where ϵ_0 and ϵ_w are the permissivity of vacuum and relative permissivity of water ($\epsilon_w = 80$) respectively, and ρ is the number of ions per volume.

$\phi(0)$ is the potential on the charged plane and can be calculated from the charge density of the

plane σ_0:

$$\phi(0) = \frac{2k_bT}{F} sinh^{-1}[\frac{\sigma_0}{\sqrt{8\epsilon_0\epsilon_w k_bT\rho}}] \tag{2.10}$$

where F is the Faraday constant and other parameters are the same as defined above. In our model, the charged plane is assumed to be O Å outside the hydrophobic core ($O = 3$ Å to mimic the distance between the phosphate and carbonyl groups of PG lipids), thus $d = |z| - T/2 - O$. Inside membrane ($d < 0$), the potential is assumed to be equal to $\phi(0)$. The surface charge density σ_0 is calculated by anionic lipid fraction times the net charge per lipid divided by area per lipid ($\sigma_0 = f_a * q * z/A_L$).

2.3. Implicit membrane model for pores

The membrane model in section 2.1 was extended to pores with two different geometric shapes [241, 242]. To describe pore shapes, the transition function $f(z')$ was replaced by $f(r', z')$ because the solvent components now change in both radial and axial directions:

$$f(r', z') = \frac{z'^n}{1 + z'^n} + \frac{1}{1 + r'^n} - \frac{z'^n}{(1 + z'^n)(1 + r'^n)} \tag{2.11}$$

in which z' was defined in previous section. r' is the normalized radial coordinate ($r' = r/R$). For a pore that possesses a cylindrical shape, the pore radius R is a constant (R_0). Typical pores that have this type of geometric shape are ion channels or barrel-stave pores. For toroidal pores that have curved pore surface, we defined another geometric shape whose R follows a parabola relationship with z':

$$R = R_0 + K_0 z'^2 \tag{2.12}$$

In Equation 2.12 the constant R_0 is the pore radius at the membrane center and K_0 is used to describe the curvature of the pore.

2.4. Numerical solution of Poisson-Boltzmann equation

The electric potential $\phi(\vec{r})$ generated by a charge distribution $\rho(\overrightarrow{r})$ in a polarizable continuum with dielectric constant $\epsilon(\overrightarrow{r})$ can be described by Poisson's equation:

$$\nabla[\epsilon(\overrightarrow{r})\nabla\phi(\overrightarrow{r})] + \rho(\overrightarrow{r}) = 0 \tag{2.13}$$

For biomolecules in electrolytes, it is convenient to assume that there are two types of charges: fixed charges of the biomolecules and mobile charges of the counter ions in solution. The distribution of the ions can be modeled as a Boltzmann distribution. As a result, Equation 2.13 can be turn into the following equation, namely Poisson-Boltzmann equation:

$$\nabla[\epsilon(\overrightarrow{r})\nabla\phi(\overrightarrow{r})] + 4\pi\sum_i c_i^{\infty} z_i q\lambda(\overrightarrow{r})exp[-\frac{z_i q\phi(\overrightarrow{r})}{k_b T}] + 4\pi\rho(\overrightarrow{r}) = 0 \tag{2.14}$$

where c_i^{∞} and z_i are the concentration and valence of the ion species i and $\lambda(\overrightarrow{r})$ is a parameter that describe the accessibility of a position to ions (0, unaccessible; 1, fully accessible).

For complex distribution of fixed charge $\rho(\overrightarrow{r})$, there is no analytical solution for Equation 2.14. Numerical solution can be achieved by Newton methods which discretize the continuous solution to a finite lattice, start with an initial guess for the $\phi(\vec{r})$ of each lattice point and iteratively improve the guess by converting the equation into a linear equation using current solution. Different software packages provided different discretization methods and equation solvers. A software package, APBS[243], utilizes cubic lattices and a multilevel solver that solves the Poisson-Boltzmann equation on a coarser level of discretion first and use the solution to speed up the calculation of finer levels [243].

To obtain an accurate $\phi(\vec{r})$, the boundary potential must be correctly given [244]. For membrane systems whose fixed charges are close to the boundary, it is difficult to give correct initial estimation. One way to solve this issue is to start with a system whose boundary is far away from the fixed charges and continuously move the boundary to the fixed charges[244]. The system to be studied is first placed in the center of a large lattice box whose boundary is far away from the system of interest. The space between system of interest and boundary is filled with ionic solutions. In this case, it is reasonable to assume that the potential at the boundary is zero. The Poisson-Boltzmann equation will be solved on the lattice and then the solution is used to calculate the boundary potential of a smaller lattice whose boundary is closer to the system of interest. By continuously reducing the lattice size and focusing on the system of interest, we can obtain more and more accurate $\phi(\vec{r})$.

3. Orientation of transmembrane peptides

The orientation of transmembrane peptides was suggested to comply with the hydrophobic mismatch theory. That is, when a peptide has a longer hydrophobic segment than the membrane hydrophobic thickness, the peptide will tilt to fit its hydrophobic segment with the membrane. Based on this theory, the tilt angles of a series of designed peptides should be moderate. This is verified by multiple methods, such as ^{15}N-NMR and FTR-IR. However, the observed tilt angles from solid state ^{2}H- NMR experiments are small. Here, we examined the peptide orientation in MD simulations using implicit and all-atom membrane models. We observed that the peptides adopted moderate tilt angles as suggested by the hydrophobic mismatch theory. We further explored the energy landscape of peptide orientation. The optimal tilt angle at each membrane thickness also agreed with the hydrophobic mismatch theory. The energy barrier for rotation is small so that the peptides can have rapid rotation motions. Using the angular information obtained from the solid state NMR experiments, we restrained the peptide side chains in the MD simulations. The tilt angles of the generated structure ensembles are small. To make the peptide orientation agree with the MD simulations, the motion averaging of the NMR spectrum at small time scales must be considered.

3.1. Method

3.1.1. Peptide conformation

The peptide conformations were constructed as ideal α-helices by assigning the ϕ/ψ angle of the peptide backbones to be -47°and -57°. The sequence of the four peptides we studied are :

WALP23 : GWW$(AL)_n$LWWA-NH_2

WLP23 : GWW(L)$_n$LWWA-NH$_2$

KALP23 : GKK(AL)$_n$LKKA-NH$_2$

KLP23 : GKK(L)$_n$LKKA-NH$_2$

The constructed conformations were minimized in implicit solvent using the steepest descent method and then used for MD simulations.

3.1.2. Implicit simulations

To simulate the peptide orientation in implicit membranes, the minimized conformation of each peptide was first oriented parallel to the membrane normal with its mass center placed at the origin of the coordinate system. For each peptide, we ran four simulations at different membrane thicknesses (see Table 3.1) in the IMM1 neutral membrane model[237] and each simulation lasted 10 ns.

Illustration of how tilt and rotation angles are defined in literature can be found in Figure 1.1. To calculate the tilt/rotation angles, we first calculated three vectors: the helix axis $\vec{H}$, the perpendicular line $\vec{R}$ from the reference atom (the C_α atom of the glycine residue) to helix axis, and the cross product of $\vec{R}$ and $\vec{H}$. Then we projected the z axis to the $\vec{R}$ and $\vec{R} \times \vec{H}$ plane. The tilt angle of the peptide was calculated as the angle between the membrane normal (z-axis) and the helix axis. The rotation angle was calculated as the angle between $\vec{R}$ and the projection of z (z'). The tilt and rotation angles were calculated as the average values of all conformations in the last 5 ns of each simulations.

3.1.3. Explicit simulation

The final conformation of WALP23 in the implicit simulation at membrane thickness 23.5 Å was used for explicit simulations.

Two completely different membrane systems were built:

In the first system, pre-equilibrated DMPC lipids were randomly placed round WALP23 to create a membrane around it. The hexagonal simulation box was used to make sure the lipids distribute

more uniformly around the peptide. Several simulations were carried out with different surface tensions or with fixed surface area (see Table 3.2). In each simulation, the system was heated and equilibrated for 4 ns with the peptide's backbone atoms that are constrained in their intial positions and then the simulation was continued for up to 20 ns with the constraints removed. CHARMM27 parameter set was used for the simulations of the first system.

In the second system, WALP23 was inserted into a well-equilibrated DMPC membrane in the orthogonal shape at a higher hydration level. The lipids that were overlapped with the peptide were removed. The system was also heated and equilibrated for 4ns with constraints on the peptide backbones and then continued 20 ns without any constraints. Only one simulation was carried out with constant surface area. CHARMM27r parameter set was used for the simulations of the second system.

The details of simulations are listed in Table 3.2. All simulations were carried out using the NAMD simulation package. The tilt and rotation angles were determined in the same way as in the previous section. The membrane thickness was calculated as the distance in z axis between the average mass centers of the carbonyl groups in the upper and lower leaflets.

3.1.4. Energy landscape

To construct the energy landscape of peptide tilt, each of the four peptides constructed in subsection 3.1.1 was tilted and inserted into membranes with thickness ranging from 10 – 30 Å and step size of 1 Å. In each membrane, the tilt angle of the peptide was changed from 0° to 90° with step size of 5°. In each tilt/thickness combination, the peptide was simulated for 200 ps to allow the peptide to find its optimal conformation and then the system was energy minimized with 1000 steps of steepest descent. To maintain the tilt angle of the peptide, its C_α atoms were restrained in a cylinder whose radius is around 2.6 Å and the main axis coincides with the initial peptide axis. The mass center of the peptide was initially placed at the center of the membrane and was allowed to move freely between $\pm T/2$ if T is the thickness of the membrane hydrophobic core. For each tilt/thickness combination, we calculated the transfer energy ΔW of the final conformation by transfering the peptide from membrane to water and calculating the difference in effective energy ($\Delta W = W_{memb} - W_{water}$) .

To construct the energy landscape of peptide rotation, only one membrane thickness was studied (T=23.5 Å). Each peptide was tilted from 0° to 90° with step size of 5°and rotated from 0° to 360° with step size of 10°. The same method was used to constrain the tilt angle and the mass center. The peptide's rotation angle was constrained by constraining C_α atom of the reference residue glycine on a plane that is parallel to the helix axis and that passes through the initial position of the C_α atom of the glycine residue. For each tilt/rotation combination, the peptide was simulated for 200 ps and then energy minimized with 1000 steps of steepest descent. For each tilt/rotation combination, we calculated the ΔW of the final conformation.

The energy landscape was constructed by plotting ΔW against tilt angle and membrane thickness or tilt and rotation angles. Because the tilt and rotation angles might deviate slightly from the constrained values, the acutal tilt and rotation angles were used to prepare the plots. The contour maps was generated with gnuplot.

3.1.5. MD simulations with angular constraints

To obtain structures that agree with solid state NMR data, we applied constraints to the intramolecular angles (β) to make them stay close to the experimental values ($\bar{\beta}$) . The constraint energy has a harmonic form:

$$E = \sum_{i}^{N} k_i * (\beta_i - \bar{\beta}_i)^2 \tag{3.1}$$

The angle β is normally a angle between a chemical bond and the direction of the magnetic field (z axis). The MMFP module was modified to provide the functionality of constraining a bond orientation to a given direction. The constraint can be called using the following command under CHARMM:

mmfp

geo vector -

force k tref $\bar{\beta}$ -

xdir 0.0 ydir 0.0 zdir 1.0 -

sele *atom1* end -

sele *atom2* end

end

where the direction of the magnetic field is defined by its three components in x (xdir), y (ydir), z(zdir) directions (in our case, it points to z axis); the bond vector is defined by two atoms ("sele ... end", the first atom is the origin of the vector, the second atom is the end of the vector).

For ^{2}H NMR, the angle $\bar{\beta}$ between C_α-C_β bond vector and magnetic field direction can be calculated from the ^{2}H NMR quadrupole splitting (QS) using the following equation (derived from Equation 1.3):

$$\bar{\beta} = \pm acos(1 \pm \frac{4\Delta v_Q}{3QCC}) \tag{3.2}$$

We calculated $\bar{\beta}_i$ of different alanines from Table 3.3. Because for each alanine there are four possible $\bar{\beta}_i$ given by Equation 3.2, combinations were generated. For each combination of $\bar{\beta}_i$ angles, a short simulation (500 ps) was carried out with each labeled alanine constrained to its experimental orientation (a force constant k of 100 $kcal/mol/rad^2$ was used for all alanines). The last 250 ps of these simulations were combined together and the conformations were ranked by their potential energy and rmsd (Equation 1.4). Conformations with both potential energy and rmsd in the lowest 10% were included in the final structure ensemble. The peptide orientation were calculated from the conformations in the final ensemble.

3.2. Peptide orientation in MD simulations

First, the tilt angles of four peptides — WALP23, WLP23, KALP23, KLP23 — that have different flanking residues and hydrophobic segments were calculated from the implicit simulations and

compared to the GALA method. Table 3.1 shows the results. The tilt angles calculated from the implicit simulations are larger and more significantly affected by the membrane thickness than the ones obtained from the GALA method. The hydrophobicity of the central segment does not affect the tilt angle critically. Compared to the interface favoring residue tryptophan (W), the polar residue lysine (K) makes the peptides tilt smaller in the implicit simulations. This is different from the observation based on the GALA method, which is understandable: the polar residues prefer to stay in the water rather than on the membrane surface, which pushes the peptides to be more closely parallel to membrane normal.

Table 3.1.: Peptide orientation in implicit MD simulations at different membrane thicknesses.

Peptide	Membrane	Hydrophobic thickness Å	GALA tilt /°	MD simulation /°
WALP23				
	di-18:1 PC	26.5	4.8	13.3
	di-14:0 PC	23.5	5.2	24.0
	di-13:0 PC	21	7.5	32.8
	di-12:0 PC	19.5	8.1	36.9
KALP23				
	di-18:1 PC	26.5	4.8	12.0
	di-14:0 PC	23.5	7.6	17.8
	di-13:0 PC	21	9	24.8
	di-12:0 PC	19.5	11.6	31.1
WLP23				
	di-18:1 PC	26.5	4.5	10.1
	di-14:0 PC	23.5	8.1	18.5
	di-13:0 PC	21	8.9	32.6
	di-12:0 PC	19.5	11.4	36.8
KLP23				
	di-18:1 PC	26.5	6.4	10.9
	di-14:0 PC	23.5	8.3	14.3
	di-13:0 PC	21	9.4	22.4
	di-12:0 PC	19.5	10.6	28.1

We also carried out simulations in all-atom models. In these simulations, the surface tension was changed to stretch the membrane to different thicknesses. The tilt angles in these simulations are even larger than the ones we found in the implicit simulations and have a correlation with the membrane thickness. Hydration level may also affect the tilt angle; in a simulation with increased hydration level (Table 3.2 MD_Orth), the tilt angle of the peptide is smaller. Even so, the tilt angle is much larger than the ones given by GALA method.

Although tryptophan residues tend to anchor the peptides to the membranes, the tilt and rotation

angle of WALP23 are not very restrained. The tilt angle can fluctuate up to ±10° and the rotation angles can vary between 0-100°. The rotation motion is especially significant: the peptide can change its Azimuthal rotation angle for 50-100° in 10 ns.

Table 3.2.: Orientation of WALP23 in the explicit DMPC membranes.

Name	P/L ratio	Periodic box	Hydration Level (L:W)	Surface Tension	Membrane thickness (Carbonyl-Carbonyl)	Tilt	Simulation Length	Force Field
MD_Hex	1/100	Hexagonal	1:13.6	55.0 $\AA^2$ fixed area	28 Å	35°	20ns	Charmm27
MD_Hex+40	1/100	Hexagonal	1:13.6	+40 dyn/cm	22.5 Å	40°	9ns	Charmm27
MD_Hex+80	1/100	Hexagonal	1:13.6	+80 dyn/cm	17 Å	62°	20ns	Charmm27
MD_Orth	1/62	Orthogonal	1:28.7	60.5 $\AA^2$ fixed area	25 Å	27°	19ns	Charmm27r

3.3. Energetic maps of peptide orientation

3.3.1. tilt angles in different membrane thickness.

Using an implicit membrane model, it is possible to explore the energy landscape of peptide tilt. We calculated the transfer energy from water to membrane (ΔW) of peptides at different tilt angles (τ) and different membrane thicknesses. This quantity (ΔW) is preferred over the absolute effective energy (W) because it shows the energy cost of inserting a peptide into the membrane.

In Figure 3.1, we plotted the ΔW against tilt angle and membrane thickness. At each membrane thickness (T), we observed that each peptide has an optimal tilt angle τ_0 at which the transfer energy ΔW is at its mimimum. τ_0 changed with T following $\tau_0 = A * acos(\frac{T}{L})$ (the red thick lines inside the figure), where L is the hydrophobic length of the peptide and A is an empirical constant that might be related with the hydrophobicity of the center segment. Based on the graph, WLP23 and KLP23 have slightly shorter hydrophobic length L but higher hydrophobicity A than WALP23 and KALP23; their optimal tilt angles increased faster with the membrane thickness.

The energy differences between the optimal tilt angles and the other tilt angles are affected by both the hydrophobicity A and the flanking residues. Buring lysine or trytophan residues in membranes is quite unfavorable, so that all four peptides have much higher energy at tilt angles larger than optimal tilt. The differences ($\Delta\Delta W$) in ΔW between those tilt angles and the optimal tilt angles are between 20-50 kcal/mol. The WALP23 also have quite unfavorable energy ($\Delta\Delta W \geq$20 kcal/mol) at small tilt angles (< optimal tilt) in thin membranes (T ~ 10-15 Å) while WLP23 have even

higher $\Delta\Delta W$. In contrast, small tilt angles are only slightly unfavorable ($\Delta\Delta$W $<$ 10 kcal/mol) for lysine flanked peptides KALP23 and KLP23.

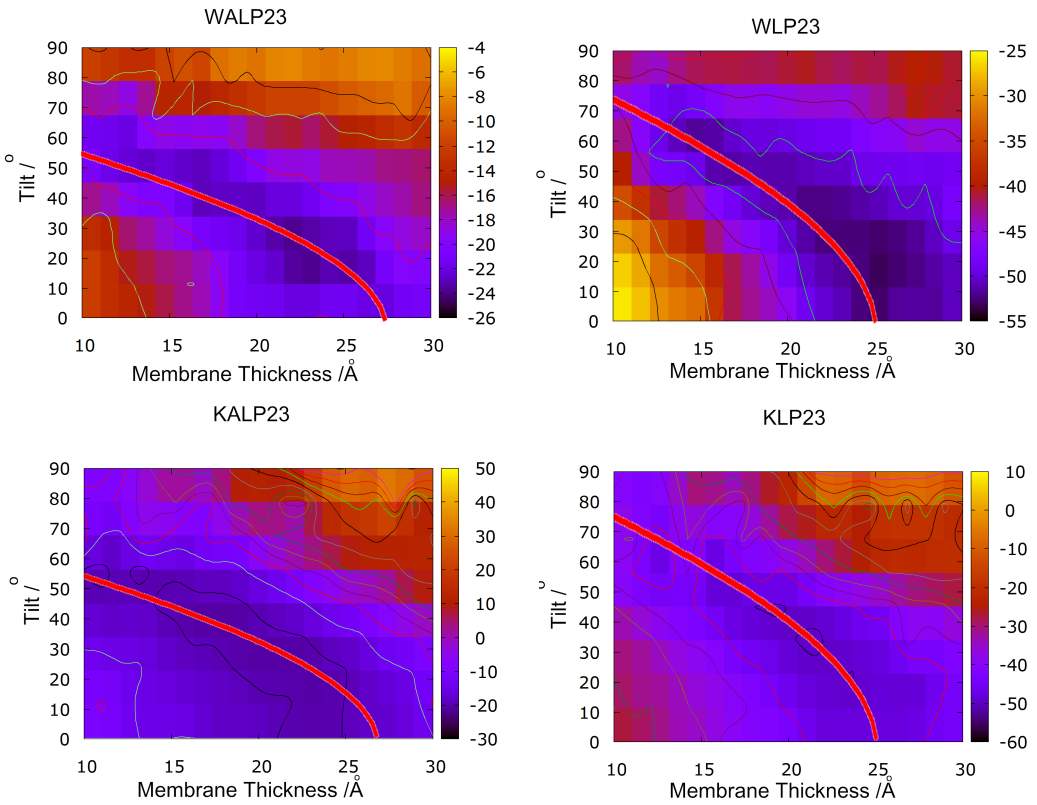

Figure 3.1.: Transfer energy ΔW of peptides at different membrane thicknesses and tilt angles. The thick red lines were drawn based on cosine functions.

3.3.2. Rotation angles of transmembrane peptides

The correlations between tilt and rotation of the peptides were also studied (Figure 3.2). Flanking residues play an important role in the rotation angle ρ. Under the optimal tilt angles (around 20-30° determined from Figure 3.1), both WALP23 and WLP23 have a range (the darker regions pointed by red arrows) of rotation angles that have more favorable ΔW (~5 kcal/mol lower) than other rotation angles. To rotate around the helix axis, WALP23/WLP23 should also overcome several energy barriers (the isolated red regions at tilt ~20-30° in which the ΔW is 5-10 kcal/mol higher than the other rotation angles). In contrast, KALP23 and KLP23 have no difficulty in rotating around the helical axis; the energy differences between different rotation angles are quite small

(<5 kcal/mol). This is understandable: tryptophan prefers anchoring the membrane interfaces and has a quite rigid structure while lysine can rotate freely. However, even for tryptophan flanked peptides, the energy barrier won't exceed 15 kcal/mol. All four peptides could have fast rotation motion around their axes.

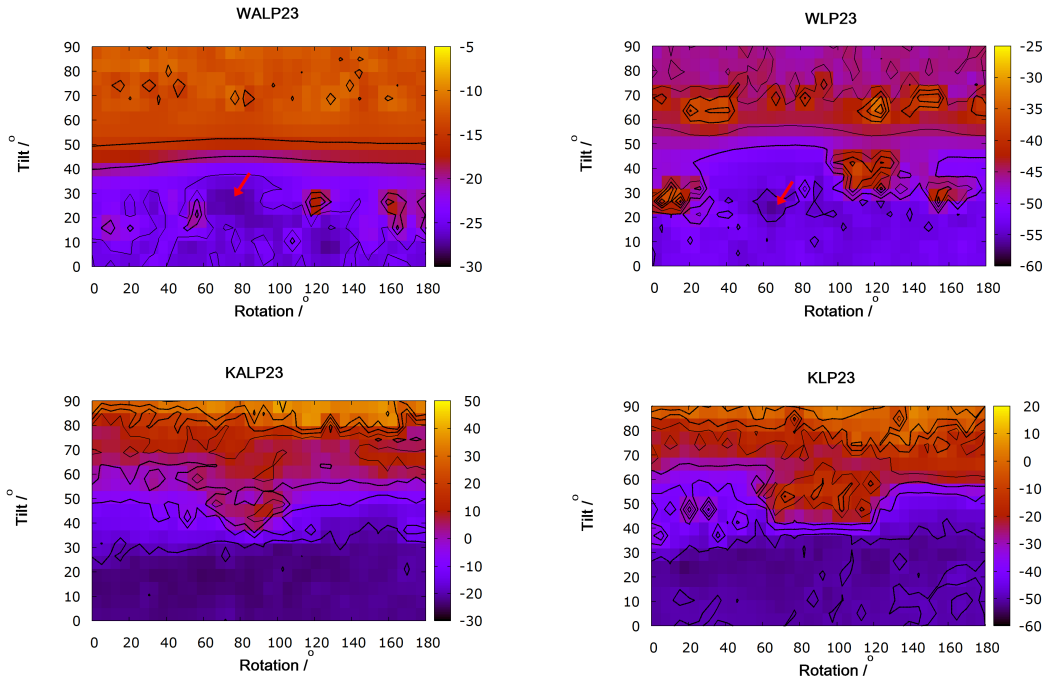

Figure 3.2.: Transfer energy ΔW of peptides at different tilt and rotation angles in DMPC membrane (hydrophobic thickness= 23.5 Å).

3.4. Refinement of peptide orientation using solid state NMR data

The traditional GALA method suffers from two major problems: 1) the peptide structure is assumed to be an ideal helix. 2) the measurement of NMR spectra subjects to molecular motions. MD simulations can be used to obtain structure ensembles from solid state NMR. Similar to the structure refinement using distance information, the angles of several NMR probes can be constrained to the experimental values and MD simulations can be carried out to sample the conformational space until structures with both low potential energy and high agreement with NMR data were found.

We modified the CHARMM source code to incorporate constraints for NMR angles. To test whether the angular constraint can be used to extract overall peptide orientation, we calculated the angles of

several alanine side chains with respect to NMR axis (assumed to be z axis) from a free simulation. Constraining a peptide with the obtained angular information in another simulation, the overall orientation of peptide in the constraint simulation matched with the original simulation (result not shown).

We thus used our method to refine the peptide orientation with the following NMR data shown in Table 3.3. The possible alanine side chain orientations were calculated from the listed quadrupole splitting $|\Delta\gamma_q|$ as stated in the method section and the corresponding alanine residues were constrained in the MD simulations to experimental orientations. Because a $|\Delta\gamma_q|$ value may correspond to four different alanine orientations, we carried out multiple simulations to explore all possible combinations. The structure ensemble with both low energy and rmsd to experimental spectra was filtered from the generated trajectories.

Table 3.3.: List of experimental ^{2}H-NMR quadrupole splittings. An asterisk beside a number means that the value was estimated from neighboring residues.

Peptide	Membrane	$\|\Delta\gamma_q\|$								Source
		Ala 5	Ala 7	Ala 9	Ala 11	Ala 13	Ala 15	Ala 17	Ala 19	
$WALP19-A_x-d4$	DLPC	7.2	3.3	11.3	2.6	14.0	0.0	NA	NA	van der Wel et al. [19]
	DMPC	6.6	7.8	8.7	4.6	12.8	0.0	NA	NA	
	DOPC	4.4	11.4	7.0	6.8	11.9	1.5	NA	NA	
$WALP23-A_x-d4$	DMPC	9.3	1.0*	11.3	2.0*	12.8	1.0*	12.3	2.0	Strandberg et al. [20]

The tilt angle and rotation angle distributions in the result structure ensembles are shown in Figure 3.3. The tilt angles are quite small ($\leq$15 °) and do not follow the trend of hydrophobic mismatch. The rotation angles are not quite restricted to certain value.

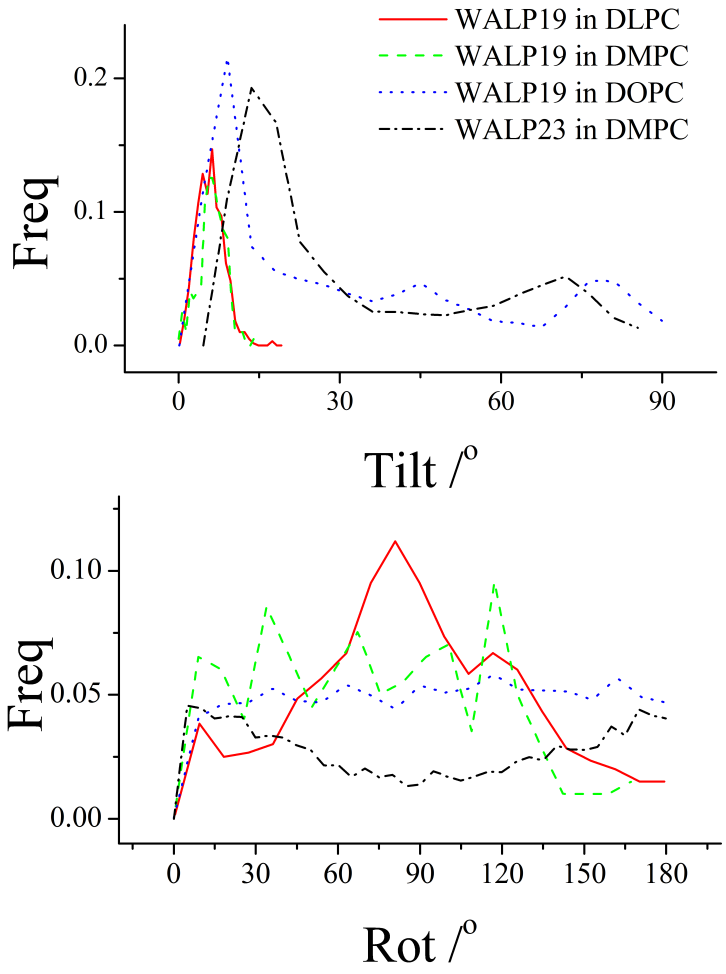

Figure 3.3.: Tilt and rotation angle distributions of WALP19 and WALP23 peptides in the structure ensembles refined with NMR restraints.

In latest studies [42], a similar method was used to incorporate the solid state NMR constraint into the simulation. Similarly, if only one peptide is used in the simulation, the determined tilt angle is small. However, if the system contains several peptides($\geq$32) and assumes the theoretical quadrupole splitting to be an average value of all peptides, the resulting tilt angle is quite close to that of explicit simulations.

In general, the intensity of the NMR spectrum indicates the probability of observing a certain conformation to exhibit certain spectrum shift. The location of the peaks should be only related to the distribution of conformations. If this is the case, simulating one peptide and 32 peptides

won't lead to dramatically different results. However, the molecule can move much faster than NMR spectrum can resolve. The interval of interconversion between different conformation states can be much smaller than the NMR time scale. Thus, we would get an unresolved spectrum which represents the average conformation of an structure ensemble. The quadrupole splitting should be calculated from that average conformation and the NMR spectrum should be a result of distribution of many of these average conformations. This raises a question: is the molecular motion fast enough to confuse the NMR spectroscopy? The retention time of peptide tilt/rotation motion is in the scale of tens of nanoseconds. The time scale of scalar coupling is normally in the range of microseconds. The rapid motion of peptide in liquid membranes will have quite a significant effect on the NMR spectrum. Fortunately, such an effect has been corrected by recent studies assuming the theoretical quadrupole splittings are calculated from a structure ensemble with various tilt and rotation angles[245, 34, 35].

4. Pore formation in anionic membranes

Many membrane active peptides induce pores, either transient or stable ones. Their abilities to induce pores are crucial for their biological actions. Two types of pores can be induced by membrane active peptides: barrel-stave or toroidal. In a barrel-stave pore, the peptides form a bundle that separates the water from the hydrophobic interior of the membrane. In a toroidal pore, the lipids themselves bend and line the pore surface with head groups. Many of the membrane active peptides are highly cationic. Their pore formation abilities should be affected by anionic lipids significantly. However, the effect of anionic lipids on the pore formation is sometimes ambiguous: magainin, a cationic peptide, induces pores in anionic membranes at lower concentration than in zwitterionic ones [203, 204]; melittin, which is even more cationic than magainin, has lower pore formation ability in membranes containing anionic lipids[83, 222, 223, 224, 217].

In this section, a theoretical method to model pores in anionic membrane is provided to explain the lipid preference of magainin and melittin by their transfer energy to anionic pores. In this method, the electrostatic potential is obtained from numerical solutions of the Poisson-Boltzmann equation and used to calculate the electrostatic interaction energy between peptides and membrane in the IMM1 implicit membrane model. A double charge layer model is used to incorporate the effects of the membrane dipole potential. The inhomogeneity of the charge density in the toroidal pores, characterized by explicit membrane simulations, is also included in the model. Using this method, the transfer energy of a peptide to different pores can be calculated. The transfer energy of magainin and melittin to toroidal pores varied with the membrane anionic content, in correlation with their lipid selectivity that had been observed experimentally. This model was also used to determine the stablility of three models of protegrin pores. We found that the NCNC parallel structure is more stable than the other two models proposed by the experiments.

4.1. Method

4.1.1. Geometric modelling

For a planar membrane, any property (dielectric constant, charge density etc.) can be described by a one-dimensional function $f(d)$, in which d is the distance to the membrane surface. To calculate the value of a property at a point $\vec{r}$ adjacent to a curved membrane surface, we can approximate the curved surface by its tangent plane at the point $\vec{r}'$ on the surface closest to $\vec{r}$. Now d becomes the distance between $\vec{r}$ and $\vec{r}'$, i.e. the shortest distance between r and the membrane. Under this approximation, the 3-dimensional function $f(\vec{r})$ can be obtained from the corresponding one-dimensional function $f(d)$ by simply calculating d. This approximation should be perfectly valid for membrane systems, because the membrane properties normally only change dramatically in the membrane interface region where d is small enough. The distance d can be calculated using a fast marching algorithm, or from an analytical solution of $\partial d/\partial(\vec{r}') = 0$ if better accuracy is desirable. The surface of the toroidal pore in our model is defined as the interface between hydrophobic core and polar head groups, given by the equation: $\{\vec{r}:\ g(\vec{r})=0\}$, where g in cylindrical coordinates is:

$$g(r,z) = \begin{cases} r - R_0 - K_0(z/(T/2))^2 & ,r < R_0 + K_0 \\ z - T/2 & ,r \geq R_0 + K_0 \quad and \quad z > 0 \\ z + T/2 & ,r \geq R_0 + K_0 \quad and \quad z < 0 \end{cases} \tag{4.1}$$

For barrel-stave pores, we assume the pore shape to be cylindrical. The head groups are not present on the pore wall and solvent environment transits sharply from hydrophobic core to water; a different method is thus used to model this discontinuity. The distribution function f(d) inside a cylindrical region of the planar membrane is set equal to the value in solution (f(∞)).

4.1.2. Explicit simulations

Explicit simulations were first carried out using NAMD[246] before we modeled the pores in implicit models to determine the charge distribution on the pore surfaces. Using the geometric modeling

method introduced above, geometric restraints were added to NAMD to create and maintain pore shapes in pure lipid membranes using the distance based harmonic and Gaussian restraint functions:

$$Harmonic\ restraint: \quad W(d) = k(d - d_0)^2 \tag{4.2}$$

$$Semi - Harmonic\ restraint(inside): \quad W(d) = \begin{cases} 0 & , \quad d - d_0 \leq 0 \\ k(d - d_0)^2 & , \quad d - d_0 > 0 \end{cases} \tag{4.3}$$

$$Semi - Harmonic\ restraint(outside): \quad W(d) = \begin{cases} k(d - d_0)^2 & , \quad d - d_0 \leq 0 \\ 0 & , \quad d - d_0 > 0 \end{cases} \tag{4.4}$$

$$Gaussian\ restraint: \quad W(d) = k(1 - exp\ (-\frac{(d - d_0)^2}{2})) \tag{4.5}$$

,in which k is the force constant, d is the distance to the membrane surface, and d_0 is the shift of restraint center from the membrane surface. To save computation time, the restraint energy values inside the periodic cell were pre-calculated at the beginning of the simulations. The restraint on each atom in the simulations was looked up from the table based on the location of the atom. The restraint forces were calculated as the first order derivatives of the restraint energy. If the location of an atom does not fall exactly on a grid point, its restraint energy and forces were calculated from tri-linear interpolation of the 8 adjacent grid points.

These restraints were applied to planar bilayers to create a $R_0 = 20$ Å, $K_0 = 20$ Å pore inside the membranes. 100% DMPG and DMPC/DMPG(1:1) mixture planar bilayers were constructed as initial systems using CHARMM-GUI[247] and equilibrated for 1 ns. Both systems were constructed

to have an area of 90 Å × 90 Å, 212 lipids and a lipid/water ratio of 1/36.5. The ion concentration (NaCl) was set to 0.1 M with additional Na^+ counterions added to neutralize the lipid charge. Then the restraints were applied using the following protocol: first, a 1 kcal/mol harmonic restraint was applied to the head groups to push them to the pore surface. At the same time, 0.5 kcal/mol semi-harmonic restraint (inside) to the lipid tails and 2 kcal/mol semi-harmonic restraint (outside) to the waters were also applied to make sure the lipid tails stay inside the membrane and the waters stay outside the membrane (the restraint force constants were empirically chosen). Under such restraints, the membrane systems were simulated for 2 ns. Then the restraints on the lipid tails and waters were removed. The restraint on the head groups was changed into a Gaussian restraint with force constant of 1.0 kcal/mol and correlation length (σ) of 0.5 Å to maintain the pore structure but not overly disturb the head group distribution. The simulations were continued for 20 ns to equilibrate the pore system. The last 1 ns was used to analyze the head group distribution. All simulations above were carried out under the $NP\gamma T$ ensemble using NAMD2.8 and the CHARMM36 force field [248]. Since this new version solved the problem of area per lipid shrinkage during the simulations, surface tension γ was kept at zero to create a tensionless membrane environment.

To calculate the head group distribution, the locations of the head group centers of mass were determined and mapped onto a 3D-lattice (0.5 Å resolution). We then counted the probability of a head group appearing in each grid point during the last 1 ns of the simulations. To get a smoother distribution, Gaussian smoothing was used by assuming that the probability p of a head group appearing at position d Å away from its center of mass is a Gaussian function of d ($p = \frac{exp(-\frac{d^2}{\sigma^2})}{\int exp(-\frac{d^2}{\sigma^2})dd}$). For each grid point on the lattice the contributions from different head groups and frames were summed up and averaged. The standard deviation σ of the Gaussian function was chosen to be 4.548 Å so that the center of mass locates within an area of 65 $\mathring{A}^2$, corresponding to the average area per lipid in membranes.

4.1.3. Electrostatic model for anionic membrane

The dielectric properties of the bilayer are represented by a five-slab model (Figure 4.1). The dielectric constant $\epsilon(d)$ depends on the distance (d) to the surface of the hydrophobic core as

follows:

$$\epsilon(d) = \begin{cases} \epsilon_{memb} & , \quad d < D \\ \epsilon_{head} & , \quad 0 \leq d \leq D \\ \epsilon_{water} & , \quad d > D \end{cases} \tag{4.6}$$

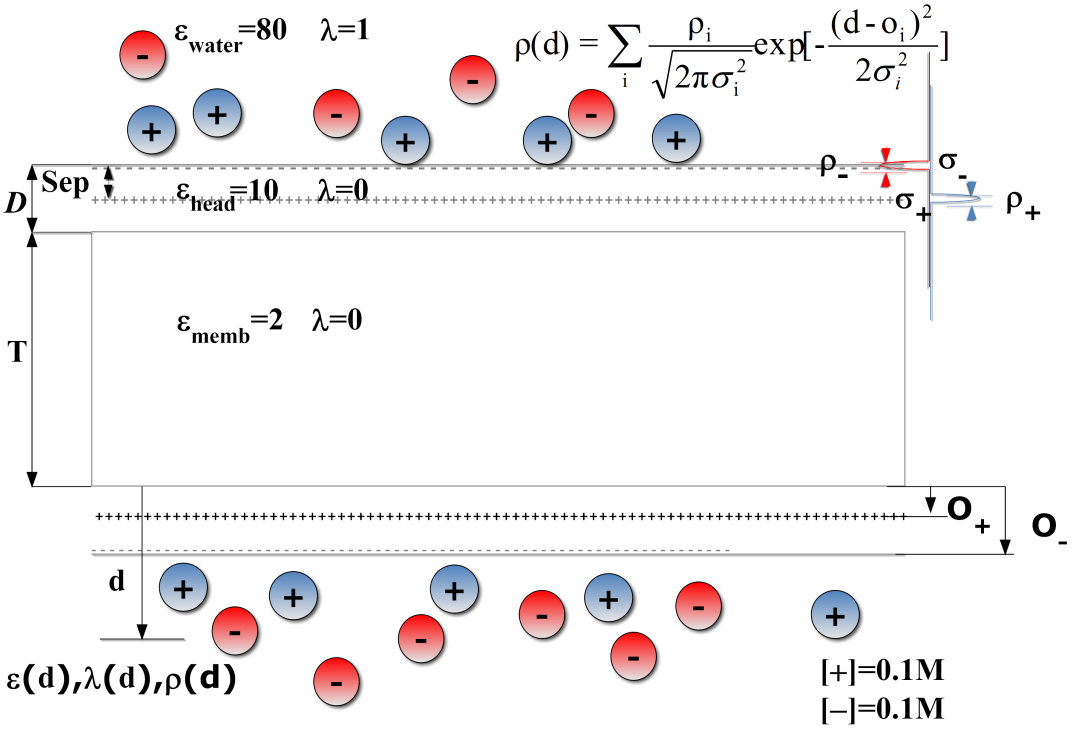

Figure 4.1.: Electrostatic model for Poisson-Boltzmann calculations illustrated for a planar membrane. The dielectric constant ϵ, ion accessibility λ and charge density ρ are defined as a function of the distance to the hydrophobic core surface (d). The charges inside the head group area are considered to be distributed in two layers of charge with opposite sign (represented by + and - respectively). Each charge layer is considered to be distributed in a Gaussian function with density $_+/\ _-$ and width $_+/\ _-$. The negative charge layer is fixed to the location of phosphate groups in PG membranes (solid line, $O_- = h$, where $h = 3\,\mathring{A}$). The separation of the two charge layers is defined as Sep ($Sep = O_- - O_+$).

where ϵ_{memb} is the dielectric constant inside the membrane and has a value of 2. Inside the interfacial region the dielectric constant, ϵ_{head} , is 10 in order to match the theoretical calculations for the region close to carbonyl groups [249, 250, 251, 252]. The width, D, of this region is 3 Å so that

the boundary is around the phosphate group. This would resemble the head group region better than considering the whole head group region dielectric medium: the region above the phosphate groups should have a dielectric constant and ion permeability similar to water [252]. In solution the dielectric constant ϵ_{water} is 80. The ion accessibility factor is defined as:

$$\lambda(d) = \begin{cases} 0 \quad , & d \leq D \\ 1 \quad , & d > D \end{cases} \tag{4.7}$$

so that ions cannot penetrate below the phosphate groups. The ions were assumed to be monovalent and have a radius of 2 Å. Setting the ion accessibility boundary on the membrane surface reproduces better the Gouy-Chapman theory [253].

In order to mimic the membrane dipole potential, we defined two layers of charges as previous work [254]. The charge density of each layer was defined as a Gaussian distribution function:

$$\rho(d) = \sum_i \frac{\rho_i}{\sqrt{2\pi\sigma_i^2}} exp[-\frac{(d-o_i)^2}{2\sigma_i^2}] \tag{4.8}$$

where ρ_i is the charge per area for each charge layer, o_i is the offset of the center of each charge layer from the membrane surface, and σ_i is the Gaussian width. i is + and – for the positive and negative charge layers, respectively. The charge density ρ_+ was set to $+1q/A$ (A is the area per lipid, 68 $\mathring{A}^2$ as for DOPC/DOPG membranes; q is the charge of a proton). ρ_- was set to–$(1 + Z_l * anfr)q/A$ ($anfr$ is the fraction of anionic lipids and Z_l is the net charge of an anionic lipid molecule). The negative charge layer is located on the plane of the phosphate groups ($o_- = h$), consistent with the implementation of the Gouy-Chapman theory in IMM1[239]. The positive charge layer was placed below the negative charge layer ($o_+ = h - Sep$) so as to create a positive dipole potential in the membrane interior. The value of Sep was adjusted to best match experimental data (see Results).

In toroidal pores, the head group density, and thus the charge density, may not be uniform on the curved surface. We considered this effect by introducing an inhomogeneous toroidal pore model. In

this model, the charge density on the pore rim is assumed to be equal to that of the planar membrane (ρ_0), while the charge density per unit area in the pore is assumed to change quadratically with $|z'|$:

$$\rho(z') = \rho_0 * [h + (1 - h) * z'^2] \tag{4.9}$$

The quadratic function is chosen based on the lipid headgroup distributions in Figure 4.2 and Figure 4.3. The homogenenity factor (h) is used to describe the ratio of the charge density in the center of pore wall over the charge density in the pore opening. If $h = 1$, $\rho(z') \equiv \rho_0$; the pore is a homogeneous toroidal pore. Explicit simulations were used to estimate the proper value of h, but the entire range of values was tested to obtain insights into its effect.

4.1.4. Finite Poisson Boltzmann Calculation

The PB equation was solved numerically using a finite element method implemented in the APBS package [243]. The space was discretized into a finite lattice box. Each grid point was assigned a dielectric constant value, ion accessibility factor, and charge density by the distribution functions presented above. Instead of using the value at the grid center, we used the average value in the grid volume for better accuracy. The distribution maps of these values are saved in openDX format, readable by APBS.

All membrane systems studied have dimensions 240Åx240Åx240Å and are centered at the origin of the coordinate system. These membranes are embedded into cubic boxes with edge length 640 Å filled with aqueous ion solution (0.1 M). The boundary potential was set to the Multiple Debye-Hückel boundary conditions. For improved accuracy, focusing was used, i.e. the calculation was successively run in cubic boxes with edges of 480 Å, 240 Å, 120 Å, and 80 Å. For each run, the potential of the previous run was used as the boundary potential. All these boxes were divided into a 161x161x161 grid. The electrostatic potential was finally obtained in a region of 80 Å x 80 Å x 80 Å of the membrane and at a final resolution of 0.5 Å.

Creating these focusing systems and carrying out the PB calculations for a single membrane took

about 20 minutes with a currently available single processor core (i7 2.0 Ghz). A membrane preparation package (mbuild) similar to APBSmem [255] was developed to automate and customize the calculation process.

4.1.5. Implicit Simulations

The IMM1 Gouy-Chapman module in the CHARMM program was modified so that the analytical Gouy-Chapman electrostatic potential (ϕ_{GC}) is replaced by the numerical solution of the Poisson-Boltzmann equation (ϕ_{PB}). Tri-linear interpolation was used to get the ϕ_{PB} value and its derivatives at any given point.

For initial application of the model we chose the well-studied antimicrobial peptides magainin [256] and melittin [207] as model peptides. The peptide structures were obtained from the PDB database[257] (PDB codes: 2mag and 2mlt, respectively). For the simulations of the peptides on planar membranes, the peptide was placed on the membrane surface with its helical axis parallel to the membrane. The peptides were oriented so that the hydrophobic side faces the membrane interior. The peptides were first restrained on the surface using a planar restraint for 5 ns, and then simulated freely for 3 ns. The simulation time is similar to the previous version of IMM1 and 1 ns simulation takes around 1 CPU hour on a single 3.0GHz core.

For pore simulations, we also rotated the peptide so that the hydrophobic residues are facing the pore wall and aligned them with the pore wall (center of mass located at z = 0, $r = R_0$, and the helical axis parallel to membrane normal). The peptides were first restrained inside the pore for 5 ns. This was done using a planar restraint , i.e. the restraint energy is zero if the peptide center of mass is inside the pore ($|z| < T/2$) or a harmonic function of the distance to the membrane surface planes ($|z| - T/2$) with force constant 5 $kcal/\mathring{A}^2$ if the peptide center of mass is outside the pore. An additional 3 ns simulation was then performed without the restraint. If the peptide did not stay inside the pore during the 3ns, the trajectory was discarded and the last 2 ns of the restrained simulation was used for analysis.

All simulations were repeated four times using different initial random velocities. In all simulations, the temperature was kept constant at 298 K and the Verlet integration method was used. The binding energy of the peptides to the membrane was estimated by the effective energy change

(ΔW) upon transferring the peptide from the membrane (W_{memb}) to water (W_{water}), keeping the conformation fixed. The preference of the peptides for pore walls relative to the planar membrane was estimated by the relative binding energy ($\Delta\Delta W_{eff} = \Delta W_{pore} - \Delta W_{planar}$). The last 3 ns of the trajectories were used to calculate the binding energy except for cylindrical pores, for which the last 2 ns of restraint simulations were used. The final values were averaged for the four simulations and the error bars were calculated as the standard deviation of $\Delta\Delta W_{eff}$ among the four simulations.

4.2. Lipid distribution in toroidal pores

For toroidal pores, it is natural to expect that the head group density on the pore surface will be lower than that on the planar membrane because the same numbers of headgroups are now distributed over a larger area. Before constructing our implicit membrane model for pores, we carried out explicit membrane simulations to study the distribution of lipid head groups in toroidal pores restrained at R_0= 20 Å and K_0= 20 Å. These simulations showed a nonuniform head group density. For pores in pure DMPG membranes, the density of lipid head groups in the pore center was determined to be about 60-70% of that at the pore opening (Figure 4.2). This conclusion is also true in DMPC/DMPG mixed membranes, where the head group densities of both DMPC and DMPG in the pore center was around 50-60% of that at the pore opening (Figure 4.3). Lipid demixing was not observed, as the DMPC and DMPG in the pore had almost the same distributions. Similar head group distributions were observed in pores formed in pure DMPC without restraints. However, the pore structures were not stable when the restraints were removed, the pore collapsed with the membrane surface tension $\gamma = 0$ dyn/cm, or enlarged to infinity when $\gamma \geq 26$ dyn/cm (results not shown).

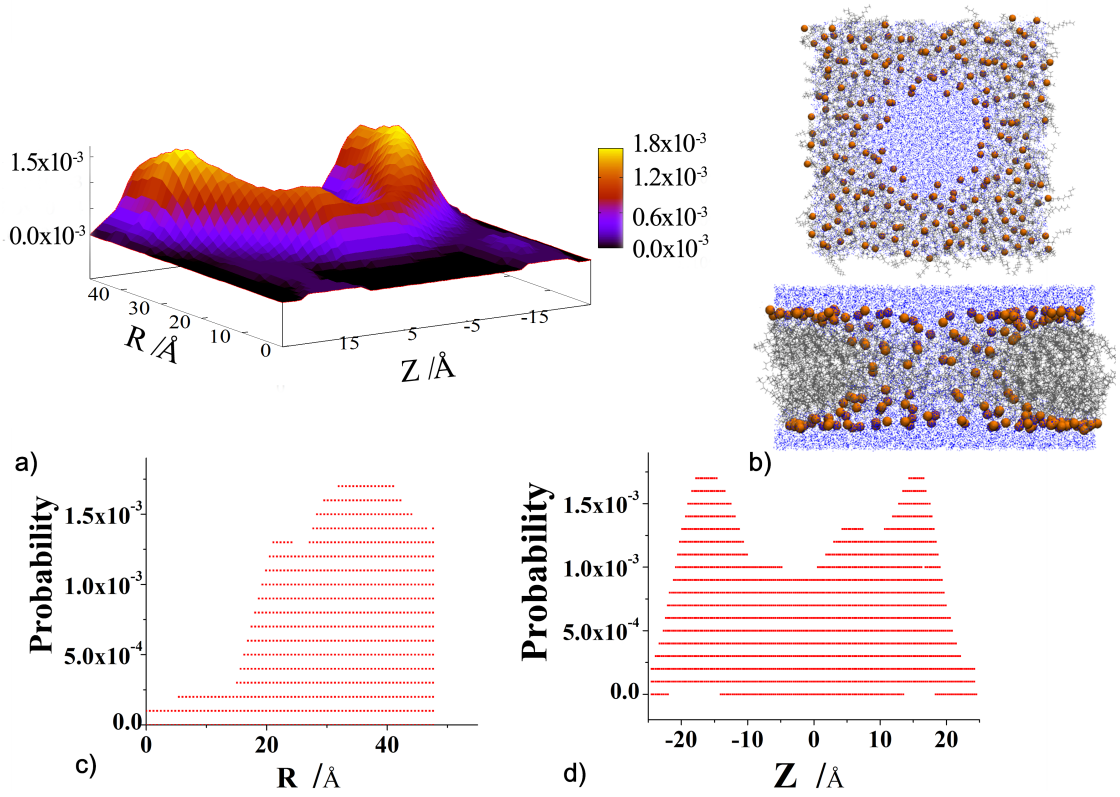

Figure 4.2.: Distribution of DMPG head groups in a toroidal pore. The pore shape is constrained to be $R_0 = 20$ Å, and $K_0 = 20$ Å. a) DMPG head group distribution in the radial (R) and axial (Z) direction. b) Top and side views of the membrane, in which the orange balls represent the DMPG head groups, the blue dots represent the water molecules and the grey lines represent the lipid tails. c) Figure a) viewed from the axial direction (Z). d) Figure a) viewed from the radial direction(R).

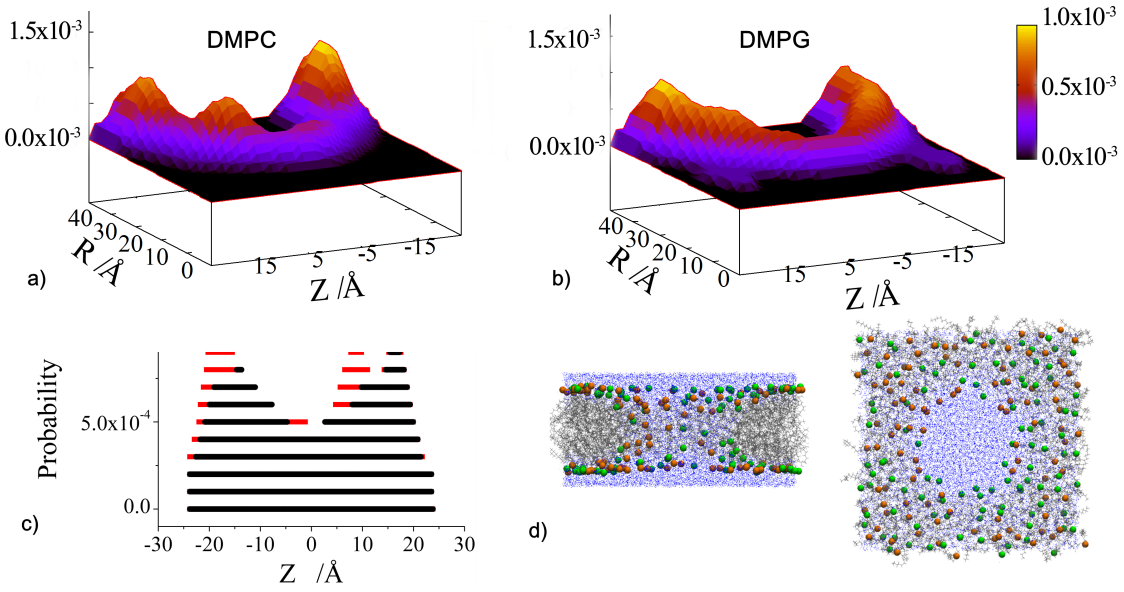

Figure 4.3.: Distribution of DMPG/DMPC head groups in a (1:1) mixed toroidal pore after 20 ns simulation. The pore shape is constrained to be $R_0 = 20$ Å, and $K_0 = 20$ Å. a) DMPC head group distribution. b) DMPG head group distribution. c) Figures a&b viewed both from the radial direction (R), in which red represents DMPC and black represents DMPG. d) side and top views of the membrane, in which the orange balls represent the DMPG head groups, green balls represent the DMPC head groups, the blue dots represent the water molecules and the grey lines represent the lipid tails.

4.3. Calculating Electrostatic potential in membrane

4.3.1. Calculating Electrostatic potential in planar membrane

We first tested the electrostatic model described in subsection 4.1.3 on planar membranes. In symmetric anionic membranes, the electrostatic potential has two major components: a positive dipole potential (ϕ_{DP}) inside the membrane and a negative surface potential (ϕ_S) outside of it. Figure 4.4a shows the dependence of the potential across the membrane on the separation between the two charge planes for a 100% anionic membrane. The surface potential calculated from the present model agrees with the one calculated using the Gouy-Chapman theory and does not depend on the value of *Sep*. Figure 4.4b shows that the surface potential is only affected by the membrane

excess charge, following an exponential relationship with the anionic lipid fraction. For lower values of the anionic lipid fraction, the calculated surface potential is still in good agreement with the Gouy-Chapman theory (deviation less than 1%, data not shown).

By changing the separation (*Sep*) between the charge layers, we can adjust the strength of the head group dipole and, consequently, the dipole potential in the membrane interior (Figure 4.4a). When *Sep* is equal to or larger than 1.0 Å the potential inside the membrane is positive. As can be observed in Figure 4.4b, the excess negative charge due to the presence of anionic lipids makes the dipole potential lower than in zwitterionic membranes.

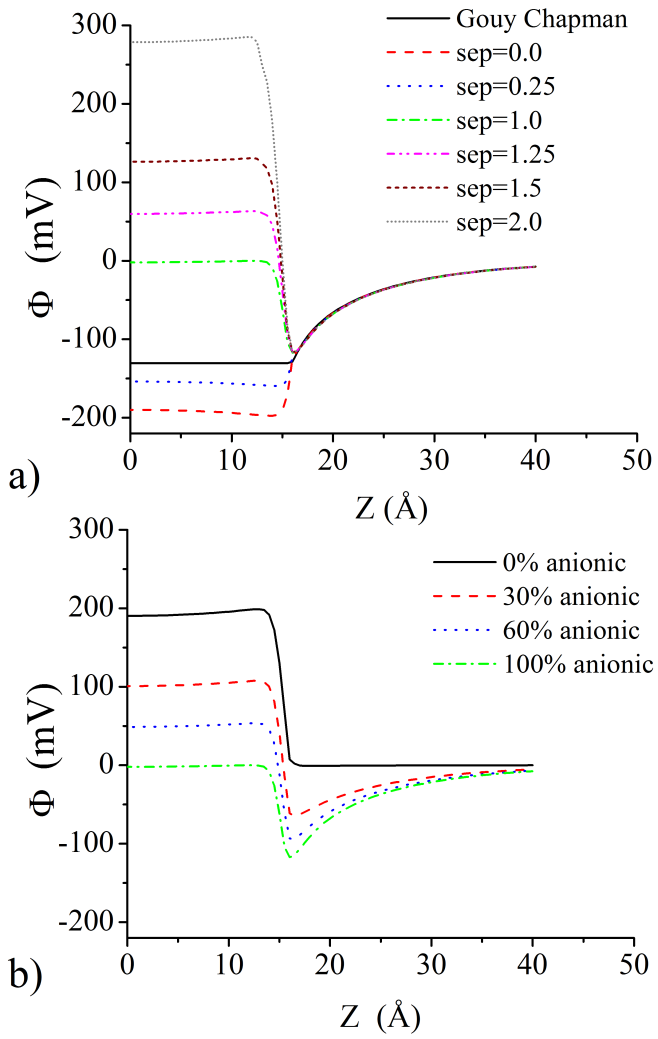

Figure 4.4.: Electrostatic potential across planar membranes. The center of the membrane is at Z = 0 Å. Only one of the symmetric sides of the membrane is shown. The boundary between the hydrophobic core and the head group area is at Z = 13 Å and the negative charge plane is at Z = 16 Å. a) Electrostatic potential for a 100% anionic membrane with different Sep values. The black line shows the potential calculated using the Gouy-Chapman theory (IMM1-GC), the potential inside the membrane in this case is set as a constant value equal to the surface potential. b) Electrostatic potential with Sep = 1.0 Å at different anionic fractions.

In the present model, the dipole potential of a 100% zwitterionic membrane is between 190-320 mV when the charge layer separation is between 1.0 and 1.5 Å. The dipole potential of a 100% anionic membrane is 191 mV lower. The true values of the dipole potential have not yet been unequivocally determined. Measurements of the transfer rate of hydrophobic ions have inferred the dipole potential of PC bilayers to be around 200-300 mV [258, 259, 260]. The value measured for a PC monolayer is about 400-500 mV [261, 262]. The values calculated from molecular dynamics

simulations of explicit lipids vary from 500 to 1000 mV depending on the hydration level and force field used [263, 264, 265, 266, 267]. Knowledge about the dipole potential inside anionic and mixed membranes is even more scarce: anionic lipids are suggested either to reduce [262] or increase [268, 269] the dipole potential of the membrane. The dipole potential values obtained with our model for zwitterionic membranes using Sep = 1.0-1.5 Å are close to the dipole potential established for PC bilayers using hydrophobic ions. The dipole potential difference between 100% zwitterionic and 100% anionic membranes is similar to the difference between PG and PC monolayers [262].

4.3.2. Calculating Electrostatic potential in membrane pores

We studied two possible types of pores induced by antimicrobial peptides: cylindrical (hydrophobic, pore lining consisting of acyl chains) and toroidal (hydrophilic, pore lining consisting of lipid head groups). Both pores were built using the models shown in Figure 4.1, as described in Methods. Figure 4.5 shows an example of the electrostatic potential distribution in a cylindrical and a toroidal pore in a 100% anionic membrane. Both pores shown have radius 13 Å and the toroidal pore has a curvature factor K_0 = 10 Å. The electrostatic potential had a similar distribution for larger pore radii and curvature factors. In a 100% zwitterionic membrane the potential distribution is qualitatively similar but the magnitude and gradient of the potential are lower outside the membrane and higher in the membrane interior.

As can be observed in the electrostatic potential map of Figure 4.5a, both the absolute value and the gradient of the potential on the wall of the cylindrical pore are very low (in absolute value) compared to those on the membrane surface. The potential inside the pore is also very low in absolute value and is hardly affected by the positive dipole potential (Figure 4.6). This indicates that the dipole potential should not have a large effect on the transportation rate of ions and peptide binding in this type of pores.

The electrostatic potential map of the homogeneous toroidal pore of Figure 4.5b shows that the potential distribution is similar to that of a planar membrane. In comparison to the cylindrical pore, the potential inside the pore is more negative due to the contribution of the charges on the interior of the pore surface. Also, the potential in the membrane interior near the toroidal pore is not uniformly distributed. However, the gradient is small compared to the head group region and

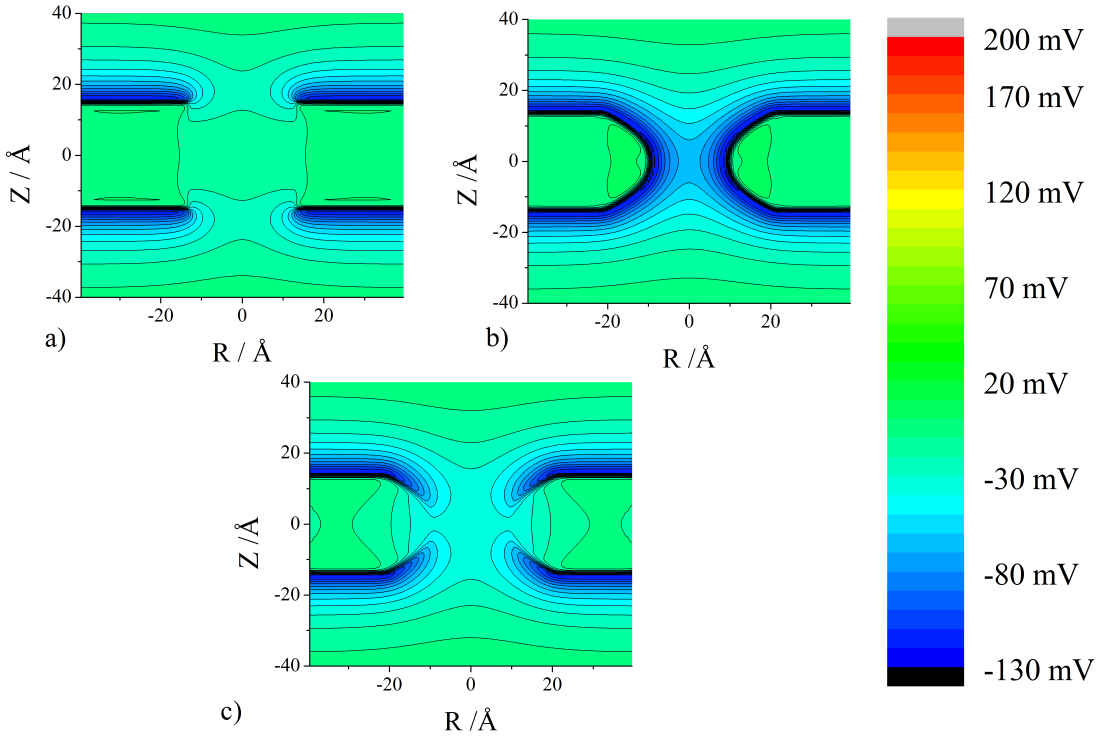

Figure 4.5.: Distribution of the electrostatic potential in pores in 100% anionic DOPG membranes (Sep = 1.0 Å) in the radial (R) and axial (Z) direction. a) Cylindrical pore with radius $R_0 = 13$ Å. b) Toroidal pore with $R_0 = 13$ Å and $K_0 = 10$ Å and $h = 1.0$. c) Toroidal pore with $R_0 = 13$ Å and $K_0 = 10$ Å and $h = 0.0$.

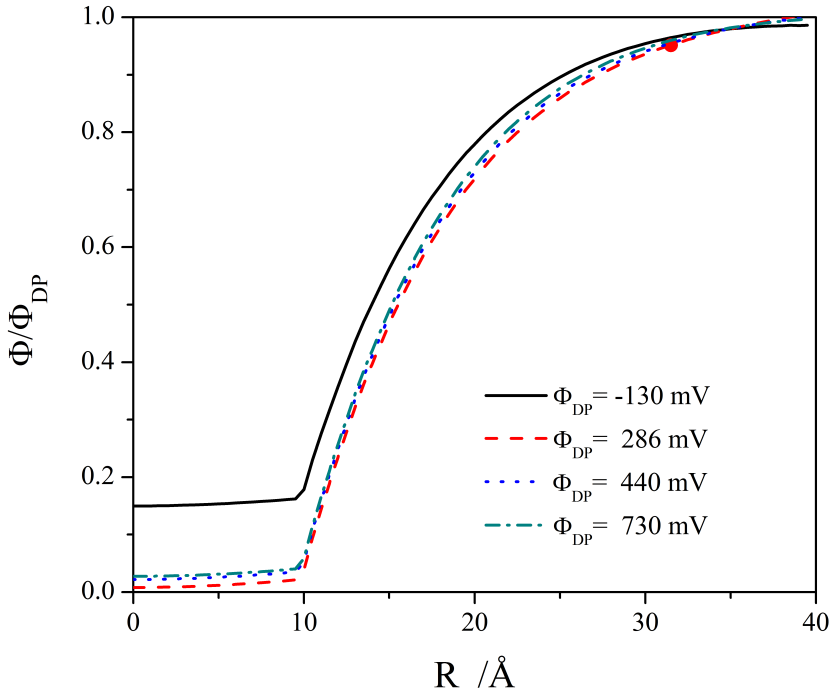

Figure 4.6.: Electrostatic potential ϕ at the membrane center (z = 0 Å) of a cylindrical pore with radius 10 Å, normalized by the dipole potential of the planar membrane region (ϕ_{DP}).

thus should not have a large effect on peptide binding.

We also considered the case of an inhomogeneous toroidal pore, where the charge density is not uniformly distributed on the pore surface. In the extreme case, when $h = 0$, the pore center has no head groups at all. Shown in Figure 4.5c, the electrostatic potential is relatively higher in the pore center than for the homogeneous toroidal pore, while the potential gradient is significantly lower. The potential distribution thus can be viewed as an intermediate between that of a homogeneous toroidal pore and that of a cylindrical pore.

4.4. Peptide Binding to Anionic Membrane

4.4.1. Binding of peptide to planar membrane

We ran simulations of magainin and melittin bound to planar membranes with varying head group dipole strength and anionic lipid fractions. The initial secondary structures were maintained in all simulations. Only in membranes with extremely high head group dipole strength did we observe significant conformational changes in some simulations.

Figure 4.7 shows the dependence of the binding energy on anionic lipid content. In all cases the binding energy followed a linear relationship with the membrane surface potential, as expected from the relationship between binding energy and surface potential ($E = q * \phi$). The results obtained for magainin using two Sep values (1.0 and 1.5) are compared in Figure 4.7 to the results of fluorescence measurements of the peptide partition coefficient [204]. It can be observed that the slope of the correlation obtained with Sep=1.0 Å agrees better with the experimental value than the one obtained with Sep=1.5 Å. The agreement with experiment is better than that of our previous model based on the Gouy-Chapman theory[239]. Furthermore, the binding energy values are of the same order as the experimental ones and those given by the Gouy-Chapman theory.

Magainin and melittin have a net charge of +4 and +6, respectively. When Sep = 1.0 Å, the effective charges of the peptides, calculated from the slope of the fitted line in Figure 4.7, are +2.3 and +4.5, respectively (+1.2 and +3.8, when Sep = 1.5 Å). The difference between the effective and the net charge can be explained by the inhomogeneous electric environment of the membrane. For

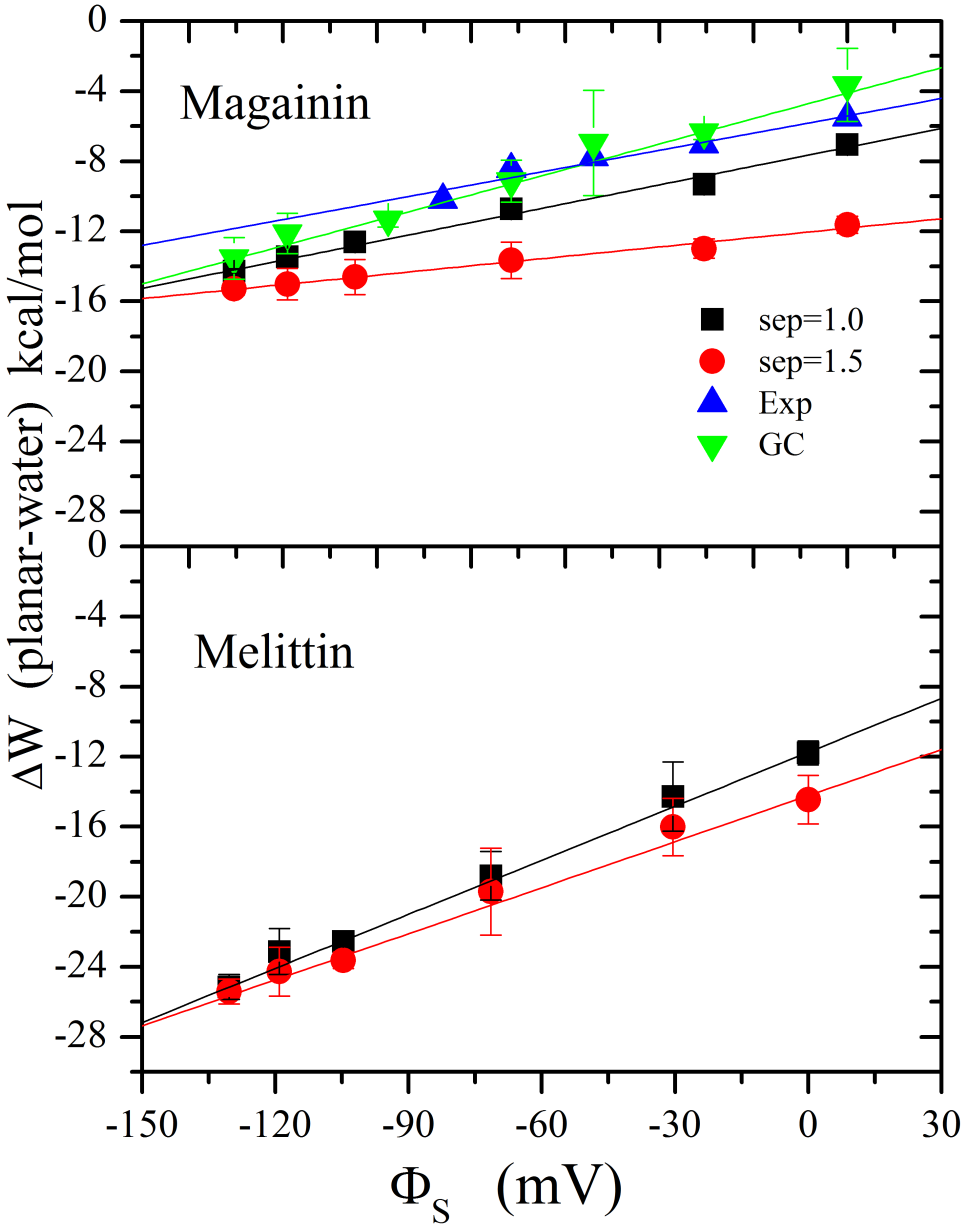

Figure 4.7.: Binding energy of peptides to planar membranes with different surface potential ϕ_S (Z = 16 Å). The experimental values for magainin are calculated from dissociation constants. Results obtained with the Gouy-Chapman theory (IMM1-GC[239]) are also included for comparison.

magainin, the effective charge calculated from fluorescence measurements of the partition coefficient [204] is +2.1. This good correlation further supports the selection of Sep = 1.0 Å .This value was thus used for the rest of this study.

4.4.2. Binding of peptide to cylindrical pores

After validation of the model on planar membranes, we ran simulations of the same peptides bound to the walls of cylindrical pores. Two hydrophobic membrane thicknesses were tested: one close to that of DMPC/DMPG membranes (23.5 Å) [270] and one close to that of DOPC/DOPG membranes (26 Å) [270, 271]. The pore radius is assumed to be half of the membrane thickness. This is done because the width of the water-membrane transition region in IMM1 depends on the thickness of the membrane or the radius of the pore and membrane binding affinity is affected somewhat by this width.

The transfer energy ($\Delta\Delta W$) reflects the intrinsic propensity of the peptide to form pores (cooperative effects are considered in Discussion). Figure 4.8a shows the transfer energies ($\Delta\Delta W_{eff}$) of magainin and melittin from the planar membrane surface to the cylindrical pore wall. Transfer of both peptides is favorable only in zwitterionic membranes. For magainin the transfer energy is more favorable in DMPC than DOPC pores, while the opposite is observed for melittin. This is likely due to the fact that the hydrophobic length of the two peptides matches better the thickness of the corresponding membrane. For both peptides, the $\Delta\Delta W_{eff}$ increases with the anionic lipid fraction in the membranes. This is largely due to the increasingly unfavorable electrostatic interaction energy $\Delta\Delta W_{PB}$ (Figure 4.8b). This is understandable: as membrane charge increases, the cationic residues of magainin and melittin increasingly prefer the charged membrane surface instead of the neutral cylindrical pore wall.

Two representative conformations of magainin and melittin in zwitterionic cylindrical pores are shown in Figure 4.8c and d, respectively. Both magainin and melittin are long enough to align with the pore wall quite well, but a slight tilt of the peptides was always observed. The tilt angle could result from the fact that the hydrophobic residues on both peptides do not align perfectly in a straight line.

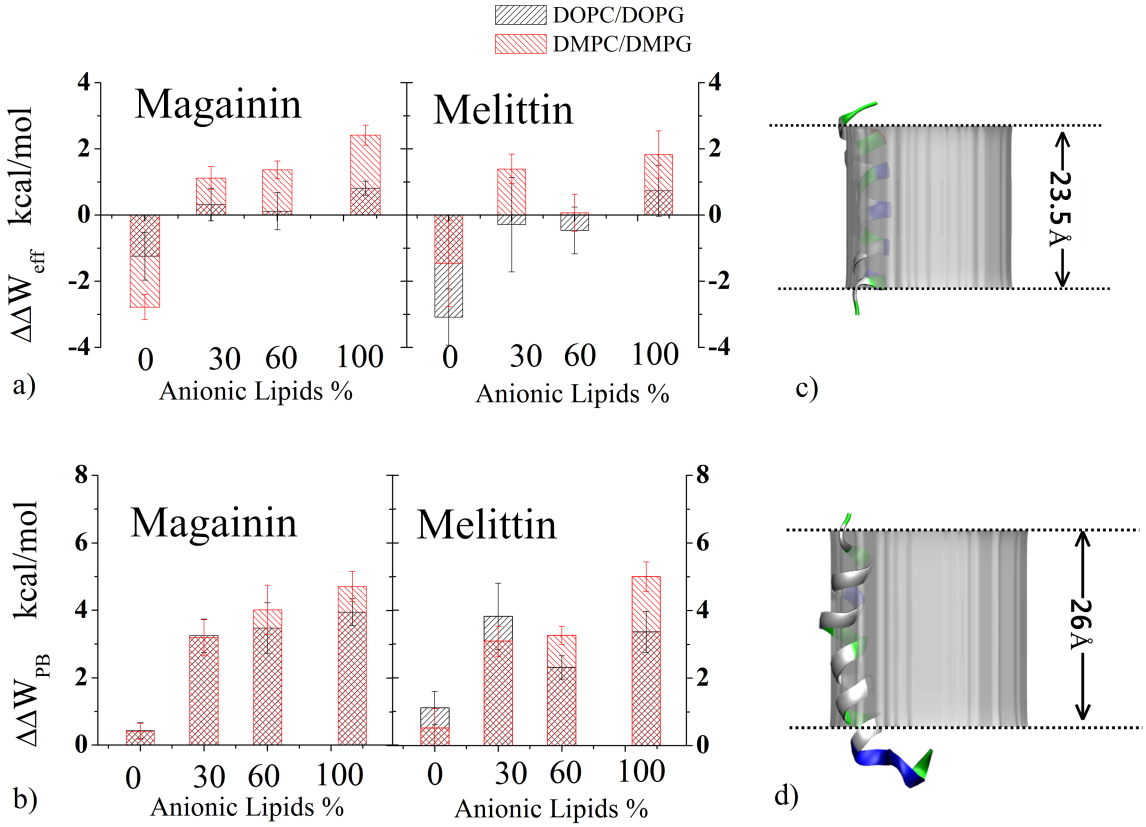

Figure 4.8.: Binding of magainin and melittin to cylindrical pores. Black bars: thicker membranes mimicking DOPC/DOPG. Red bars: thinner membranes mimicking DMPC/DMPG. a) Transfer energy of magainin and melittin from planar membrane to cylindrical pore calculated from the restrained simulations. b) Electrostatic interaction energy difference of magainin and melittin from planar membrane to cylindrical pore calculated from the restrained simulations. c) Lowest energy conformation of magainin when bound to a cylindrical pore with radius $R_0 = 11.75$ Å in DMPC membrane (T = 23.5 Å). d) Lowest energy conformation of melittin when bound to a cylindrical pore with radius $R_0 = 13$ Å in DOPC membrane (T = 26 Å). Colors on the peptides: red, negatively charged residues; blue, positively charged residues; green, neutral polar residues; white, nonpolar residues.

4.4.3. Binding of peptide to toroidal pores

The transfer energy of both peptides from flat membrane to toroidal pores was always found to be negative. The dependence of the transfer energy on the curvature factor of the pore did not exhibit a clear trend. Below, we focus on the data in pores with $K_0 = 15$ Å because they connect more smoothly with the planar membranes surrounding the pores than pores with $K_0 = 10$ Å but have lower curvature at the pore center compared to pores with $K_0 = 20$ Å.

Since there is no need for the peptide to span the full length of the toroidal pore surface, it is natural to expect that peptide binding to toroidal pores should be insensitive to membrane thickness. Indeed, the preference for the thinner membrane was no longer observed for magainin in toroidal pores: the binding energy of peptides to toroidal pores is not correlated with membrane thickness. However, melittin binds more favorably to pores in the thicker membranes (hydrophobic thickness 26 Å).

In toroidal pores, the transfer energies of magainin and melittin showed a different pattern of dependence on anionic lipid content and h factor (Figure 4.9). In pores with $h \leq 0.6$ the transfer energy of magainin decreases with anionic content while that of melittin increases. At $h = 0.6$ the dependence of both peptides on anionic content is small and for $h = 1.0$ the transfer of both peptides becomes less favorable as anionic content increases. It is also observed that for both peptides $\Delta\Delta W_{eff}$ decreases when h increases in zwitterionic membranes (0% anionic). In 100% anionic membranes this trend diminishes for magainin but is maintained for melittin.

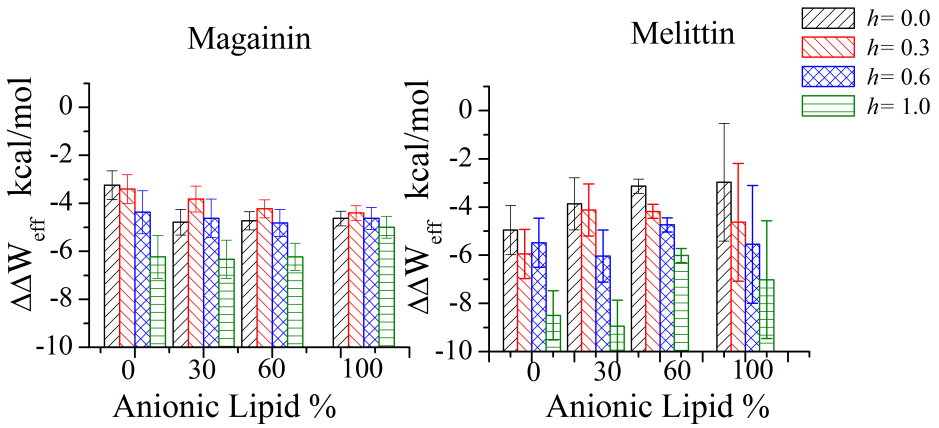

Figure 4.9.: The transfer energy ($\Delta\Delta W_{eff}$) from planar membranes to toroidal pores with different anionic lipid fractions and inhomogeneous factors (h). The pore radius R_0 is 13 Å and the curvature factor K_0 is 15 Å. a) $\Delta\Delta W_{eff}$ for magainin. b) $\Delta\Delta W_{eff}$ for melittin.

Insights into the origin of these trends are obtained by Figure 4.10 and Figure 4.11, which provide the lowest energy configurations of the two peptides at different conditions. In zwitterionic membranes ($anfr = 0$), both peptides locate closer to the center of the pore as h increases, accompanied by a more favorable transfer energy. This is due to favorable interactions of the peptides with the double charge layer of the model (mimicking the lipid headgroups). When the headgroup density is low at the pore center, the peptides stay close to the rim and the transfer energy is smaller. In 100% anionic membranes, as h increases, magainin remains on the membrane surface but its orientation flips. This flip, which is observed at all anionic fractions between $h = 0.3$ and 0.6, may be the reason that the transfer energy does not change much with h at high anionic fraction. Melittin on the other hand, changes configuration dramatically as h increases. It inserts into the hydrophobic core at low h (which incurs a desolvation cost of the Thr residues) and is on the membrane surface at high h. This is likely the cause of the decrease in transfer energy as h increases in the fully anionic membranes. Examining now Figure 4.10 and Figure 4.11 horizontally, in pores with $h \leq 0.3$ the behavior of the two peptides is very different as anionic fraction increases. Magainin stays on the membrane surface but locates deeper in the pore as anionic fraction increases. Melittin on the other hand, driven by the strong interactions of the charged residues near the termini with the membrane surface charge, straddles the pore and inserts its neutral middle segment into the membrane hydrophobic core, and thus the transfer energy becomes less favorable. In pores with $h = 1.0$, the transfer energy of both peptides increases with anionic fraction as the energy on the

flat membrane decreases more rapidly than that in the pore.

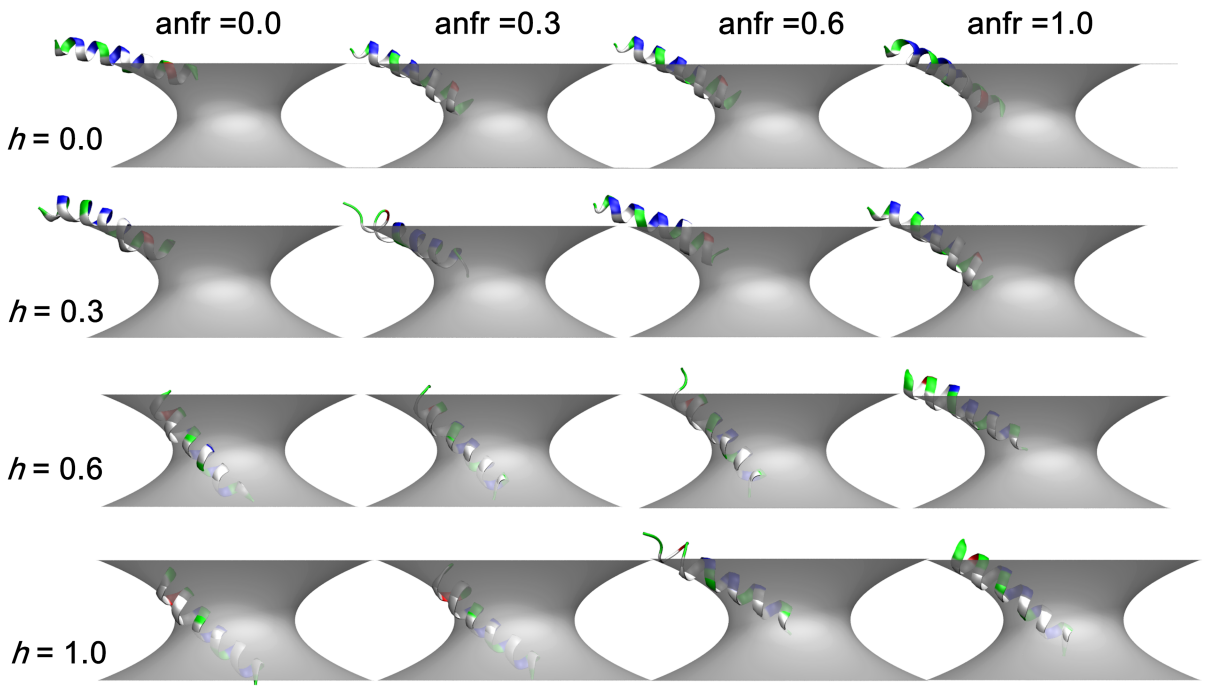

Figure 4.10.: Lowest energy conformations of magainin in toroidal pores with different anionic lipid fractions (anfr) and inhomogeneous factors (h). The pore radius R_0 is 13 Å and the curvature factor K_0 is 15 Å. Colors on the peptides: red, negatively charged residues; blue, positively charged residues; green, neutral polar residues; white, nonpolar residues.

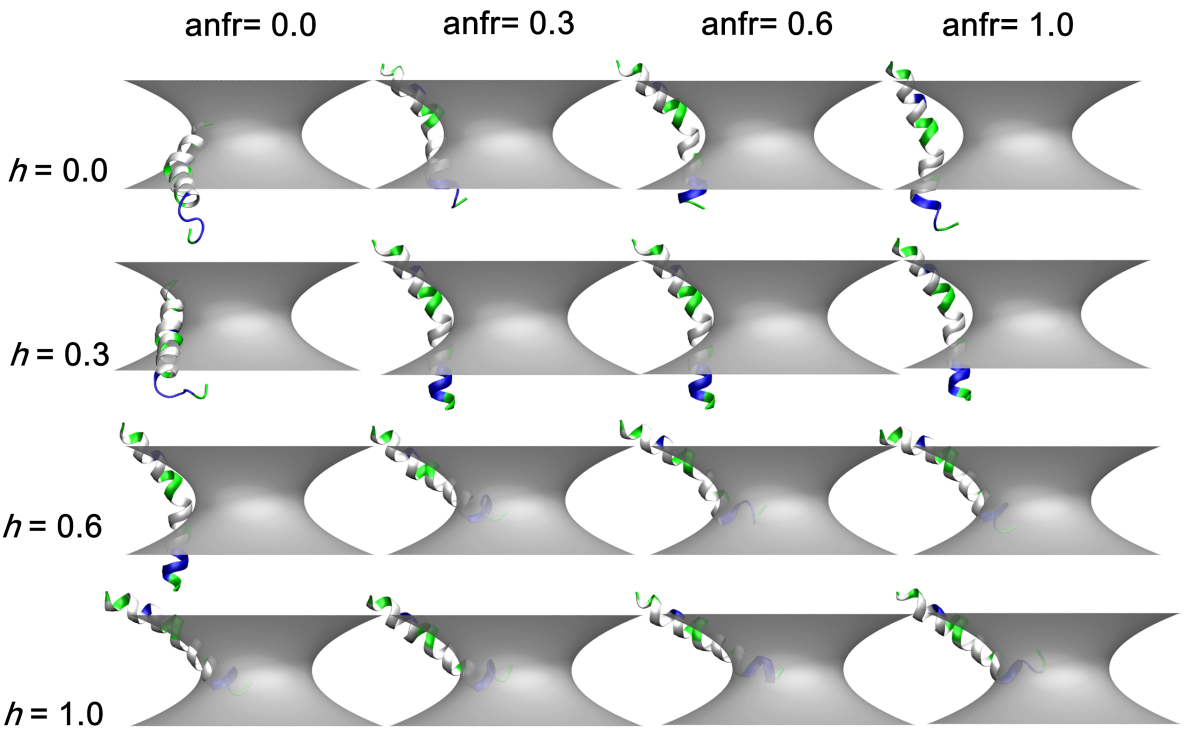

Figure 4.11.: Lowest energy conformations of melittin in toroidal pores with different anionic lipid fractions (anfr) and inhomogeneous factors (h). The pore radius R_0 is 13 Å and the curvature factor K_0 is 15 Å. Colors on the peptides: red, negatively charged residues; blue, positively charged residues; green, neutral polar residues; white, nonpolar residues.

4.5. Binding of protegrin octamers to anionic membrane pores

Protegrin has been suggested to form NCCN parallel dimers in membranes[272]. Such structure is unlikely to be energetically optimal because the hydrophobic faces of the two monomers are pointing to different directions. However, many proposed protegrin pore structures rely on assemblies of NCCN dimers [230, 232]. We constructed three different models for protegrin octameric pores and tested their transfer energy and stability in the implicit membrane model.

Shown in Table 4.1, out of the three models, NCNC)par barrel has the most favorable effective energy (<W>) and transfer energy to pre-formed lipidic pores (<ΔW>). The effective energy and transfer energy of NCCN)par is significantly lower than NCCN)anti and NCNC)par. Assuming the line tension is 7 pN[273], the formation energy of a pore with radius R_0= 15 Å is

9.5 kcal/mol ($2\pi R_0\gamma$). Formation of octameric pores in neutral membranes is energetic favorable for both NCCN)anti and NCNC)par models, providing a possible explanation for the toxicity of protegrin.

Table 4.1.: Average effective energies and transfer energies (kcal/mol) from water to the pore of octameric barrels in toroidal pores from 5-ns simulations.

		K_0 = 10 Å	K_0 = 15 Å	K_0 = 20 Å
Neutral membrane				
NCCN)par	<W>	-3311±19	-3335±10	-3364±13
	<ΔW>	+10.9±1.0	+11.2±0.3	+10.9±0.6
NCCN)anti	<W>	-3366±10	-3378±4	-3374±11
	<ΔW>	-5.8±0.5	-10.3±0.9	-12.8±0.6
NCNC)par	<W>	-3388±11	-3393±7	-3395±8
	<ΔW>	-19.1±0.7	-19.3±1.0	-20.4±0.2
30% Anionic membrane				
NCCN)par	<W>	-3568±11	-3563±6	-3579±15
	<ΔW>	-37.6±1.4	-39.5±4.1	-37.7±4.0
NCCN)anti	<W>	-3598±3	-3592±7	-3590±5
	<ΔW>	-61.1±1.1	-59.9±3.3	-58.8±2.8
NCNC)par	<W>	-3625±8	-3616±8	-3613±8
	<ΔW>	-72.5±0.8	-69.0±0.4	-66.6±1.0

Correspondingly, shown in Figure 4.12, the NCCN)par barrel quickly collapsed to a two-layer β-sheet in the simulations. Both NCCN)anti and NCNC)par are stable in the simulations. Our finding suggested that the NCCN)par dimer observed in solid state NMR[272] is not favorable in pores; instead the NCNC)par structure is most favorable. Interestingly, the NCCN)par was found to be more stable in aqueous solution [274], consistent with the energy calculated from IMM1 (not shown). The observed NCCN)par structure might exist primarily in the water layer interacting with the two lipid bilayers at the same time.

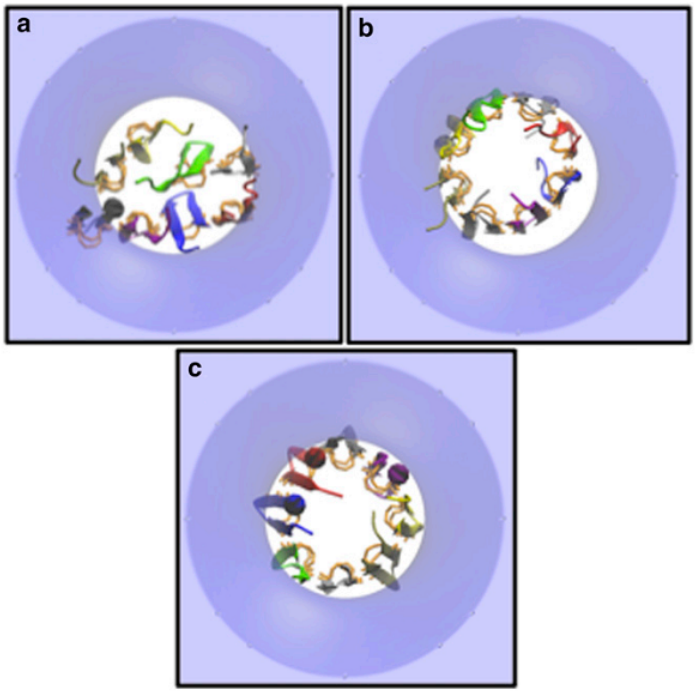

Figure 4.12.: Top views of the lowest-energy conformation of protegrin octamer models in 30% anionic toroidal pores of $R_0 = 15$ Å, $K_0 = 15$ Å . (a) NCCN)par. (b) NCCN)anti. (c) NCNC)par. The latter has the lowest effective energy and the most favorable transfer energy to the membrane. The disulfide bonds are highlighted by orange licorice.

5. Linking biological activity with biophysical parameters

Antimicrobial peptides have many advantages over conventional antibiotics, which make them excellent targets for drug design. They can selectively kill bacteria, being relatively benign to eukaryotic cells. Their selectivity is assumed to be a result of their different affinity for bacterial and eukaryotic cell membranes. In this section, MD simulations with an implicit membrane model are used to study the binding of these peptides to planar membranes or pores. The theoretical transfer energies calculated from the implicit membrane model are compared with the binding free energies collected from experiments. Even though the transfer energy could not completely reproduce the binding free energy, a linear relationship was observed between them.

Using the information obtained from the implicit membrane simulations, we tried to verify: 1) whether the selectivity of the peptides can be explained by their different affinties to membranes with different anionic lipid content. 2) whether their binding affinities to planar membrane surfaces constitute the dominant factor for their biological activities. If not, what other factors would affect their biological activities. 3) whether the "carpet" model represents an upper limit for the activities of antimicrobial peptides. 4) whether pore formation activity would enhance the activity of these peptides. Finally, we tried to establish a quantitative relationship between physical properties of the peptides and their activities against different organisms.

We observed that: 1) the hemolytic and antibacterial activities correlate differently with the anionic lipid content of the membranes: hemolytic activity correlates best with 10% anionic membrane and antibacterial activity correlates best with $\geq$30% anionic membrane. 2) Although the correlations between biological activities and binding affinity to corresponding membranes are statistically sig-

nificant, they are not extremely high. Other physical factors, such as surface area occupation, insertion depth, and structural fluctuation, may also significantly affect the biological activities. 3) The membrane surface coverage by many peptides at the MIC is estimated to be much lower than what would be required by the "carpet" mechanism. Those peptides that are active at low surface coverage tend to be those identified in the literature as pore-forming. 4) The transfer energy from planar membrane to cylindrical and toroidal pores was also calculated for these peptides. The transfer energy to toroidal pores is negative in almost all cases while that to cylindrical pores is more favorable in neutral than in anionic membranes. The transfer energy to pores correlates with the deviation from the prediction of the carpet model. Quantitative Structure-Activity Relationships can also be established using the crucial physical properties.

5.1. Method

5.1.1. Implicit simulation of antimicrobial peptides.

MD simulations of AMPs were conducted in planar membranes with anionic lipid fraction ranging from 0% to 100% in physiological salt solutions (0.1 M monovalent salt), using the membrane model presented in the Methodology. The structures of the studied peptides were obtained from the PDB database. For NMR structures (most common) the lowest energy model for each peptide was selected and energy minimized using the steepest descent method for 300 steps. The peptides were placed on the membrane surface with their long axis parallel to the surface and rotated with the nonpolar residues facing the membrane. Four simulations with different random initial velocities were carried out. Each simulation consisted of 2 ns equilibration followed by 2 ns production. The latter was used for analysis. To calculate the Δ<W>, we simulated the peptide for 100 ns and used the last 50 ns for analysis. All simulations were carried out using the CHARMM program [275].

AMPs were also simulated inside cylindrical and toroidal pores using the standard IMM1 model for neutral pores [242] and the numerical Poisson-Boltzmann approach for anionic pores [276]. All pores have a radius of R_0 = 13 Å. The toroidal pores have K_0= 15 Å and h=0.6. Two anionic fractions were studied: 10% and 30%. The peptides were placed adjacent to the pore wall with their long axis parallel to the pore axis and their nonpolar residues facing the pore wall. Four

simulations with different random initial velocities were carried out. Each simulation consisted of 3 ns equilibration followed by 3 ns production. The latter was used for analysis. The transfer energy to the pores, $\Delta\Delta$W, was calculated as the difference between the ΔW to the pore and the ΔW to the planar membrane. To be consistent with the pore simulations, the ΔW to planar membrane was calculated using the Poisson-Boltzmann potential [276] instead of the Gouy-Chapman theory.

5.1.2. Calculating physical properties from MD simulation

A list of the physical descriptors considered is shown in Table 5.3. The first five are standard descriptors that can be obtained from the sequence.The overall hydrophobicity (H), hydrophobic dipole moment (μ_H) and hydrophobic quadrupole moment (Q_H) of the peptides were calculated using the method and the consensus scale introduced by Eisenberg[116]. The original PDB structures were used to calculate these values. The net charge (n_{charge}) was calculated as sum of the charges of all ionizable groups at pH 7.

Additional descriptors were obtained from the MD simulations. The binding energy of the peptides to the membrane was estimated by the average effective energy change ($\Delta W_{w\rightarrow m}$) upon transferring the peptide from the membrane surface (W_{memb}) to water (W_{water}), with conformation fixed. The immersed volume V was calculated by constructing a grid lattice around the peptide and counting the number of grids (0.1 Å) that are occupied by peptide atoms and at the same time are inside the membrane (z< T/2) . The occupied area A_S was calculated as the volume of peptide inside a 1 Å slab centered at the membrane surface (z = T/2) divided by the slab thickness.

The tilt angle of the peptide was calculated as the angle between the principal axis of the peptide and the membrane normal (z axis). The insertion depth was calculated as the distance of the lowest residue of the peptide to the membrane surface. It is a negative value when the peptide has parts that are buried inside the membrane. The helix percentage was calculated using DSSP [277]. The electric dipole of the peptide was calculated using the coor dipole command of CHARMM. Because the charged residues are neutralized in EEF1 and IMM1, we added back the charge to the charged residues before the calculation. The origin of the coordinate system was transferred to the peptide mass center when calculating the electric dipole. The number of hydrogen bonds nhbond was calculated with cutoff distance 2.5 Å and cutoff angle 100°. The maximum fluctuation

of the peptide (rmsf) is defined as the maximum value of the root mean square fluctuation of each residue.

5.1.3. Data set

For comparison between experimental free energy and theoretical binding energy, 11 peptides were simulated and their ΔW was calculated. Experimental binding free energies (ΔG) were collected from the literature and summarized in Appendix B. All binding free energy values were converted to the molarity standard state (ΔG_0 , see Appendix A).

The study was then extended to a total of 53 helical or partially helical peptides with known PDB structure selected from the APD database[53]. Large antimicrobial peptides ($>$ 50 residues) and beta structured peptides were not included in this study to avoid the complexity of additional structural variables. The activities of the peptides against *E. Coli*, *P. Aeruginosa* (typical Gram-negative bacteria), and *S. Aureus* (typical Gram-positive bacterium) were collected from literature data. These three organisms are most commonly used for measuring antimicrobial activity. A table listing the PDB id and activity of studied peptides can be found in Appendix B, where peptides are grouped by their origin and family. All the data collected come from experiments with standard or a variation of broth microdilution assay [278]. However, different colony formation units (CFU) are normally used in different studies so we listed the CFU conditions together with the MIC values in Appendix C. Data reported in $\mu g/ml$ were converted to μM.

For comparing hemolytic activity, the peptide concentrations required to generate a certain extent of hemolysis are also listed in Appendix C. Although the hemolytic assays were carried out in a standardized way, the incubation time and cell suspension concentration vary in different studies. These conditions are also listed in Appendix C. Only the concentration to generate 50% hemolysis (EC50) was used to determine the relationship between hemolytic activity and peptide physical descriptors.

5.1.4. Fitting the biological acitivity to the "Carpet" model

Based on Equation 1.7, we can obtain that:

$$MIC = P^* : L \frac{1}{v_L exp(-\frac{\Delta G_c^0}{RT})} \tag{5.1}$$

In the carpet model, it is reasonable to assume that the membrane loses its integrity when the peptide covers a critical fraction (f^*) of area of the lipids. f can be calculated as:

$$f = \frac{n_p A_S}{n_p A_S + n_L A_L} \tag{5.2}$$

Thus the critical P*:L is:

$$P^* : L = \frac{f^* A_L}{(1 - f^*) A_S} \tag{5.3}$$

and

$$MIC * A_S = \frac{f^* A_L}{(1 - f^*) v_L} exp(\frac{\Delta G_c^0}{RT}) \tag{5.4}$$

For the carpet model, we expect f^* to be a constant value. In implicit simulations, A_s can be easily obtained and ΔG_c^0 can be estimated from the transfer energy ΔW (see section 5.2).

5.2. Can the implicit membrane model correctly predict binding free energy?

Thermodynamic data for membrane binding in the literature are reported in a variety of standard states. For comparison between them they need to be converted to the same standard state. Appendix A describes how this is done and presents a compilation of data on AMPs.

The membrane binding free energy can be broken up into the following contributions: a) the change in average effective energy, $\Delta\langle W\rangle$, which includes intramolecular and solvation free energy changes, b) translational and rotational entropy changes, c) the free energy of folding, if the soluble form is disordered and the membrane-bound form has secondary structure, and d) the disaggregation free energy, if the peptide is aggregated in solution [279]. Using an implicit model it is relatively straightforward to obtain $\Delta\langle W\rangle$: for each peptide, we place it on the membrane or in water and calculate the difference in average effective energy in MD simulations. However, peptides that are unfolded or aggregated in solution this simple approach is not sufficient.

For peptides that are disordered in solution and fold into a helix upon membrane binding, a useful approach might be to calculate the free energy of the transition from membrane-bound helix to a helix in solution. This value should be added to the free energy of helix unfolding in solution, which for these peptides should be a small number, not more than 2-3 kcal/mol [239]. The translational-rotational entropy of peptide adsorption to a membrane has been estimated as 1.3 kcal/mol [280] and is likely to be similar for different peptides. The effective energy of membrane binding of the helix is estimated from the average transfer energy, $\langle\Delta W\rangle$, obtained by averaging the difference in effective energy between membrane and aqueous phase for every conformation generated during the membrane simulation. $\langle\Delta W\rangle$ has the added advantage of a lower statistical uncertainty than $\Delta\langle W\rangle$. According to this rationale, $\langle\Delta W\rangle$ should be systematically more negative than the experimental binding free energy by a few kcal/mol.

We pursued both approaches and computed $\langle\Delta W\rangle$ from 4-ns simulations on the membrane and $\Delta\langle W\rangle$ from separate 100-ns simulations both on the membrane and in solution. The results are listed and compared with the experimental binding free energies in Table 5.1. $\langle\Delta W\rangle$ is more negative than the ΔG in all cases except for Dermadistinctin K and mastoparan X. Compared to $\langle$

ΔW>, the values of Δ<W> are closer to the values of ΔG. In these long simulations, we observed that most peptides maintained their initial structure on the membrane but became partially or completely unfolded in water. Only Dermadistinctin K and mastoparan X stayed mainly helical in water. This may indicate that, although these peptides are unstructured in solution [281, 282], the free energy of helix unfolding we neglected in <ΔW> is smaller in these two cases than usual.

Table 5.1.: Comparison of the experimental binding free energy with Δ<W> and <ΔW>. * Interpolated from other anionic fractions.

Peptide	PDBid	Lipids	ΔG_c^0	$<\Delta W>$	$\Delta<W>$	Ref
Alamethicin	1amt	DOPC	-5.77	-8.6±0.2	-8.2±0.4	Lewis and Cafiso [283]
Mastoparan X	2czp	POPC	-4.7	-4.2±0.8	-4.0±0.6	Almeida and Pokorny [284]
δ-hemolysin	2kam	POPC	-6.0	-12.6±0.5	-17.6±7.7	Clark et al. [285]
CM-15	2jmy	DMPC	-4.72	-8.3±0.9	-5.1±1.8	Bastos [75]
		DMPG	-5.49	-15.5±0.3	-14.1±3.2	
Dermadistinctin K	2k9b	egg PC	-3.97	-3.1±1.7	-2.5±3.1	Verly et al. [286]
LL-37	2k6o	SOPC	-6.16	-12.7±0.4	-1.8±3.8	Sood et al. [287]
		SOPC/POPG(7:3)	-8.79*	-19.1±1.9	-6.9±3.6	
Magainin	2mag	POPC	-3.7	-5.4±0.6	-1.8±3.1	Gregory et al. [204]
		POPC:POPG(3:1)	-5.98	-10.7±1.0	-7.6±2.8	
Melittin	2mlt	DOPC	-5.1	-13.1±0.7	-5.4±1.2	Beschiaschvili and Seelig [288]
		POPC/POPG(8:2)	-8.2	-18.6±2.5	-17.0±4.1	
Pardaxin	1xc0	POPC	-6.21	-22.1±0.8	-7.0±2.3	Rapaport and Shai [289]

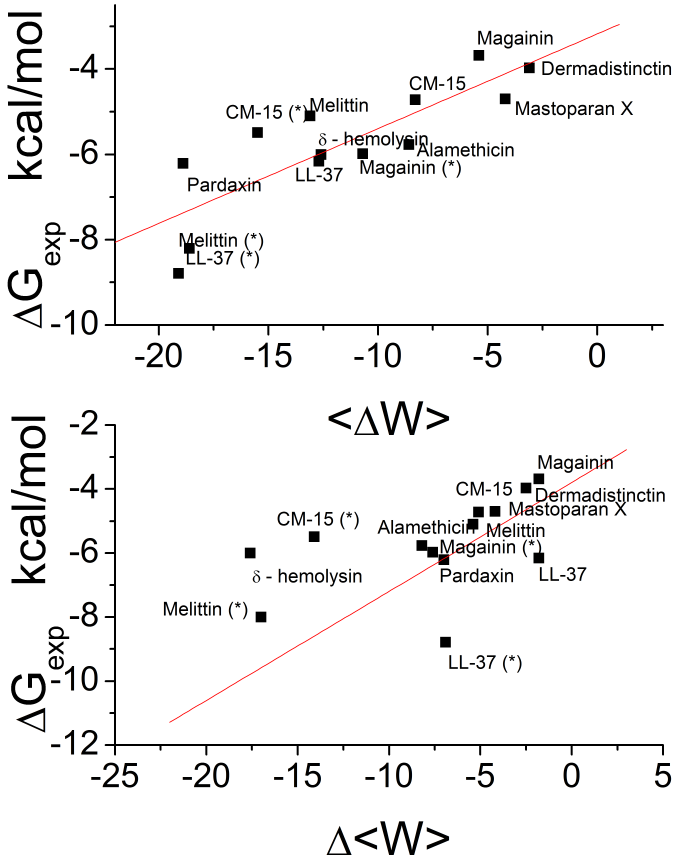

Figure 5.1.: Correlation between theoretical binding energy and experimental binding energy ΔG_{exp}. Binding energy values that are measured in anionic membranes are marked with (*). Upper panel, $<\Delta$ W>. Lower panel, $\Delta <$ W>.

Scatter plots that compare ΔG with $<\Delta$W> and $\Delta<$W> are shown in Figure 5.1. A strong linear relationship can be found between $<\Delta$W> and ΔG_{exp}:

$$\Delta G_{exp} = 0.196 \pm 0.045 * \Delta < W >_{w \to m} -3.43 \pm 0.60,\ R^2 = 0.71 \tag{5.5}$$

The correlation between ΔG and $\Delta<$W> is much weaker (Figure 5.1b). Extending some of the simulations up to 1000 ns did not improve the results significantly. Excluding the points that clearly do not fit (CM-15(*), Melittin(*), pardaxin), a linear relationship between $\Delta<$W> and ΔG_{exp} can

also be established but with higher uncertainty:

$$\Delta G_{exp} = 0.341 \pm 0.176 * \Delta < W >_{w \to m} -3.80 \pm 0.97,\ R^2 = 0.32 \tag{5.6}$$

All-atom explicit simulations also exhibit significant deviations from experimental binding free energies. Several cases are listed in Table 5.2 and compared to transfer energies using the present implicit model. In some cases, the binding free energies calculated from explicit simulations are comparable to <ΔW>. In other cases, the <ΔW> from implicit simulations is closer to the experimental value than the explicit simulation result. As explained above, an important missing factor in these calculations is conformational entropy. For β antimicrobial peptides which have relative rigid structure, the transfer energy <ΔW> is closer to the binding free energy.

Even though not directly comparable with experimental binding free energy, <ΔW> can still be quite useful in practice thanks to its linear relationship with ΔG_{exp}. Calculating <ΔW> also requires much less computing effort because 4 ns simulations can already give good correlation between <ΔW> and ΔG_{exp}.

Table 5.2.: Comparison of transfer energy with binding free energy calculated from umbrella sampling. + The experimental value is obtained for a truncated lactoferricin which has less charge, so the actual value should be more negative. * The standard state of the experiment is assumed to be ΔG_c^0.

Peptide	Membrane	$\Delta G_{c,sim}^0$	ΔG_c^0	< ΔW>	Ref.
Lactoferricin	DOPC	-1.05±0.39		-0.9 ±0.1	Vivcharuk et al. [290]
	DOPG	-5.4±1.3	-7.38^+	-7.9±0.7	Jing et al. [291], Tolokh et al. [292]
Protegrin	DMPC/DMPG(7:3)	-2.4±0.8	-7*	-5.3 ±1.1	Lai et al. [293], Vivcharuk and Kaznessis [294]
Indolicidin	DOPC	-0.05±0.46	-7.25	-1.1±1.2	Andrushchenko et al. [74], Yeh et al. [295]
	DOPC/DOPG(7:3)	-1.94±0.56	-8.97	-5.5±0.8	
Melittin	DOPC	-13.92 ±1.35	-5.4	-13.1±0.7	Allende et al. [221], Irudayam and Berkowitz [212]

5.3. Correlation between binding energy and biological activity.

5.3.1. Correlation between experimental membrane binding free energy ΔG_{exp} and biological activity

To examine the relationship between membrane partition and biological activity, we collected from the literature minimum inhibitory concentrations (MIC) for antibacterial activity and 50% hemolysis concentrations (EC50) for hemolytic activity. Appendix C lists the collected data. Appendix B lists experimental binding free energies from the literature. Because concentrations are exponentially related to energies (see Equation 5.4), we plot the natural log of MIC and EC50 against the binding energy to neutral or anionic membranes in Figure 5.2. There is considerable scatter in the data, but some correlations are visible. The linear correlation coefficient (R) between the ln(MIC) and binding energy to anionic membrane is 0.46 and 0.62 for anionic lipid fraction 25-30% and 50% respectively. The correlation for 100% anionic membrane, however, is negative largely due to a single data point: CM-15 is quite effective even though its membrane binding is rather weak. The binding energy to neutral membrane has a weak negative correlation (R= -0.32) with the ln(MIC), indicating that the electrostatic interaction between anionic lipids and cationic peptides is important for antibacterial activity.

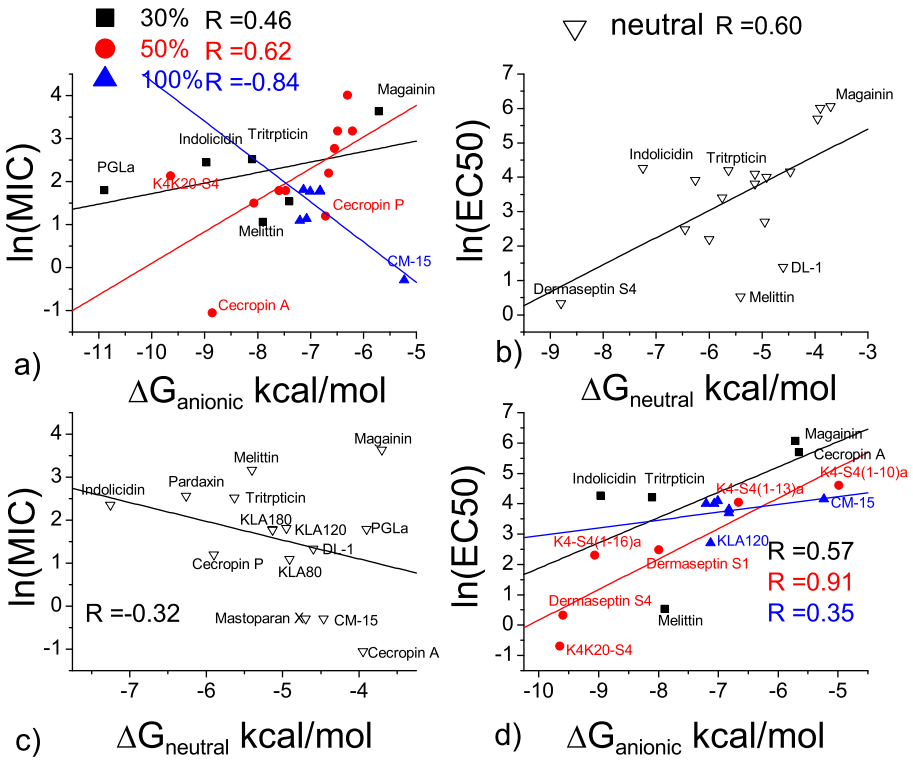

Figure 5.2.: Correlation between experimental binding energy and biological activity. The lines are the best fit lines. a) $\Delta G_{anionic}$ in 25-100% anionic lipid and antibacterial activity against E. Coli. b) $\Delta G_{neutral}$ and hemolytic activity. c) $\Delta G_{neutral}$ and antibacterial activity. d) $\Delta G_{anionic}$ and hemolytic activity. The data points are chosen from Appendix B. The unit of MIC and EC50 is μM.

The linear correlation coefficient between the ln(EC50) and neutral membrane is 0.60. However, the correlation between ln(EC50) and anionic membrane is similar (R= 0.57 and 0.91 for anionic lipid fraction 25-30% and 50% respectively).

5.3.2. Correlation between theoretical transfer energy $< \Delta W >$ and biological activity

For many peptides, the experimental binding free energy is not available, especially to anionic lipids. These can be obtained theoretically for different anionic fractions using an implicit membrane model and molecular dynamics simulation. We ran simulations under different anionic fraction (anfr) and calculated the correlation coefficient (R) between <ΔW> and natural log of biological effective concentrations (Figure 5.3a). The antibacterial activity against all three organisms correlates best with transfer energy to $\geq$ 30% anionic lipid membrane and quickly diminishes as the anionic

fraction approaches 0%. The correlation to hemolytic activity is largely independent of anionic fraction; it is actually somewhat larger for 10% anionic fraction. It is difficult to say whether this slight increase in correlation is significant. It is worth noting, however, that the erythrocyte membrane contains around 30% phosphatidylserine (PS) in the inner leaflet [103]. Considering that the antimicrobial peptides can form pores, translocate through the membrane or induce lipid flip-flop in the membrane, it is conceivable that they could interact with the anionic lipids in the inner leaflet. Also, the outer leaflet of erythrocyte membrane contains glycoproteins and glycolipids which all possess chains of anionic sialic acid [296, 297].

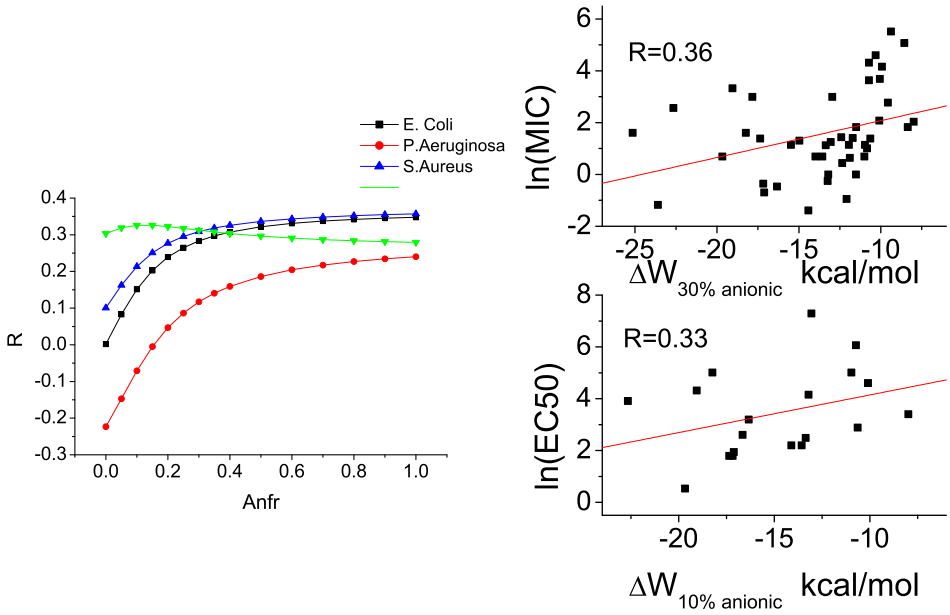

Figure 5.3.: Correlation between transfer energy and biological effective concentrations. a) The effect of anionic lipid fraction (Anfr) on the correlation coefficient (S) between transfer energy <ΔW> and biological effective concentrations. b) ln(MIC) against E. Coli c). ln(EC50) against red blood cells. The <ΔW> and effective concentration values shown here are listed in Appendix C. The unit of MIC and EC50 is μM.

Specific scatter plots of the data are shown in Figure 5.3b&c. The linear correlation coefficient is slightly lower, due to the increased sample size and the difference between <ΔW> and ΔG, but still is statistically significant. These data, together with those of the previous section lead to similar conclusions: a) there is a statistically significant correlation between binding energies and biological activities, b) electrostatic interactions are important for antimicrobial activity but much

less so for hemolytic activity, and c) the scatter in the plots shows that membrane affinity is not the sole determinant of activity.

5.4. Correlation between other properties and biological activity.

The correlation between biological activity and binding energy is evident but not strong. This strongly indicates that membrane binding energy is not the only factor affecting the biological activities. Antimicrobial peptides are well known for their structure diversity. Even when we limited the range to helical peptides, the peptide can be as short as 13 residues (IsCT) or as long as 42 residues (moricin, 1kv4); the charge can range from -2 (alamethicin,1amt) to +12 (CAP18, 1lyp); the peptide can be highly helical (alamethicin ,1amt) or mainly unfolded (SMAP29, 1fry); it can also be highly linear (mastoparan M, 1d7n) or have multiple flexible hinge (moricin,1kv4). As a result, the behavior of the peptides on the membrane interface is quite different. Figure 5.4 shows several typical conformations on anionic membranes. The peptide can insert deep into the hydrophobic core (8 Å, alamethicin, 1amt) or only penetrate shallowly (1 Å, such as fowlicidin-2, 2gdl); the tilt angle of the peptide can range from 80° (pardaxin) to 120° (such as fowlicidin-1, 2amn). The structure can be quite stable (rmsf $<$ 0.9 Å, such as mastoparan M, 1d7n) or can have large fluctuations (rmsf $>$ 5 Å, such as moricin). The conformations on neutral and anionic membranes are similar. The only difference is that the binding energy is less negative and the peptide inserted less into the membrane.

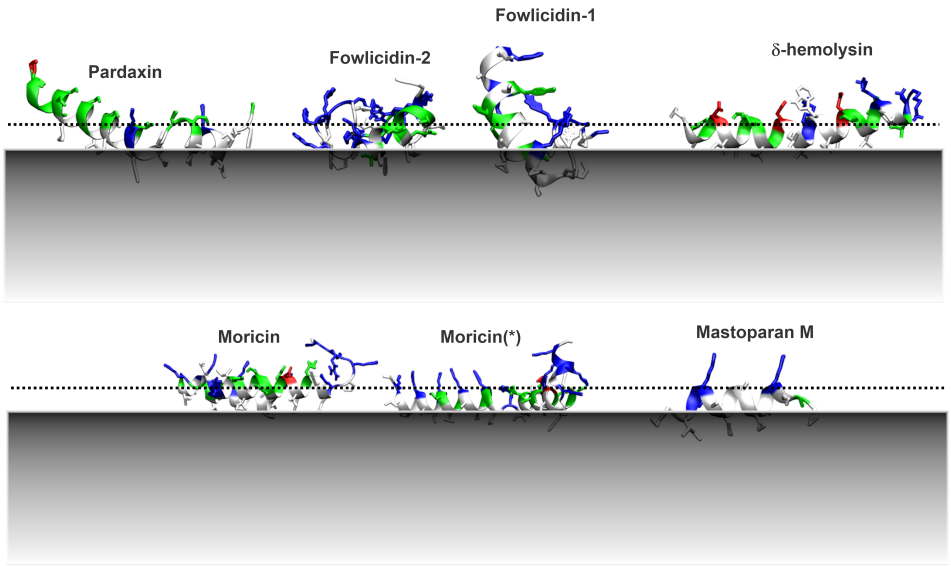

Figure 5.4.: Example conformations of antimicrobial peptides on anionic membranes. The grey area indicates the hydrophobic core of the membrane. The dotted line indicates the location of phosphate groups. The colors on peptides indicate the residue type: Red: acidic residues; Blue: basic residues; white: polar residues; green: uncharged polar residues. Moricin(*): an alternative conformation of moricin with same total energy.

Empirical correlations between peptide physicochemical properties and their antimicrobial activities have been investigated in the past [142, 298, 143, 149, 138, 299]. MD simulations offer additional descriptors that go beyond peptide sequence and secondary structure (Table 5.3). The correlations between these descriptors and the biological effective concentrations are shown in Table 5.3. The Spearman correlation coefficient is used because it is not affected by the actual mathematical relationship between effective concentration and descriptor. Because the MIC and EC50 increase when the activity of the peptide decreases, positive correlation in Table 5.3 means unfavorable effect on the activity.

Table 5.3.: Correlation between the biological effective concentrations and biophysical descriptors. The p values are given in the parenthesis (two tails T-test, probability that the actual correlation is below the given value). The descriptors were calculated from 30% anionic membrane simulations and neutral membrane simulations respectively for correlating with MIC and EC50.

Biophysical Factor		MIC E.Coli. $N_{pept} = 44$	EC50 Hemolytic $N_{pept} = 19$
ΔW	Transfer energy of peptide from water to membrane surface.	0.46 (1.7E-03)	0.30 (2.1E-01)
H	Hydrophobicity.	-0.09 (5.8E-01)	-0.08 (7.4E-01)
μ_H	Hydrophobic moment.	-0.45 (2.4E-03)	-0.56 (1.3E-02)
Q_H	Hydrophobic quadrupole	-0.39 (8.2E-03)	-0.45 (5.1E-02)
n_{charge}	The net charge of the peptides.	-0.46 (1.7E-03)	-0.13 (5.9E-01)
n_{res}	Number of residues.	-0.36 (1.3E-02)	-0.23 (3.4E-01)
V	The immersed volume of peptide in the hydrophobic core of the membrane.	-0.15 (3.4E-01)	-0.22 (3.6E-01)
A_s	Area of peptide occupied on the membrane surface.	-0.40 (7.6E-03)	0.12 (6.3E-01)
Tilt	The angle between peptide helix axis and membrane normal.	0.05 (7.6E-01)	0.29 (2.2E-01)
Depth	The penetration depth of peptide residue into the hydrophobic core. Calculated as the distance between the deepest residue and the membrane surface.	-0.14 (3.7E-01)	-0.48 (3.7E-02)
Helix%	The percentage of helical structure.	0.25 (9.8E-02)	0.05 (8.3E-01)
nhelix	The number of helical residues.	-0.13 (3.9E-01)	-0.25 (3.0E-01)
$< n_{hbond} >$	The number of hydrogen bonds per residue that were formed inside the peptide.	-0.02 (8.8E-01)	-0.02 (9.2E-01)
n_{hbond}	The number of hydrogen bonds.	-0.28 (6.5E-02)	-0.08 (7.4E-01)
rmsf	The maximum fluctuation of any residue in the simulation.*	-0.42 (4.3E-03)	-0.17 (4.9E-01)
D_{elec}	The electric dipole possessed by the peptide.	-0.25 (9.6E-02)	0.39 (0.9E-01)

Not surprisingly, the electrostatic interaction is crucial for selectivity: ncharge correlated significantly with the antibacterial activity but not so well with the hemolytic activity. Peptide size (n_{res}) also correlates positively with the biological activity as previously revealed [300]. As found by previous studies [142, 143], amphipathicity is an important factor determining the activity of the peptide, even surpassing in importance the overall hydrophobicity [301]. Interestingly, the hydrophobic quadrupole, which can serve as measure of imperfect amphipathicity [242], is also an important determinant of biological activity.

MD simulation provides additional information that could help us identify important new activity determinants. As described in previous sections, the transfer energy ΔW correlates with both antibacterial and hemolytic activity. We observed that the antibacterial activity and hemolytic activity are affected differently by membrane insertion, tilt angle and A_S . The membrane insertion (both insertion volume V and insertion depth, the latter showing stronger correlation) positively correlates with the hemolytic activity but not antibacterial activity, consistent with the result for the tilt angle; the closer the tilt angle is to 90°, the less active the peptide is against erythrocytes. The surface area occupation A_S is positively correlated with the antibacterial activity but not the hemolytic activity. It has been found that the angle subtended by polar residues is important to

both antimicrobial activity and hemolytic activity [120]. Decreasing the angle will increase both the insertion into the membrane and the membrane surface area occupation of the peptide. The fact that electric dipole of the peptide is unfavorably correlated with hemolytic activity is also consistent with this trend: increasing the peptide dipole increase interactions with the head groups and will enhance the binding to membrane interface while at the same time reduce the insertion into membrane hydrophobic core.

The effect of helicity and structural flexibility is sometimes ambiguous in experiments. Increasing the number of proline residues in a peptide significantly reduced its channel-forming activity and thus both antimicrobial and hemolytic activities [302]. The increased flexibility and reduced helicity of D-amino acid containing peptides normally abrogated their hemolytic activity but did not diminish their antibacterial activity [71, 70, 303, 67]. Recent research however showed that proline-containing peptides have higher antibacterial activity and lower hemolytic activity Vermeer et al. [304]. We observed that the structural flexibility (reflected by the structural fluctuation in the MD simulations) is positively correlated with both antibacterial and hemolytic activities. This may be due to a lower entropy cost upon membrane binding, and thus a lower membrane binding free energy. Alternatively, flexibility might be required at subsequent steps, such as pore formation. The number of helical residues (n_{helix}) and hydrogen bonds (n_{hbond}) are positively correlated with the biological activities. However, increasing the helical percentage has a negative effect on the biological activities, possibly because structural flexibility is reduced. The average number of hydrogen bonds per residue ($< n_{hbond} >$) also has no correlation with biological activity. Hemolytic activity generally correlates more with helix formation and antibacterial activity correlates more with structural flexibility.

Using the collected biophysical descriptors, we can also establish a relationship between biological activity and biophysical factors using multiple linear regression:

$$ln(MIC) = 12.63 + 0.01821 * \Delta W_{30\%\, anionic} - 0.03737 * A_s + 3.919 \times 10^{-5} * A_s^2 - 0.2741 * depth + 0.3614 * sin(tilt) - 0.1310 * rmsf - 0.2430 * n_{charge} \quad R^2 = 0.46 \quad (5.7)$$

$$ln(EC50) = 11.93 + 0.1574 * \Delta W_{10\%\, anionic} + 0.01342 * D_{elec} - 0.1814 * depth$$
$$- 1.223 * rmsf - 0.08303 * helix\% - 0.1410 * n_{charge} \qquad R^2 = 0.79 \qquad (5.8)$$

In the above equation, adding or dropping a descriptor will reduce the correlation. The minimum set of parameters one needs to describe the biological activities is quite different for antibacterial activity and hemolytic activity. Using these two equations, the predicted value agreed quite well with the actual values (Figure 5.5). The mean square error is between ± 1.5. Compared to other QSAR studies, the correlation of predicted ln(MIC) with actual values is rather low. Considering that the protocol of MIC/EC50 measurement allows difference in concentration of 2 fold and the fact that our data points are chosen in different peptide families, the observed error is reasonable.

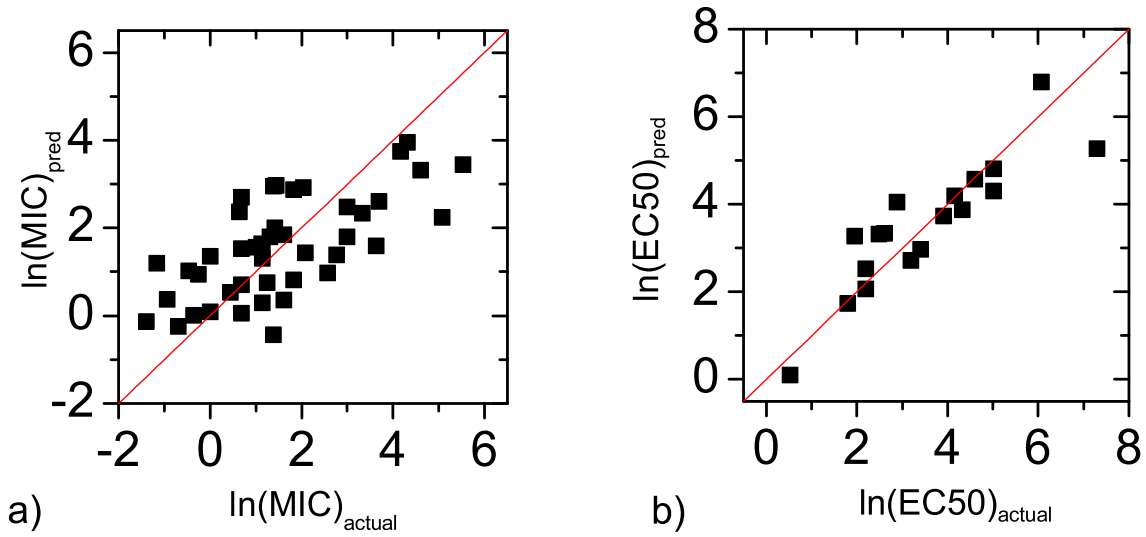

Figure 5.5.: The predicted biological activity compared with the actual biological activity. a) the ln(MIC) calculated for E.Coli. membrane. b) the ln(EC50) calculated for Erythrocyte membrane.

5.5. Quantitative relationship between other biological factors and biological activity.

5.5.1. Prediction of the "carpet" model

The "carpet" model of AMP action proposes that peptides accumulate on the membrane surface until a critical point is reached at which the membrane disintegrates [12, 305]. In this simple model, AMP activity depends on only two parameters: the membrane affinity of the peptide and the critical surface coverage that a certain type of membrane can withstand. The latter is not known, but it is reasonable to assume that it will fall in the range 50-90%. In subsection 5.1.4 we derived a simple equation relating the MIC or the EC50 to these two parameters. If we insert Equation 5.5 into Equation 5.4, we obtain:

$$ln(MIC * A_s) = \frac{0.196 < \Delta W >}{RT} - \frac{3.43}{RT} + ln\frac{f^*}{1-f^*} + lnA_L - lnv_L + ln(1 \times 10^6) \qquad (5.9)$$

where the last term is a converstion factor from μM to M. Figure 5.6 plots the calculated <ΔW> against ln(MIC*A_s) or ln(EC50*A_s) and the Equation 5.9 with A_L=65 Å and v_L=0.76 M^{-1} [132] and different values of f^*. The f^*=0.9 line is close to the upper points in the plot, corresponding to peptides that are rather inactive compared to their computed binding affinity. A large number of points fall below the f^*=0.5 line, i.e. they are more active than the carpet model predicts. This could be an indication that these peptides act by a more efficient mechanism, for example pore formation.

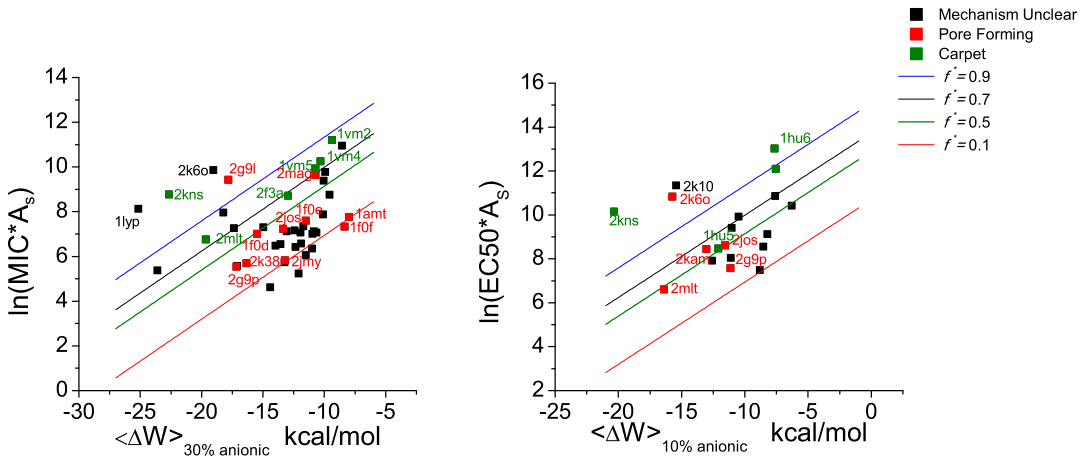

Figure 5.6.: Biological activity of peptides plotted against theoretical transfer energy. a) activity against E. Coli. b) activity against red blood cells. The lines correspond to the theoretical expectation from the carpet model for different value of the critical surface fraction covered. The red points are the peptides proposed to adopt "pore forming" mechanism. The green points are the peptides proposed to adopt "carpet" mechanism. The black points are the peptides that have unknown mechanism.

It is interesting to compare the position of each peptide in these graphs to experimental data suggesting their mechanism of action. In Appendix D, we collected information on the mechanism of various peptides suggested in the literature. It should be noted that most of these proclamations are based on circumstantial evidence that may be in conflict with another. For example, LL-37 was found to orient mainly parallel to membrane surface by Polarized ATR-FTIR spectroscopy [67] but partly perpendicular to the membrane surface by oriented CD spectroscopy [177]. Another example is pardaxin, which was originally referred to as a pore forming peptide [306] but more recent experiments suggested that it could adopt the "carpet" mechanism in the presence of anionic lipid or cholesterol [98, 307, 308]. Sometimes, the conflict is reconcilable: magainin is suggested to act through the "carpet" mechanism on eukaryotic cell membranes but not on bacterial membranes [110]. However, the stable pore formed in anionic membranes is preceded by formation of a large opening [173], similar to the ones observed in "carpet" mechanisms. Also, many of the suggestions are based on in vitro experiments that may not be entirely relevant to in vivo activities.

Keeping these caveats in mind, we marked the data points on Figure 5.6 according to the proposed mechanism for each peptide. The peptides proposed to be "carpet" like are marked by green color. They distribute above the $f^* = 0.5$ line. The peptides proposed to be "pore forming" are marked by

red color. The majority of them lie below the $f^* = 0.5$ line, but there are some outliers, primarily gaegurin-4 (2g9l) and LL37 (2k6o). The mechanism of LL-37 (2k6o) is controversial: it has been suggested to form pores [177] but also to act as a "carpet" [67, 309, 310, 311].

5.5.2. Correlation between transfer energy to pores and deviation from the "carpet" model

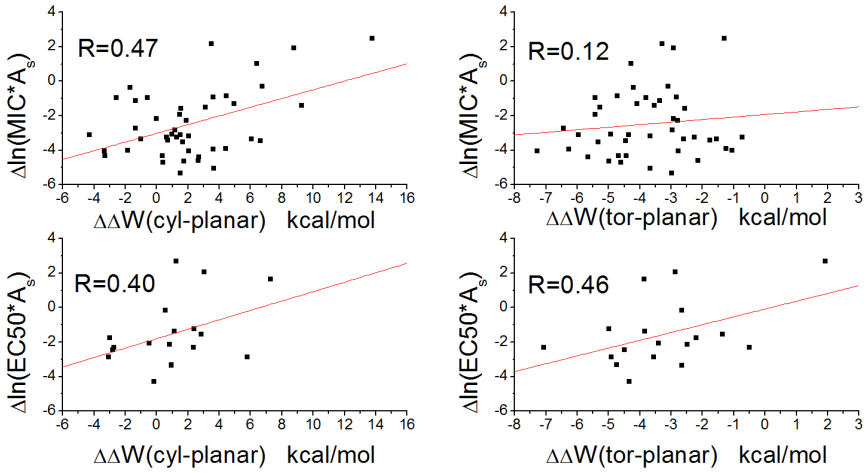

Figure 5.7.: The correlation between transfer energy to pores and deviation of $ln(MIC * A_s)$ and $ln(EC50 * A_s)$ from predictions of the "carpet" model. cyl: the pore is a cylindrical pore with R_0=13 Å. tor: the pore is a toroidal pore with R_0=13 Å, K_0=15 Å, h=0.6. The anionic fractions of the lipids are 10% and 30% respectively for $ln(MIC * A_s)$ and $ln(EC50 * A_s)$. The red lines are the best fit lines.

Pore formation is a complex process with many contributions: peptide-lipid interaction, possibly peptide-peptide interaction, and the lipid deformation energy. But since forming a lipidic pore is energetically unfavorable [167], if a peptide tends to induce pore formation, the transfer energy of a single peptide to lipidic pores should be favorable. In previous work [242], four antimicrobial peptides were found to bind more strongly to toroidal pores than to the planar membrane. Here we extend this work to a larger number of peptides and to anionic pores [276]. We calculated the transfer energy of the peptides to pre-formed cylindrical and toroidal pores in neutral, 10% anionic and 30% anionic membrane of radius R_0= 13 Å. The values are shown in Appendix E. We observed that all peptides have favorable transfer energy to anionic toroidal pores. Transfer

energy to cylindrical pores in anionic membranes is only favorable for a few peptides. In neutral membrane, the transfer energy to both pores is favorable for most peptides. Pardaxin (1xc0) has unfavorable transfer energy to any type of pore in neutral and 10% anionic membranes even though a pore formation mechanism was proposed for it [306]. The peptide changed into a hairpin like structure in the toroidal pores. It may be that the peptide adopts a specific structure that we have not been able to sample and that this is a metastable structure. Peptide-peptide interactions, which we haven't taken into account in this study, may also contribute to stabilizing the pore [312].

If pore formation makes the peptide more effective than the "Carpet" model would predict, we should observe that the reduction in $ln(MIC * A_s)$ and $ln(EC50 * A_s)$ from the value expected from the carpet model is positively correlated with the transfer energy to pores. Figure 5.7 shows that this indeed is the case: the more negative the $\Delta\Delta$W, the more likely is the $ln(MIC * A_s)$ or $ln(EC50 * A_s)$ to be lower than the values predicted by "Carpet" model using f^*= 0.9. The correlation is significant (p-Value $\leq$ 0.1) except between $\Delta ln(MIC * A_s)$ and $\Delta\Delta W_{tor}$. Interestingly, the transfer energy to cylindrical pores is more highly correlated with $\Delta ln(MIC * A_s)$ than the transfer energy to toroidal pores, even though the transfer energy to the latter is more favorable. This might be due to simplifications in the analysis, for example, toroidal pores induced by different peptides may have different curvature K_0 and inhomogeneous factor h, but we are assuming they are constant in our simulations.

6. Summary and Perspective

This thesis has studied various aspects of membrane active peptides. In this chapter, we summarize our findings and propose future work that could extend our current findings.

6.1. Summary

Implicit membrane model provides an important tool to model membrane active peptides. It is extraordinarily efficient and is able to estimate several important properties of peptides. It can also be used to represent different geometric shapes other than planar membrane. For example, two types of pores, barrel-stave (cylindrical) pores and toroidal (parabola) pores, that antimicrobial peptides normally form can be modeled. In this thesis, we further extended it to include the electrostatic interaction between cationic peptides and membranes pores. In this new model, the head group dipoles were represented by a double layer model and the inhomogenous distribution of charges on the pore surfaces was also considered.

In the first study, we proved that peptide orientation can be correctly predicted by the implicit membrane model. The tilt angles of transmembrane peptides in the implicit membranes follow the hydrophobic mismatch theory rather than the incorrectly interpreted NMR experiments.

The implicit membrane model can also be used to estimate the peptides' binding affinity to the membrane surface. By calculating the theoretical transfer energy, our study confirmed that the binding affinity to membrane surface is an important factor in determining the antimicrobial peptides' activity but it is not the only one. Based on the correlation analysis, we are also able to suggest the best representation of the respective biological membranes.

Other properties collected from the implicit simulation were also found to be critical for antimicrobial peptides' activities. Such information, hard to obtain from experiments, provides useful insights that help us to identify new design criteria for novel antimicrobial peptides. Quantitative structure-activity relationship can also be established using these properties.

The pore model provides additional information. As revealed in our study, the "Carpet" model cannot describe the activities of all antimicrobial peptides. Most antimicrobial peptides can adopt a more effective mechansim such as pore formation. The enhancement in biological activity by forming pores is also directly correlated with the pore formation energy. Focusing on two antimicrobial peptides, magainin and melittin, the pore model can be used to explain their different activities in response to anionic lipids. The pore model can also help us to correctly identify the more stable conformation of protegrin octameric pores.

6.2. Future work

Implicit membrane models have already provided useful information that can help us understand the behavior of antimicrobial peptides. However, more efforts are still needed in the following areas:

6.2.1. Data quality

In our study, the biological activity data was collected from the different literature and the selected antimicrobial peptides originated from different organisms. As a result, we observed highly scattered data in the correlation studies. Using more standardized data sources and focusing on single peptide property (while maintaning other properties the same), the complexity of research would be significantly reduced. If we were able to acquire data from large-scale mutation studies, we would be able to test our model in a more systematic way.

6.2.2. Quantitative model for ion flux through pores.

In this study, we observed that the transfer energy to pores affects the biological activity. However, we remain unable to formulate a model that can connect the pore formation to the biological events

such as cell death. Cell death is normally accompanied by the breakdown of the ion gradient. A quantitative model that can connect the transfer energy to pores to the ion flux through pores would be extremely helpful for predicting the activity of antimicrobial peptides. Bolintineanu et al. [313], Bolintineanu and Kaznessis [314] have already done some pioneering work in this area. Huang [315] also made some efforts in calculating biological effective concentrations from pore formation energies. As a first step, we could collect the equilibrium constant of pore formation through fluorescent measurements. A direct correlation between the transfer energy to pores and the number of pores can thus be acquired.

6.2.3. Determine the peptide mechanism from the transfer energy to pores

In this study, we have calculated the transfer energy of several peptides to pores. We observed that most peptides have favorable transfer energy to toroidal pores, at least in anionic membranes. These peptides, however, are not limited to antimicrobial peptides. Many fusion peptides, cell penetrating peptides, and apolipoprotein segments also transfer favorably into toroidal pores. Understanding the reason why these distinct peptides all bind to toroidal pore favorably could help us find the common features of these peptides and may also help us identify the difference between these peptides.

6.2.4. Verify the transfer energy to pores through explicit simulations.

Since implicit membrane model may sometimes be a little over-simplified, we need to verify whether the transfer energy calculated from implicit membrane model is reasonable before we can confidently use it in our studies. In the thesis study, we provided a constraint method that can keep pores stable in the explicit simulations, which allows us to calculate the potential of mean force of transfering a single peptide from membrane pores to water. The calculated transfer free energy could be compared with the values that are calculated from implicit model to validate the latter.

6.2.5. Determining the pore formation energy.

In the current verion of implicit membrane model, the elastic deformation energy of pores is not considered. This is an important quantity that determines whether the pore is stable or not. There are already some theoretical studies focusing on the pore formation energy [154, 160, 172]. However, these methods either require the simplification of the molecules that prevents modeling the effect of peptides[172], or require indirect measurements of pore formation energy[154, 160]. The geometric constraint method we introduced in the thesis can be used to constrain the lipids to certain shapes. With some adaptation, this method can be used to calculate the pore formation energy through umbrella sampling. The effect of peptide binding on the pore formation energy can also be obtained easily. Based on this, we can even estimate the minimum number of antimicrobial peptides to stabilize a toroidal pore. Such information can in turn enhance the implicit modeling of pores.

6.2.6. Geometric Modeling of the membrane.

In this thesis, we have developed a tool to model complicated geometric shapes. It can be used to build models for Poisson-Boltzmann calculation or constrain the shapes of lipid ensembles in the explicit simulations. Although only two geometric shapes were provided so far, it is fairly easy to extend the program to more complicated shapes. Extending the model to interesting geometric shapes such as curved bilayers, micelles, tubules, fusion pores, etc. will help us understand a variety of membrane activities that can be induced by membrane active peptides.

Appendices

A. Experimental methods for determining binding affinity to membrane

A.1. Calculation of standard states

The standard membrane binding free energy can be defined based on a number of different equilibrium constants. One is based on the peptide molarities in the lipid [PL] and aqueous phase [P_w] [316]:

$$\Delta G_c^0 = -RTlnK_c \quad , where\ K_c = [P_L]/[P_w] \tag{A.1}$$

where [PL] is defined as moles of peptide per volume of the lipid phase for membrane-inserting peptides or per volume of the interfacial region for interfacially adsorbed peptides. An alternative definition of the standard free energy is based on the mole fraction partition coefficient K_x :

$$\Delta G_x^0 = -RTlnK_x \quad , where\ K_x = \frac{n_b/(n_b + n_L)}{n_f/((n_f + n_w)} \tag{A.2}$$

in which n_b, n_f, n_L and n_w are the moles of bound peptide, free peptide, lipid and water molecules, respectively . Because under most experimental conditions, $n_b << n_L$ and $n_f << n_w$, K_x can be

approximated as:

$$K_x \approx \frac{n_b/n_L}{n_f/n_w} \tag{A.3}$$

ΔG_x^0 can be converted to ΔG_c^0 as follows [316]:

$$\begin{aligned}\Delta G_c^0 &= -RTln\frac{[P_L]}{[P_w]} = -RTln\frac{n_b/V_L}{n_w/V_w} = -RTln\frac{n_b/(n_L v_L)}{n_f/(n_w v_w)} \\ &= -RTln\frac{n_b/n_L}{n_f/n_w} + RTln\frac{v_L}{v_w} \\ &\approx \Delta G_x^0 + RTlnv_L/v_w\end{aligned} \tag{A.4}$$

where V_L and V_w are the total volume of the lipid and water, v_w and v_L are the molar volumes of water (0.018 M^{-1}) and lipid (0.76 M^{-1} , based on DOPC volume [317]) respectively. At room temperature (298 K), used here and in most experiments, the term $RTln(\frac{v_L}{v_w})$ is equal to 2.2 kcal/mol.

K_x can be obtained by measuring the fraction of peptide bound to the membrane f_b ($f_b = n_b/(n_b + n_f)$) at different lipid concentrations [L]:

$$\begin{aligned}f_b &= \frac{n_b}{n_b + \frac{n_b/n_L}{K_x/n_w}} \\ &= \frac{K_x n_L}{K_x n_L + n_w} \\ &= \frac{K_x[L]}{K_x[L] + [W]}\end{aligned} \tag{A.5}$$

where [W] is the water concentration, close to 55.3 M at room temperature. Another definition of the binding free energy is based on the association or dissociation constant (K_a or K_d) of peptide

to membrane. So:

$$P + L \rightarrow PL \tag{A.6}$$

$$K_d = \frac{1}{K_a} = \frac{[P_f][L]}{[PL]} \tag{A.7}$$

$$\Delta G_a^0 = -RTlnK_a = RTlnK_d \tag{A.8}$$

where $[P_f]$ and [PL] are the concentration of free peptides and peptide/lipid complexes over the entire volume of the system. The definition of [L] is a little ambiguous: because of the collective behavior of the lipids, the membrane should be treated as an ensemble of lipids [133]. Here, we assume the binding sites are lipid ensembles composed of n lipid molecules on average. [L] is thus defined as the concentration of binding sites $[L_n]$. Because the lipid concentration is normally low, $V_{system} \quad V_w$, thus $[P_f]$ is close to $[P_w]$. So:

$$\begin{aligned}
\Delta G_c^0 &= -RTln\frac{[P_L]}{[P_w]} \approx - RTln\frac{n_b/V_L}{[P_f]} \\
&= -RTln\frac{[PL_n]V_{system}/V_L}{[P_f]} \\
&= -RTln\frac{V_{system}/V_L}{K_d/[L_n]} \\
&= RTlnK_d v_L^{'} = \Delta G_a^0 + RTlnv_L^{'}
\end{aligned} \tag{A.9}$$

where $v_L^{'}$ is the molar volume of the lipid binding site. K_d can be measured from binding kinetics or by fitting the titration curve to a binding model (see below). In most papers reporting K_d, $v_L^{'}$ is treated as v_L. Because a lipid binding site can contain up to 10-20 lipids [318, 286, 319], neglecting

this can result in an energy difference of 1.36 to 1.77 kcal/mol.

K_d can be obtained from binding kinetics [320] or by one-site model[96]. In the latter, lipid membrane is assumed to be a single site receptor that can be saturated with enough peptides and the concentration-independent dissociation constant K_d can be calculated from fitting the following equation:

$$R_b = \frac{R_{max}[P_w]}{K_d + [P_w]} \tag{A.10}$$

R_b is the molar ratio of bound peptide in the lipid ($R_b = n_b/n_L$). R_{max} is the maximum capacity of the binding site (R_{max}= 1/n). Equation A.10 can be transformed into:

$$K_d = \frac{(1 - f_b)[L]}{n f_b} - [P](1 - f_b) \tag{A.11}$$

if the fraction of bound peptide f_b ($f_b = n_b/(n_f + n_b)$) is measured. In this equation, [P] and [L] is the total concentration of peptide and lipid respectively.

In this paper we adopt ΔG_c because of two main advantages over ΔG_x and ΔG_a. First, molarities arise naturally in statistical thermodynamic treatments (see below) and second, it is independent of the relative molecular size of the lipid and water, as it should intuitively. One disadvantage of ΔG_c is that the definition of the volume of the lipid phase V_L is somewhat arbitrary and differs for membrane-inserting and adsorbed peptides.

Alternative equilibrium constants can be found in the literature, for example [321]:

$$K_{app} = R_b/[P_w] \tag{A.12}$$

K_{app} can be used to calculate ΔG_c^0:

$$\begin{aligned}\Delta G_c^0 &= -RTln[P_L]/[P_w] = -RTln\frac{n_b/V_L}{[P_w]} \\ &= -RTln\frac{R_b n_L)/V_L}{[P_w]} \\ &= -RTln\frac{K_{app}}{v_L} \\ &= \Delta G_{app}^0 + RTlnv_L \end{aligned} \tag{A.13}$$

One disadvantage of K_{app} is that K_{app} is not constant but changes with peptide concentration [288]. This is because the peptide could saturate the membrane and prevent further binding; when peptides get too crowded on the membrane, the electrostatic repulsion between charged antimicrobial peptides becomes significant. For anionic membranes, the saturation happens easier because the higher affinity of peptide to the membrane. To obtain a concentration-independent partition coefficient, many papers maintained the peptide to lipid ratio at a very low value so that the peptide-peptide interaction is negligible. This makes experimental measurements more difficult. To allow a wider concentration range, some authors removed the electrostatic interaction component from the binding free energy [288, 322, 323] using the following method.

Because of the electrostatic interaction between the membrane and peptide, the peptide concentration in the aqueous solution immediately adjacent to the membrane $[P_m]$ is:

$$[P_m] = [P_w]exp\ (-zF_0\frac{\phi_0}{RT}) \tag{A.14}$$

where z is the charge of the peptide, F_0 is the Faraday constant, and $_0$ is the electrostatic potential on the membrane surface, which can be obtained from the Gouy-Chapman theory:

$$\sigma^2 = 2000\ _0\ _R RT\sum\nolimits_i C_{i,eq}(e^{-\frac{z_i F_0 \Phi_0}{RT}} - 1) \tag{A.15}$$

where $\epsilon_0\epsilon_R$ is the dielectric constant, $C_{i,eq}$ is the concentration of each ion species in the solution,

z_i is the charge of each ion species. σ is the charge density on the membrane surface, defined as a sum of charges on anionic lipids and on surface bound peptides (e_0 is the unit charge, A_L and A_p are the area of lipid and peptide molecules, X_{PG} is the fraction of anionic lipid):

$$\sigma = \frac{(e_0/A_L)(-X_{PG} + X_b z_p)}{[1 + X_b(A_p/A_L)]} \tag{A.16}$$

Using $[P_m]$, a partition coefficient K'_{app} that is independent of peptide concentration can be obtained:

$$K'_{app} = R_b/[P_m] \tag{A.17}$$

However, the binding energy $\Delta G'_c$ calculated from K'_{app} does not include the electrostatic interaction between peptide and anionic lipids, which makes it unsuitable for our purposes. We corrected such reported binding free energies by adding back the electrostatic interaction energy between peptide and membrane:

$$\Delta G^0_c = \Delta G'_c + z\phi \tag{A.18}$$

where z is the effective charge of the peptide and is the membrane surface potential calculated from Gouy-Chapman theory.

A.2. Experimental Methods

The following experimental methods are commonly used to determine the binding energy:

CD titration In CD experiments [288, 119], the moles of bound peptide n_b can be calculated from the change in ellipticity θ because of conformational change upon peptide transfer from water

solution to the membrane. By titrating a small amount of peptide solution into the lipid solution or a small amount of liposome solution into the peptide solution, the binding isotherm can be established. Or, the fraction of bound peptide f_b can be obtained and used to calculate K_x or K_d using Equation A.5 and Equation A.11.

Isothermal titration calorimetry (ITC) Small amounts of peptide are injected into liposome solutions periodically (or reversely, liposomes are titrated into a peptide solution) [322, 324]. Heat is generated in the binding reaction. The number of membrane-bound molecules is calculated from the molar binding enthalpy and is used to calculate the molar ratio of bound peptide Rb. The binding free energy can be calculated using the same method as CD experiments.

Fluorescence titration Another method used to obtain the binding isotherm is to measure the fluorescence intensity of a tryptophan residue on the peptide or fluorophore labels attached to peptide sidechains [63, 66]. The molar ratio of bound peptide R_b can be calculated from the fluorescence intensity. R_b can be used to further calculate K_d using Equation A.10.

Fluorescence kinetics In this method, the resonance between a tryptophan residue on the peptide and a fluorescent probe in the membrane indicates the extent of peptide binding. The rate of peptide association ($k_{on}[L]$) and dissociation (k_{off}) to membrane surface can be measured [204]:

$$P_w \underset{k_{off}}{\overset{k_{on}[L]}{\rightleftharpoons}} P_L \tag{A.19}$$

One has to note that [L] is used in the literature instead of $[L_n]$ so the reported K_d is actually nK_d. The fluorescence intensity can be expressed as:

$$F(t) = a_0[1 - exp\,(-k_{app}t)] + a_1 \tag{A.20}$$

where a_0 and a_1 are constant and the apparent rate constant k_{app} is the sum of both directions:

$$k_{app} = k_{on}[L_n] + k_{off} \tag{A.21}$$

k_{app}can be obtained by fitting the kinetic curves. By changing the lipid concentration, the rate constant k_{on} and k_{off} can be determined. The dissociation constant K_d can be calculated as:

$$K_d = \frac{k_{off}}{k_{on}} \tag{A.22}$$

K_d can be used to calculate the binding free energy using the relationship shown above. The binding free energy calculated from the reported K_d is:

$$\Delta G_c^0 = RTlnK_d v_L \tag{A.23}$$

Surface plasmon resonance Another way to measure binding kinetics is surface plasmon resonance [325]. By injecting peptide solution to a membrane surface illuminated by surface plasmon polaritons, we can obtain the change in surface response with time during the association process. The kinetics of association is assumed to be two steps: 1) fast association with lipid. 2) peptide insertion into the membrane to form a tighter complex.

$$P_w + L_n \underset{k_{d1}}{\overset{k_{a1}}{\rightleftharpoons}} P_L \underset{k_{d2}}{\overset{k_{a2}}{\rightleftharpoons}} PL^* \tag{A.24}$$

The rate constants k_{a1}, k_{a2}, k_{d1}, k_{d2} can be calculated from the following differential equations:

$$\frac{(dR_1)}{dt} = k_{a1}[P](R_{max} - R_1 - R_2) - k_{d1}1R - k_{a2}R_1 + k_{d2}R_2 \tag{A.25}$$

$$\frac{dR_2}{dt} = k_{a2}R_1 - k_{d2}R_2 \tag{A.26}$$

where R_1, R_2, R_{max} are the surface response contributed by peptide lipid complex produced by first step, second and 100% peptide-lipid complex respectively. The dissociation constant of step 1 and step 2 are k_{d1}/k_{a1} and k_{d2}/k_{a2} respectively. The overall dissociation constant is the product of K_{d1} and K_{d2}. The overall dissociation constant can be used to calculate the binding free energy using Equation A.8.

Ultrafiltration or Reverse HPLC The peptide is mixed with lipid for sufficient time to allow full binding. Then the solution is centrifuged through a filter [326] or run through HPLC [327] where membrane and free peptide solution can be separated. The peptide concentration that remained in solution and bound to the membrane thus can be determined. In this method, the partition coefficient K_p is defined as:

$$K_p = \frac{[P_b]/v_w}{[P_f]/v_L} \tag{A.27}$$

Thus the binding free energy can be calculated as:

$$\Delta G_c^0 = -RTlnK_p + RTln\frac{v_L}{v_w} \tag{A.28}$$

Tryptophan time-resolved fluorescence Because the life-time (τ) of tryptophan fluorescent excited by a laser pulse is dependent on the surrounding environment, the τ measured in peptide-lipid mixtures has the following relationship with the fluorescence life time τ_w in water and τ_L in lipid [75]:

$$\tau = \frac{\tau_w + K_p v_L [L]_L}{1 + K_p v_L [L]} \tag{A.29}$$

where $K_p = \frac{n_b/(n_L v_L)}{n_f/(n_w v_w)}$. K_p can be obtained by fitting the above equation under different lipid concentration. Based on the definition, K_p is actually K_c. Thus the binding free energy can be calculated as:

$$\Delta G_c^0 = -RTlnK_p \tag{A.30}$$

EPR The resonance intensity can be used to calculate the bound peptide ratio $\lambda = n_b/n_f$. By titrating lipid into peptide solution, the partition coefficient K_c can be calculated from fitting the following equation [283]:

$$1/\lambda = \frac{1}{K_c v_L^{'}}(1/[L] - v_L) \tag{A.31}$$

in the above equation, $v_L^{'}$ is the effective molar volume available for peptide and can be defined as:

$$v_L^{'} = \frac{A_L(d/2)}{n_L N_a} \tag{A.32}$$

The obtained binding free energy is ΔG_c.

For all of the above experiments, because not all lipids of the vesicle are available for binding, the

actual peptide/lipid ratio R_b^* is higher than the measured value R_b. For SUV, the outer leaflet is about 60% of the total lipids, so the R_b^* should be $R_b/0.6$.The binding energy is 0.30 kcal/mol lower if this is not considered. This correction may not be valid if the peptide can translocate across the membrane. Unless there is strong evidence for translocation, we added 0.30 kcal/mol to the binding free energy values when this effect had not already been corrected in the experiments.

A.3. Theoretical methods

The binding energy can be estimated using several theoretical methods:

Hydrophobicity scale An empirical way to calculate the membrane binding free energy is to use a hydrophobic scale. The free energy contribution of transferring each amino acid from water to the POPC interface was determined by Wimley and White [328]. The transfer free energy of a peptide can thus be calculated as the sum of the contributions from all residues. This method utilizes the peptide sequence and thus neglects the effects of secondary and tertiary structure. The calculated values are not always in agreement with the measured binding free energy [285]. In this method the reported binding free energy is ΔG_x.

Binding free energy from the potential of mean force Umbrella sampling simulations can produce the binding free energy as a function of a reaction coordinate in MD simulations. The binding free energy is calculated by integration of the PMF curves [290, 292]:

$$\Delta G_c^0 = RTln([P_L])/([P_w]) = -RTln[\frac{1}{d}\int_0^d dz e^{-\frac{W(z)}{k_b T}}] \tag{A.33}$$

where z is the distance of the peptide center of mass from the membrane center and d is a cutoff for z that defines the membrane-bound state. A similar method was originallly proposed by Ben-Tal

et al. [329]:

$$\Delta G = -RTlnK \tag{A.34}$$

$$where\ K = CA_L N_A \int_0^\infty dz(e^{-\frac{W(z)}{k_b T}} - 1) \tag{A.35}$$

$A_L$is the area per lipid, N_A is the Avogadro constant, C is a unit conversion factor. In this equation, the K is actually K_x/[W], so the $\Delta G_c^0 = -RTlnK + RTlnv_L = \Delta G + RTlnv_L$.

This method was used to compute the binding free energy of lactoferricin to POPC [290] and POPG membrane [292], the binding free energy of protegrin to POPE/POPG(3:1) bilayers [294], the binding free energy of indolicidin to DMPC and DMPC/DMPG(3:1) bilayers [295], and the binding free energy of melittin to POPC bilayers [212] .

Starting from Equation A.35 one can express the standard free energy as the sum of the average effective energy relative to the bulk (<W>) and terms of the form plnp corresponding to translational and rotational entropy [236]. The entropic terms have been found to be rather small [280] . This allows a faster estimate of the membrane binding free energy by simple implicit solvent simulations without the need to compute the potential of mean force. This approach was followed in a calculation of pH-dependent membrane binding free energies [330].

B. Collected literature values for binding free energy

The listed experiments are carried out in temperature close to room temperature. Unless specifically stated, the room temperature is assumed to be 25°C. a-f, the conversion and correction done to the peptides. No conversion is needed for those articles reporting ΔG_c.

a. Converted from ΔG_{app}. With Gouy-Chapman correction, where in the parenthesis is the effective charge of the peptide and after the slash is the energy value with electrostatic interaction added back.

b. Converted from ΔG_{app}. The ΔG_{app} is measured at low peptide/lipid ratio. If present, the value inside the parenthesis is the peptide concentration at which the K_{app} was measured.

c. Converted from ΔG_a, which is independent of peptide concentration. $\Delta G_c = RTln(K_d v_L)$.

d. Converted from ΔG_a but considering the binding site size. $\Delta G_c = RTln(nK_d v_L)$. The binding site size n is in the parenthesis.

e. Converted from ΔG_x.

f. Monolayer correction applied, where the peptide is considered to bind only to the outer leaflet of the membrane (the effective lipid volume $V_L^{'}$=0.6V_L).

g. Interpolated.

In red font are the data used in Figure 5.1.

Peptide	Method	Membrane	Binding Energy ΔG_c^0 (kcal/mol)	Original Data	Ref
Magainin	ITC	POPC / POPG (75:25)	-2.54 (3.7-3.8)/-7.50a -5.72 (1 M)b	K_{app}=55.5M^{-1} K_{app}=1.2×$10^4 M^{-1}$	Wenk and Seelig [322]
	ITC	POPC SUV	-4.74a	K_{app}=2000 M^{-1} under 30°C	Wieprecht et al. [324]
	ITC	POPC/POPG 3:1		under 45°C	Wieprecht et al. [323]
		LUV	-3.14/-8.16a	K_{app}=110 M^{-1}	
		SUV	-2.64/-7.65a	K_{app}=50 M^{-1}	

Peptide	Method	Membrane	Binding Energy ΔG_c^0 (kcal/mol)	Original Data	Ref
	ITC	POPC/POPG (3:1)		under 23°C	Wieprecht et al. [331]
		SUV	-6.0b	K_{app}=2x10^4 M^{-1}	
		POPC SUV	-3.7b	K_{app}=400 M^{-1}	
	CD titration	POPC:POPG(3:1)	-5.98(0M)b	K_{app}=2×10^4 M^{-1}	Wieprecht et al. [119]
	Fluorescence Kinetics	POPC:POPG(1:1)	-7.99c	K_d=1.8 μM	Gregory et al. [204]
		POPC:POPG(7:3)	-6.23c	K_d=35 μM	
		POPC:POPG(8:2)	-5.56c	K_d=110 μM	
		POPC:POPG(9:1)	-4.84c	K_d=370 μM	
		POPC:POPG(10:0)	-3.30c	K_d=5000 μM	
I6A8L15I17 M2a	ITC	POPC SUV	-5.6a	K_{app}=7700 M^{-1} under 30°C	Wieprecht et al. [324]
I6V9W12T15I17 M2a	ITC	POPC SUV	-6.1a	K_{app}=20000 M^{-1} under 30°C	
I6L15 M2a	CD titration	POPC:POPG(3:1)	-6.11(0M)b	K_{app}=25000 M^{-1}	Wieprecht et al. [119]
L2R11A20 M2a		POPC:POPG(3:1)	-5.40(0M) b	K_{app}=7400 M^{-1}	
I6A8L15I17 M2a		POPC:POPG(3:1)	-6.96(0M) b	K_{app}=105000 M^{-1}	
PGLa	ITC LUV	POPC/POPG(3:1)	-4.5(5)/-11.1a	K_{app}=1500 M^{-1}	Wieprecht et al. [332]
		POPC	-4.1a	K_{app}=800 M^{-1} under 30°C	
Melittin	Surface potential measurement	Lethicin	-7.55(10mM Salt) -7.96(100mM Salt)f		Schoch and Sargent [333]
	CD	POPC/POPG(9:1)	-6.5(1.9)/-7.7 a,f	K_{app}=4.5×10^4 M^{-1}	Beschiaschvili and Seelig [288]
			-6.3 (0.77 M)b,f	K_{app}=3.19×10^4 M^{-1}	
		POPC/POPG(8:2)	-6.5/-8.2a,f	K_{app}=4.5×10^4 M^{-1}	
	Fluorescence NBD	POPC LUV200	-4.92(2.2)a,f	K_{app}=6×10^3 M^{-1}	Rex and Schwarz [216]
		LUV100	-4.82(1.5) a,f	K_{app}=5×10^3 M^{-1}	

Peptide	Method	Membrane	Binding Energy ΔG_c^0 (kcal/mol)	Original Data	Ref
		SUV	-5.16(1.2) a,f	K_{app}=9×10^3 M^{-1}	
		DOPC LUV200	-4.82(1.6) a,f	K_{app}=5×10^3 M^{-1}	
		LUV100	-5.01(1.3) a,f	K_{app}=7×10^3 M^{-1} under 30 ºC	
	Ultrafiltration	EPC	-5.1 e,f	ΔG_x=-7.6 kcal/mol	Allende et al. [326]
		EPC:PS(85:15)	-6.4 e,f	ΔG_x=-8.9 kcal/mol	
	Ultrafiltration	DOPC	-5.1 e,f	ΔG_x=-7.6 kcal/mol	Allende et al. [221]
	CD			ΔG_x= kcal/mol	Fernández-Vidal et al. [334]
		POPC/POPG(10:0)	-3.7e,f	-6.2	
		POPC/POPG(9:1)	-4.3(1.0)/-5.5 e,f	-6.8/-8.0	
		POPC/POPG(3:1)	-4.62/-6.0 e,f	-7.12/-8.5	
		POPC/POPG(1:1)	-5.0/-6.4 e,f	-7.5/-8.9	
Pardaxin	Fluorescence NBD-label	POPC	-6.21 b,f	K_{app}=3.3×10^4 M^{-1}	Rapaport and Shai [289]
Dermaseptin	Fluorescence NBD-label	PC	-5.28 b,f	K_{app}=6.6×10^3 M^{-1}	
		PC/PS(1:1)	-6.12 b,f	K_{app}=2.8×10^5 M^{-1}	
Dermaseptin S1	Surface Plasmon Resonance	PC	-6.47 c,f	K_d=14.29 μM	Pouny et al. [63]
		PC/PA(1:1)	-8.0 c,f	K_d=1.01 μM	
Dermaseptin S4		PC	-8.86 c,f	K_d=0.25 μM	Gaidukov et al. [325]
		PC/PA(1:1)	-9.64 c,f	K_d=0.067 μM	
K4K20-S4		PC/PA(1:1)	-9.68 c,f	K_d=0.0625 μM	
K4-S4(1-16)a		PC/PA(1:1)	-8.10 c,f	K_d=0.91 μM	
K4-S4(1-13)a		PC/PA(1:1)	-6.68 c,f	K_d=10 μM	
K4-S4(1-10)a		PC/PA(1:1)	-5.01 c,f	K_d=167 μM	

Peptide	Method	Membrane	Binding Energy ΔG_c^0 (kcal/mol)	Original Data	Ref
DD K	ITC	PC-LUVs	-3.97 (9.7) d,f	K_d=100 μM	Verly et al. [286]
CecropinP	Fluorescence NBD	PC	-5.98b,f	K_{app}=3.1×10^3 M^{-1}	Gazit et al. [66]
		PC/PS(1:1)	-6.78b,f	K_{app}=1.2×10^4 M^{-1}	
CecropinA	Fluorescence kinetics	POPC:POPG(1:1)	-8.88 c,f	K_d= 0.24 μM	Gregory et al. [320]
		POPC:POPG(7:3)	-5.66 c,f	K_d= 56 μM	
		POPC:POPG(8:2)	-5.03 c,f	K_d= 270 μM	
		POPC:POPG(10:0)	-3.95 c,f	K_d=1000 μM	
	Fluorescence Trp	POPC:POPA(8:2)	-5.92 (27.8) d,f	K_d=1.28 μM	Silvestro et al. [318]
δ -lysin	Fluorescence Kinetics	POPC	-6.0 c,f	K_d=30 μM	Clark et al. [285]
DL-1 δ –lysin D->K		POPC	-4.5 c,f	K_d=400 μM	
DL-2a		POPC	- 4.9 c,f	K_d=200 μM	
DL-2b		POPC	- 3.2 c,f	K_d=3400 μM	
CE-1		POPC	- 4.5 c,f	K_d=400 μM	
CE-2		POPC	- 3.0 c,f	K_d=4700 μM	
MG-1		POPC	-4.9 c,f	K_d=200 μM	
MG-2		POPC	-3.9 c,f	K_d=1100 μM	
Tp10W	Fluorescence Kinetics	POPC	- 5.1 c,f	K_d=140 μM	Almeida and Pokorny [284]
Tp10W-COO		POPC	- 4.9 c,f	K_d=200 μM	
Tp10-7MC		POPC	- 6.3 c,f	K_d=20 μM	
mastoparan X		POPC	-4.7 c,f	K_d=300 μM	
Alamethicin	EPR	DOPC	-5.77f	K_c=17100	Lewis and Cafiso [283]
Gramicidin S 14dK4	ITC LUV	POPC/POPG(3:1)	-6.2 (11.1) d	K_d=3.1 μM	Abraham et al. [96]
		POPC/POPS(3:1)	-6.5 (14.3)d	K_d=1.7 μM	
		POPG	-8.3 (5) d	K_d=22 μM	
		POPS	-7.6 (5.3)d	K_d=62 μM	
		POPC	-2.0 (166.7)d	K_d=278 μM	
CM15	Tryptophan time-resolved fluorescence	DMPC	-4.72	K_c=2.9x10^3	Bastos [75]

Peptide	Method	Membrane	Binding Energy ΔG_c^0 (kcal/mol)	Original Data	Ref
		DMPG	-5.49	K_c=1.06×10^4	
	EPR	POPE/POPG(8:2)	-4.86b,f	K_{app}=0.28×10^4 M^{-1}	Bhargava and Feix [335]
LL37(F27W)	Tryptophan fluorescence	SOPC	-6.16c,f	K_d=23.8 μM	Sood et al. [287]
		SOPC/POPG(9:1)	-8.44c,f	K_d=0.51 μM	
		SOPC/POPG(8:2)	-8.58c,f	K_d=0.40 μM	
		SOPC/POPG(7:3)	-8.79c,f,g		
		SOPC/POPG(6:4)	-9.29c,f	K_d=0.12 μM	
Indolicidin	ITC	POPC	-7.26c,f	ΔG_a=-7.4 kcal/mol	Andrushchenko et al. [74]
	LUV	E Coli lipid	-8.98c,f	ΔG_a=-9.12 kcal/mol	
	Reverse HPLC LUV	POPC	-6.3e,f	ΔG_x=-8.8 kcal/mol	Ladokhin et al. [327]
		POPG	-9.0e,f	ΔG_x=-11.5 kcal/mol	
Tritrpticin	ITC LUV	POPE/POPG (7:3)	-8.59 c,f	ΔG_a=-8.73 kcal/mol	Andrushchenko et al. [74]
		POPC	-5.63 c,f	ΔG_a=-5.77 kcal/mol	
		E Coli lipid	-8.14 c,f	ΔG_a=-8.28 kcal/mol	
Tritrp1		POPE/ POPG(7:3)	-9.86 c,f	ΔG_a=-10.0 kcal/mol	
		POPC	-6.75 c,f	ΔG_a=-6.89 kcal/mol	
Tritrp2		POPC	-5.28 c,f	ΔG_a=-5.42 kcal/mol	
Tritrp3		POPE/ POPG(7:3)	-9.09 c,f	ΔG_a=-9.23 kcal/mol	
		POPC	-6.99 c,f	ΔG_a=-7.13 kcal/mol	
LAP1	Fluorescence Trp	DMPC:DMPG 1:1	-6.47 (19.5) d,f	K_d=0.728 μM	Yamamoto and Tamura [319]
LAP2			-6.53 (22.0) d,f	K_d=0.581 μM	
LAP3			-6.19 (21.0) d,f	K_d=1.09 μM	
LAP4			-6.28 (21.8) d,f	K_d=0.898 μM	
LAP5			-7.63 (15.4) d,f	K_d=0.129 μM	

Peptide	Method	Membrane	Binding Energy ΔG_c^0 (kcal/mol)	Original Data	Ref
LAP6			-7.45 (15.4) d,f	K_d=0.175 μM	
KLA80	CD titration	POPC	-4.91b,f	K_{app}=5100 M^{-1}	Dathe et al. [336]
		POPG	-7.20 b,f	K_{app}=2.5×10^5 M^{-1}	
KLA100		POPG	-7.07 b,f	K_{app}=2 ×10^5 M^{-1}	
KLA120		POPC	-4.95 b,f	K_{app}=5500 M^{-1}	
		POPG	-7.13 b,f	K_{app}=2.2 ×10^5 M^{-1}	
KLA140		POPC	-5.14 b,f	K_{app}=7500 M^{-1}	
		POPG	-6.83 b,f	K_{app}=1.3×10^5 M^{-1}	
KLA160		POPC	-5.14 b,f	K_{app}=7500 M^{-1}	
		POPG	-7.02 b,f	K_{app}=1.8×10^5 M^{-1}	
KLA180		POPG	-6.83 b,f	K_{app}=1.3×10^5 M^{-1}	

C. Collected biological activity of antimicrobial peptides

minimum inhibitory concentrations(MIC) have been converted into μM. The colony formation unit (CFU, cell/ml) is the bacterial concentration at which bactericidal activity is measured. Hemolytic activity is described as the percentage of erythrocyte (RBC represents Red Blood Cell, hRBC is from human) lysis after treatment of certain concentration of the peptide and certain time (30min-3hr).

A) Peptides from arthropods.

* CecropinA-Magainin hybrid △ Built as ideal alpha-helix ? No data available NE No Effect.

PDB	Name	10% Anionic	30% Anionic	MIC(μM)			CFU	Hemolytic	Ref.
				G-		G+			
				E. Coli	P.A.	S. Aureus			
1f0d	CA(1−8)−MA(1−12)*	-9.3±2.2	-15.6±0.3	3.125	1.56	3.125	2×10^6	0%at100 μM 4% hRBC	Shin et al. [337]
1f0f	CA(1−8)−MA(1−12), G9I10G11 deletion*	-5.0±2.8	-9.5±1.5	6.25	3.125	3.125	2×10^6	0%at100 μM 4% hRBC	
1f0e	CA(1−8)−MA(1−12), G9I10G11 → P*	-5.5±0.5	-12.1±2.4	6.25	1.56	3.125	2×10^6	0%at100 μM 4% hRBC	
2jmy	CM15, CecropinA-Melittin hybrid	-10.5±0.9	-13.2±0.3	0.5-1	2-4	0.5-2	1×10^5	45%at64 μM 1% hRBC (1hr)	Sato and Feix [338, 339]
2mlt	Melittin	-16.4±0.6	-19.7±2.5	2,3.8	2	0.5	2×10^6	50%at1.7 μM 1×10^9 hRBC(1hr)	Zhu et al. [208], Pandey et al. [127]
	Cecropin A△	-15.5±1.4	-19.5±1.9	0.35	2.6	?	2×10^5	13%at 145 μM Sheep RBC	Andreu et al. [340], Steiner et al. [76]
1t51	IsCT	-8.5±1.1	-10.6±0.5	4	2	2	2×10^6	72%at50 μM 50%at18 μM 4% hRBC (1hr) 50%at70 μM (sheep RBC 1hr)	Lee et al. [341]
1t52	IsCT E7K	-9.6±0.5	-11.0±1.5	2	2	2	2×10^6	30%at50μM 4% hRBC	
1t54	IsCT W6A	-8.4±0.9	-9.9±0.5	64	32	64	2×10^6	5.0%at50 μM 4% hRBC	

PDB	Name	10% Anionic	30% Anionic	MIC(μM)			CFU	Hemolytic	Ref.
				G-		G+			
				E. Coli	P.A.	S. Aureus			
1t55	IsCT E7K, G8P, S11K	-9.2±0.6	-14.0±1.1	2	2	2	2×10^6	0.0%at50 μM 4% hRBC	
2pco	Latarcin 1	-2.1±0.5	-11.5±1.9	0.7,1.0	4.1	?	1×10^5	20%at80 μM 2×10^7 Rabbit RBC 3hr	Kozlov et al. [342], Vasilevskiĭ et al. [343]
2g9p	Latarcin 2a	-11.1±1.4	-17.2±1.6	0.5,0.7	6.7	?	1×10^5	50%at6 μM 20%at5 μM hRBC	Shlyapnikov et al. [344], Grishin et al. [345]
1zrw	Spinigerin	-9.8±1.8	-9.6±2.2	16	16	8	(2-4)$\times 10^6$	0%at100 μM 4% hRBC	Lee et al. [346]
1zrx	Stomoxyn	-7.8±0.4	-12.1±0.7	0.19-0.39	0.39-0.78	?	?	8%at100 μM 4% hRBC	Boulanger et al. [347]
2l3i	Oxyopinin 4a	-11.1±0.7	-17.1±0.6	0.5		10	?	50%at 7 μM	Dubovskii et al. [348]
1kv4	Moricin	-16.7±1.4	-21.3±3.3	0.31	0.81	0.21	?	?	Satoe et al. [349]
2jr8	Manduca Sexta Moricin	-10.8±0.7	-19.2±0.6	1.38		1.38-2.76	5×10^5		Dai et al. [350]
2k38	Cupiennin 1a	-11.0±0.5	-16.3±1.1	0.31-0.63	0.31-0.63	0.31-0.63	(1.7-3.8)$\times 10^5$	50%at24.4 μM	Kuhn-Nentwig et al. [351]
1d7n	Mastoparan M	-10.5±1.1	-12.0±1.6	4.22	4.22	2.11	1×10^5	10% at50 μM 1% sheep RBC 1hr	Li et al. [352], Murata et al. [353]
2czp	Mastoparan X	-5.9±0.8	-8.5±0.2					Visible at 9.6μM	Hirai et al. [354]

B) Peptides from amphibian skin secretions.

△ Built as ideal alpha-helix + Inconsistent values reported by different articles.

PDB	Name	10% Anionic	30% Anionic	MIC(μM)			CFU	Hemolytic	Ref.
				G-		G+			
				E. Coli	P.A.	S. Aureus			
1vm2	mutant peptide A2	-8.2±0.1	-9.4±0.2	250	?	?	1×10^6	?	Wang et al. [355]
1vm3	mutant peptide A3	-8.8±0.4	-9.4±0.1	NE	?	?	1×10^6	?	
1vm4	mutant peptide A4	-8.7±0.5	-10.3±0.1	100	?	?	1×10^6	?	
1vm5	Aurein 1.2	-9.1±0.8	-10.7±0.1	75	?	8	1×10^6	?	
1o53	Nontoxic membrane anchor E. coli enzyme IIA(Glucose)	-5.3±0.7	-7.4±0.9	NE	?	?	1×10^6	?	
2f3a	LLAA (LL-37 derived Aurein 1.2 analog)	-9.6±0.8	-13.0±0.3	20	?	?	1.8×10^6	?	Li et al. [356]
2jpy	Phylloseptin-H2	-13.9±0.5	-14.9±0.3	3.7	7.6	1.9	1×10^5	2.05%at64 μM hRBC(30min)	Bloch et al. [357], Bechinger et al. [358]
2jq0	Phylloseptin-H1	-10.3±0.2	-11.9±0.2	1.9	7.9	3.9	1×10^5	0.98%at32 μM hRBC(30min)	
2jq1	Phylloseptin-H3	-10.6±0.9	-11.7±0.1	4.1	8.2	4.1	1×10^5	?	
2g9l	Gaegurin -4	-14.7±0.9	-17.8±0.8	20.00	26.67		1×10^6	2%at100 μM 10% hRBC	Park et al. [359], Won et al. [360], Chi et al. [361]
2k10	Ranatuerin-2CSa	-15.4±1.3	-18.2±0.5	5	?	10	1×10^6	50%at150 μM 1×10^7 hRBC(1hr)	Conlon et al. [362], Subasinghage et al. [363]
2k9b	Dermadistinctin K	-5.0±2.2	-8.8±2.3	?	?	?	?	35%at46.7 μM Peritoneal cell(4hr)	Brand et al. [364]
	Dermaseptin-S1\triangle	-7.7±0.1	-11.2±1.2	12	>24	6	5×10^5	50%at>100μM 109 hRBC (30min) 50%at 12 μM hRBC(3hr)	Savoia et al. [365]
1xkm	Distinctin	-6.6±1.6	-9.5±0.5	14.5	28,29	28,29	1×10^4	No hemolysis upto 1mM	Batista et al. [366], Raimondo et al. [367]
2mag	Magainin 2	-7.6±0.6	-10.7±1.0	38+	76		(1-5)$\times10^5$	50%at430 μM 1.8x108 hRBC(30min)	Zasloff et al. [47], Wieprecht et al. [119]

C) Peptides from cathelicidin family.

+ Inconsistent values reported by different articles.

PDB	Name	10% Anionic	30% Anionic	MIC(μM)			CFU	Hemolytic	Ref.
				G-		G+			
				E. Coli	P.A.	S. Aureus			
1fry	SMAP-29(sheep cathelicidin)	-10.5±3.3	-17.0±0.6	0.25	1.25	0.5	(1.0-2.0)×10^5	19.4%at20 μM 10%hRBC	Skerlavaj et al. [368]
1hu5	Ovispirin-1	-12.1±1.2	-16.5±1.1	?	1.66	1	4×10^5	70.2% at 35 μM 5% hRBC 50% at 13.5 μM 3.5% hRBC 30min	Sawai et al. [369], Steinstraesser et al. [370], Eckert et al. [371], Jacobsen et al. [372]
1hu6	Novispirin G10	-7.6±2.5	-13.0±0.2	3.5	2.97	4.6	4×10^5	2.50%at 36 μM 5% hRBC 50% at 1470 M	
1hu7	Novispirin T7	-6.3±2.6	-11.4±0.4	?	4.64	3.3	4×10^5	10%at35 μM 5% hRBC	
2k6o	LL-37(human cathelicidin)+	-15.7±0.5	-19.1±1.9	27.8	27.8	55.6	1×10^5	50%at~75 μM 5% hRBC(1hr)	Bals et al. [373], Oren et al. [67]
2lmf	LL-27(LL-37 N terminus 1-27)	-5.1±2.0	-8.6±0.4	160		24			Wang et al. [374]
2f3a	LLAA(LL37 derived Aurein1.2 analog)	-9.6±0.8	-13.0±0.3	20	?	?	1.8×10^6	?	Li et al. [375]
2fbs	FK-13(LL37 core peptide)	-6.7±0.9	-10.1±1.0	40	?	?	2×10^6	?	Li et al. [375]
1lyp	CAP18 (rabbit)	-14.7±1.6	-25.2±1.5	2.5	5.0	>5.0(~20?)	5-10×10^3	0% upto 500 μM	Larrick et al. [376], Travis et al. [377]
2amn	Fowlicidin-1(chicken cathelicidin)	-8.8±1.0	-17.4±0.6	4.0	?	0.5	5×10^5	50%at6 μM 0.5% hRBC 2hr	Xiao et al. [378]
2gdl	Fowlicidin-2(chicken cathelicidin)	-6.3±3.0	-10.1±3.8	4-8	?	1	4×10^5	50%at100 μM hRBC	Xiao et al. [379]
2hfr	Fowlicidin-3(chicken cathelicidin)	-12.6±2.0	-13.6±1.6	2	?	1	4×10^5	50%at9 μM hRBC	Xiao et al. [379]

D) Miscellaneous peptides.

△ Built as ideal alpha-helix + Inconsistent values reported by different articles.

PDB	Name	10% Anionic	30% Anionic	MIC(μM)			CFU	Hemolytic	Ref.
				G-		G+			
				E. Coli	P.A.	S. Aureus			
1z64	Pleurocidin+	-8.2±0.6	-10.8±0.7	2.75	35	26.35	2×10^7	29%at50 μM 4% hRBC	Cole et al. [380], Yoshida et al. [381], Lee and Lee [382]
2jos	Piscidin 1	-11.6±0.7	-13.4±1.0	3.1	12.5	3.1	1×10^5	50%at12 μM 5% hRBC 30min	Silphaduang and Noga [383], Chekmenev et al. [384]
	Warnericin-RK△	-12.7±0.9	-13.3±0.3	20.0	20.0	20.0	1×10^6	50%at1.2 μM 1% hRBC 30min	Verdon et al. [385]
2kam	δ-hemolysin	-13.0±0.6	-14.1±0.4	NA	NA	NA	NA	50% at8-10 μM(guinea pig RBC 30min)	Dhople and Nagaraj [386], Verdon et al. [385]
1p0g	HP(2-20)	-7.6±0.8	-11.0±0.4	3.13,12.5	6.25	12.5	?	50% at ~150 μM (low salt buffer) 15% at 215 μM (high salt buffer)	Ribeiro and Medina-Acosta [387], Lee et al. [388]
1p0j	HP(2-20) Analog1	-8.6±0.4	-13.2±0.6	0.78,6.25	3.13	3.13			
1p0l	HP(2-20) Analog2	-7.4±0.6	-11.9±0.2	3.13,6.25	6.25	6.25			
1p0o	HP(2-20) Analog3	-8.2±1.3	-12.4±0.3	1.56,3.13	3.13	1.56,3.13		0% at 100μM 8% hRBC	
1amt	Alamethicin	-8.2±0.2	-8.0±0.2	7.64	?	?	?	50%at 30μM 1.8×10^8cell/ml hRBC(30min)	Wenschuh et al. [389], Dathe et al. [390]
1xc0	Pardaxin	-20.3±2.0	-22.7±2.8	13	25	?	1×10^6	50%at 50 μM 5% hRBC 30min	Rapaport and Shai [289], Oren and Shai [306]

D. List of peptide mechanisms

Peptide	Mechanism
CA-MA hybrid peptides	Possibly pore forming because of voltage induced conductance [391]. But membrane broke down after certain amount of time.
CM15	Osmoprotection reveals that the pore size in bacterial membranes is 2.2-3.8 nm in diameters [338].
Melittin	Pore forming in zwitterionic membrane (DTPC bilayer, R_{in}=21 Å, R_{out} =38.5 Å) [392] but detergent-like in anionic membranes [77, 393].
Cecropin A	Possibly ion channel because voltage-dependent single channel conductance is recorded [394].
Latarcins	Latarcin1 or Latarcin7 seems to form pore in DOPE/DOPG and DPhPC [342]. But the rest latarcins may adopt detergent-like mechanism [395]. Evidences are not solid though. Latarcin2a is pore-forming in erythrocyte membrane suggested by osmoprotection [396].
Oxyopinins	Oxt1 and 2a were suggested to form pore on PC vesicles but not on PA/PE vesicles [397]. Oxt4a has a Rana-box at the terminus which resembles the structure of C terminus of gaegurin-4 and ranatuerin-2CSa [348]. Pore mechanism is speculated.
Cupiennin 1a	Toroidal pore mechanism is suggested in anionic lipids [398] to explain the mobility of head groups but may also attack intra-cellular target(inhibits nitric oxide synthase)[399]. However, the effect of peptide on DMPC is different from the anionic lipids.
Mastoparan M	No information but Mastoparan-X forms pore [400].
Aurein 1.2	Surface active instead of pore formation [401].
Gaegurin -4	Pore forming indicated by the ion permeability experiment [402].
Ranatuerin-2CSa	No information available but the peptide has a structure quite similar to Gaegurin-4
Dermadistinctin K	Possibly toroidal pore [281]. ^{31}P NMR line shape can only be explained if 50% head groups are randomly aligned and 50% head groups are oriented 2-30o
Dermaseptin-S1	Suggested to be detergent-like because it only induces leakage at extremely high peptide/lipid ratio [63].
Magainin 2	Form toroidal pore in both neutral(DMPC) and anionic membranes [175]. It may adopt detergent-like mechanism in eukaryotic cell membranes [110].
SMAP-29	Possibly pore forming [403]. But no actual evidence was given.
Ovispirin	It orient predominately parallel to the membrane surface, thus is considered to be adopting carpet mechanism [404].

Peptide	Mechanism
LL-37	Previously suggested to be ”carpet” mechanism because it orients parallel to membrane surface [67]. The pore structure in DOPC/DOPE bilayers is however determined from neutron diffraction [177]. The radius of the pore is 23-33 Å.
CAP18	Formation of transient lesions under voltage [405]. Possibly pore forming.
Fowlicidin	Fowl-1 aggregates in membrane mimicking solvents [406]. But no actual evidence for pore formation.
Indolicidin	Tryptophan location indicates “Carpet” model on PC membranes [407] but with increased fraction of PG in the membrane, indolicidin starts to order the lipid acyl chains and this may be an indication of pore formation [408].
Human granulysin	Possibly intra-cellular pathways [409] because cell died in apoptotic but not necrotic ways.
Pleurocidin	Indicated by dye release experiment, it forms pore like magainin [381].
Piscidin 1	Single channel experiments indicate toroidal pore [410].
Warnericin-RK	Osmotic protection show that the pore in erythrocyte membranes can be as large as 5.7nm in diameter [411]. The author suggested that pore formation is not likely to be stable.
δ-hemolysin	Crystal structure shows that the pore is formed by 6-8 peptides [412].
HP(2-20)	Generates size dependent dype release in osmoprotection experiment for both PC and PG vesicles [413]. Supporting pore forming mechanism.
Alamethicin	Barrel-stave pore in DLPC membrane [414].
Pardaxin	Voltage induced multi-level channel in neutral membrane [415]. However, it is suggested to adopt detergent-like mechanism in the presence of PG [308].

E. Transfer energy from planar membrane to pores

cyl: cylindrical pores. tor: toroidal pores.

Peptide	ΔΔW(cyl-planar)			ΔΔW(tor-planar)		
	30% Anionic	10% Anionic	Neutral	30% Anionic	10% Anionic	Neutral
1amt	-3.3±1.3	-3.1±1.5	-2.4±0.5	-4.4±0.5	-3.1±0.9	-3.4±0.3
1d7n	1.3±0.6	-1.7±1.0	-0.7±1.2	-2.3±0.8	-3.9±0.9	-2.7±1.6
1f0d	1.9±1.5	2.8±1.0	-0.8±2.5	-2.8±2.7	-0.8±2.3	-2.8±2.0
1f0e	2.0±2.2	2.7±2.9	-0.5±3.4	-3.7±2.3	-3.4±2.1	-3.6±3.0
1f0f	1.7±1.9	2.6±0.8	-3.6±0.5	-5.0±2.0	-2.4±1.0	-5.4±0.9
1fry	3.7±2.5	2.6±4.0	-2.4±4.7	-3.7±4.3	-4.2±3.0	-2.2±3.7
1hu5	3.4±5.2	-0.5±1.1	-1.1±1.9	-6.3±3.7	-1.8±7.7	-6.8±1.2
1hu6	1.0±2.4	-1.0±1.6	-1.2±2.5	-4.9±1.4	-5.1±1.4	-5.1±2.6
1hu7	2.0±2.0	-0.4±1.2	-2.6±2.9	-4.9±2.0	-5.2±1.4	-6.3±2.5
1kv4	4.5±2.8	1.5±3.3	0.2±1.3	-4.7±2.7	-1.6±6.8	-5.6±1.7
1lyp	13.8±1.2	12.1±1.8	3.1±1.2	-1.3±1.8	-0.4±2.3	-7.5±1.6
1o53	-6.6±1.3	1.1±0.8	-2.8±1.2	-2.6±0.6	-1.9±0.8	-4.8±0.7
1p0g	3.6±1.3	1.2±2.4	-0.2±1.8	-6.3±0.8	-2.8±1.3	-4.1±1.5
1p0j	2.7±3.0	-0.6±1.2	-2.4±0.4	-5.7±1.3	-5.0±0.6	-5.2±0.4
1p0l	1.7±2.8	-0.5±0.9	-1.9±0.8	-5.3±2.1	-4.9±0.7	-5.2±0.7
1p0o	2.1±2.5	-2.1±1.1	-0.2±1.7	-7.3±1.6	-6.0±0.3	-6.1±1.3
1t51	-1.8±1.8	0.9±1.7	-1.5±1.2	-1.0±0.8	-1.5±1.5	-2.7±1.5
1t52	2.6±0.8	2.0±1.0	-0.9±1.0	-2.2±1.3	-2.4±0.9	-3.7±0.9
1t54	1.5±0.9	0.5±1.0	-1.4±1.4	-2.6±0.3	-1.9±1.4	-2.8±0.9
1t55	6.1±1.3	1.7±0.3	-1.9±1.4	-1.5±1.2	-0.9±0.8	-3.2±1.0
1vm2	-1.7±1.1	-0.4±0.5	-2.1±0.4	-4.2±0.5	-2.5±0.5	-4.4±0.3
1vm3	-0.1±0.3	-2.0±1.0	-2.1±0.4	-3.1±0.3	-2.9±0.8	-4.2±0.4
1vm4	-0.6±0.5	-1.5±0.7	-2.7±0.5	-3.8±0.5	-3.9±1.1	-4.2±0.8
1vm5	-1.3±0.4	-1.0±0.9	-1.9±0.8	-3.4±0.4	-2.5±0.6	-3.8±0.8
1xc0	11.3±2.3	1.2±2.5	3.3±2.1	-3.3±2.7	1.9±2.8	2.1±1.7
1xkm	-8.2±3.5	4.3±2.1	-1.8±2.0	-2.1±2.9	-0.1±1.7	-4.0±1.8
1z64	4.4±1.6	2.6±2.2	-1.2±1.9	-1.2±0.5	0.0±0.7	-2.0±0.9
1zrw	-1.4±4.3	-1.3±4.0	-1.6±4.2	-6.4±5.5	-11.1±3.4	-5.0±4.1
1zrx	1.5±1.8	3.3±1.3	-1.9±1.7	-3.0±2.8	-1.3±3.1	-2.5±2.1
2amn	4.9±2.9	-0.2±2.9	-2.4±4.2	-4.1±3.8	-4.5±3.6	-6.0±1.7
2czp	-4.9±5.0	1.1±0.5	-2.1±0.9	-1.1±0.7	-2.0±0.6	-3.6±1.1
2f3a	3.1±1.2	0.7±0.9	-1.0±1.6	-5.3±1.4	-2.3±0.8	-4.3±0.9
2fbs	1.5±0.9	0.0±1.8	-2.4±1.2	-5.4±0.5	-4.1±1.2	-4.5±1.3

Peptide	ΔΔW(cyl-planar)			ΔΔW(tor-planar)		
	30% Anionic	10% Anionic	Neutral	30% Anionic	10% Anionic	Neutral
2g9l	6.4±2.6	3.4±1.2	1.1±1.3	-4.3±4.2	-1.6±2.3	-3.4±1.4
2g9p	1.5±1.2	0.9±3.1	0.7±4.1	-4.4±1.0	-3.9±2.3	-3.7±1.5
2gdl	0.7±3.1	2.4±3.8	-2.5±2.7	-1.8±3.5	-0.7±5.1	-3.1±2.9
2hfr	6.6±3.7	-2.8±3.5	-2.8±2.3	-4.5±4.3	-4.3±3.8	-3.1±2.1
2jmy	0.4±0.9	2.4±1.1	-1.8±1.1	-4.7±0.4	-3.9±0.6	-4.2±0.9
2jos	1.2±2.8	0.8±3.2	1.8±2.0	-3.0±0.9	-2.2±1.3	-4.1±0.7
2jpy	0.0±1.1	-1.6±0.6	-0.8±1.0	-2.9±1.0	-1.4±0.6	-3.5±0.6
2jq0	-3.3±0.7	-0.5±1.8	-1.8±1.0	-2.8±1.1	-2.0±0.9	-3.1±2.4
2jq1	-1.0±0.9	-0.8±1.6	-1.3±1.1	-2.6±1.1	-2.1±0.8	-4.8±0.8
2jr8	7.1±2.6	4.2±3.3	-2.6±1.1	-2.5±1.4	-3.5±2.2	-6.2±1.7
2k10	6.8±2.0	3.0±1.1	-0.5±5.4	-3.1±1.2	-2.4±0.5	-4.5±1.3
2k38	0.6±1.7	2.9±3.1	-2.0±1.1	-0.7±3.9	-2.5±3.3	-4.0±2.6
2k6o	8.8±1.4	7.3±2.7	2.4±3.5	-2.9±2.2	-3.8±4.1	-1.0±4.6
2k9b	1.3±3.0	3.7±1.5	-1.6±2.5	-1.7±1.4	-2.3±1.6	-3.6±2.6
2kam	6.2±0.8	-3.0±1.8	-1.0±2.0	-5.5±1.8	-3.0±1.5	-2.3±0.9
2l3i	3.5±4.7	5.8±3.6	0.7±3.2	-6.0±3.1	-1.0±4.4	-4.5±2.9
2lmf	-4.3±2.9	2.5±1.4	-0.3±2.2	-2.8±2.0	-1.7±3.4	-3.8±3.1
2mag	3.6±1.9	0.6±1.3	-3.1±2.4	-3.5±2.8	-2.8±1.4	-6.0±0.7
2mlt	9.3±2.0	-2.7±2.2	-0.5±3.3	-5.4±1.2	-5.3±2.5	-3.0±3.0
2pco	-2.6±2.2	0.1±3.3	-2.8±1.9	-4.6±3.1	-7.1±3.0	-6.6±1.5

Bibliography

[1] Yeaman, M. R., and Yount, N. Y. (2003) Mechanisms of Antimicrobial Peptide Action and Resistance. *Pharmacological Reviews 55*, 27–55.

[2] Kaiser, E. T., and Kézdy, F. J. (1983) Secondary structures of proteins and peptides in amphiphilic environments. (A review). *Proceedings of the National Academy of Sciences 80*, 1137–1143.

[3] King, G. F. (2011) Venoms as a platform for human drugs: translating toxins into therapeutics. *Expert Opinion on Biological Therapy 11*, 1469–1484.

[4] Heitz, F., Morris, M. C., and Divita, G. (2009) Twenty years of cell-penetrating peptides: from molecular mechanisms to therapeutics. *British Journal of Pharmacology 157*, 195–206.

[5] Epand, R. M. (2003) Fusion peptides and the mechanism of viral fusion. *Biochimica et Biophysica Acta (BBA) - Biomembranes 1614*, 116–121.

[6] Kiyota, T., Lee, S., and Sugihara, G. (1996) Design and Synthesis of Amphiphilic -Helical Model Peptides with Systematically Varied Hydrophobic−Hydrophilic Balance and Their Interaction with Lipid- and Bio-Membranes. *Biochemistry 35*, 13196–13204.

[7] Holt, A., and Killian, J. A. (2010) Orientation and dynamics of transmembrane peptides: the power of simple models. *European Biophysics Journal 39*, 609–621.

[8] Gordon-Grossman, M., Zimmermann, H., Wolf, S. G., Shai, Y., and Goldfarb, D. (2012) Investigation of Model Membrane Disruption Mechanism by Melittin using Pulse Electron Paramagnetic Resonance Spectroscopy and Cryogenic Transmission Electron Microscopy. *The Journal of Physical Chemistry B 116*, 179–188.

[9] Park, C. B., Yi, K.-S., Matsuzaki, K., Kim, M. S., and Kim, S. C. (2000) Structure–activity analysis of buforin II, a histone H2A-derived antimicrobial peptide: The proline hinge is responsible for the cell-penetrating ability of buforin II. *Proceedings of the National Academy of Sciences 97*, 8245–8250.

[10] Gandhi, C. S., Clark, E., Loots, E., Pralle, A., and Isacoff, E. Y. (2003) The orientation and molecular movement of a k(+) channel voltage-sensing domain. *Neuron 40*, 515–25, 3.

[11] Shenkarev, Z. O., Paramonov, A. S., Lyukmanova, E. N., Shingarova, L. N., Yakimov, S. A., Dubinnyi, M. A., Chupin, V. V., Kirpichnikov, M. P., Blommers, M. J., and Arseniev, A. S. (2010) NMR structural and dynamical investigation of the isolated voltage-sensing domain of the potassium channel KvAP: implications for voltage gating. *J Am Chem Soc 132*, 5630–7, 16.

[12] Bechinger, B. (1999) The structure, dynamics and orientation of antimicrobial peptides in membranes by multidimensional solid-state NMR spectroscopy. *Biochimica et Biophysica Acta (BBA) - Biomembranes 1462*, 157–183.

[13] Strandberg, E., Esteban-Martín, S., Ulrich, A. S., and Salgado, J. (2012) Hydrophobic mismatch of mobile transmembrane helices: Merging theory and experiments. *Biochimica et Biophysica Acta (BBA) - Biomembranes 1818*, 1242–1249.

[14] Mouritsen, O. G., and Bloom, M. (1984) *BIOPHYSICAL JOURNAL Mattress model of lipid-protein interactions in membranes*, 141–153.

[15] Weiss, T. M., van der Wel, P. C. A., Killian, J. A., Koeppe, R. E., and Huang, H. W. (2003) Hydrophobic Mismatch between Helices and Lipid Bilayers. *Biophysical Journal 84*, 379–385.

[16] Schäfer, L. V., Jong, D. H. d., Holt, A., Rzepiela, A. J., Vries, A. H. d., Poolman, B., Killian, J. A., and Marrink, S. J. (2011) Lipid packing drives the segregation of transmembrane helices into disordered lipid domains in model membranes. *Proceedings of the National Academy of Sciences 108*, 1343–1348.

[17] Marassi, F. M., and Opella, S. J. (2000) A Solid-State NMR Index of Helical Membrane Protein Structure and Topology. *Journal of Magnetic Resonance 144*, 150–155.

[18] Wang, J., Denny, J., Tian, C., Kim, S., Mo, Y., Kovacs, F., Song, Z., Nishimura, K., Gan, Z., Fu, R., Quine, J. R., and Cross, T. A. (2000) Imaging Membrane Protein Helical Wheels. *Journal of Magnetic Resonance 144*, 162–167.

[19] van der Wel, P. C. A., Strandberg, E., Killian, J. A., and Koeppe, R. E. *Biophysical Journal*; 2002; pp 1479–1488.

[20] Strandberg, E., Özdirekcan, S., Rijkers, D. T., van der Wel, P. C., Koeppe II, R. E., Liskamp, R. M., and Antoinette Killian, J. (2004) Tilt Angles of Transmembrane Model Peptides in Oriented and Non-Oriented Lipid Bilayers as Determined by 2H Solid-State NMR. *Biophysical Journal 86*, 3709–3721.

[21] Dürr, U. H., Waskell, L., and Ramamoorthy, A. (2007) The cytochromes P450 and b5 and their reductases—Promising targets for structural studies by advanced solid-state NMR spectroscopy. *Biochimica et Biophysica Acta (BBA) - Biomembranes 1768*, 3235–3259.

[22] Burnett, L. J., and Muller, B. H. (1971) Deuteron Quadrupole Coupling Constants in Three Solid Deuterated Paraffin Hydrocarbons: C2D6, C4D10, C6D14. *The Journal of Chemical Physics 55*, 5829–5831.

[23] Killian, J. A., Taylor, M. J., and Koeppe, R. E. (1992) Orientation of the valine-1 side chain of the gramicidin transmembrane channel and implications for channel functioning. A 2H NMR study. *Biochemistry 31*, 11283–90, 46.

[24] Bechinger, B., Resende, J. M., and Aisenbrey, C. (2011) The structural and topological analysis of membrane-associated polypeptides by oriented solid-state NMR spectroscopy: Established concepts and novel developments. *Biophysical Chemistry 153*, 115–125.

[25] Venturoli, M., Smit, B., and Sperotto, M. M. (2005) Simulation studies of protein-induced bilayer deformations, and lipid-induced protein tilting, on a mesoscopic model for lipid bilayers with embedded proteins. *Biophys J 88*, 1778–98, 3.

[26] Kandasamy, S. K., and Larson, R. G. (2006) Molecular Dynamics Simulations of Model Trans-Membrane Peptides in Lipid Bilayers: A Systematic Investigation of Hydrophobic Mismatch. *Biophysical Journal 90*, 2326–2343.

[27] Koehorst, R. B., Spruijt, R. B., Vergeldt, F. J., and Hemminga, M. A. (2004) Lipid Bilayer Topology of the Transmembrane -Helix of M13 Major Coat Protein and Bilayer Polarity Profile by Site-Directed Fluorescence Spectroscopy. *Biophysical Journal 87*, 1445–1455.

[28] Duong-Ly, K. C., Nanda, V., DeGrado, W. F., and Howard, K. P. (2005) The conformation of the pore region of the M2 proton channel depends on lipid bilayer environment. *Protein Science 14*, 856–861.

[29] Ramamoorthy, A., Kandasamy, S. K., Lee, D.-K., Kidambi, S., and Larson, R. G. (2007) Structure, Topology, and Tilt of Cell-Signaling Peptides Containing Nuclear Localization Sequences in Membrane Bilayers Determined by Solid-State NMR and Molecular Dynamics Simulation Studies. *Biochemistry 46*, 965–975.

[30] Park, S. H., and Opella, S. J. (2005) Tilt Angle of a Trans-membrane Helix is Determined by Hydrophobic Mismatch. *Journal of Molecular Biology 350*, 310–318.

[31] Petrache, H. I., Zuckerman, D. M., Sachs, J. N., Killian, J. A., Koeppe, R. E., and Woolf, T. B. *Langmuir*; 2002; pp 1340–1351.

[32] Özdirekcan, S., Rijkers, D. T. S., Liskamp, R. M. J., and Killian, J. A. (2005) Influence of Flanking Residues on Tilt and Rotation Angles of Transmembrane Peptides in Lipid Bilayers. A Solid-State 2H NMR Study. *Biochemistry 44*, 1004–1012.

[33] Vostrikov, V. V., Grant, C. V., Daily, A. E., Opella, S. J., and Koeppe, R. E. (2008) Comparison of "Polarization Inversion with Spin Exchange at Magic Angle" and "Geometric Analysis of Labeled Alanines" Methods for Transmembrane Helix Alignment. *Journal of the American Chemical Society 130*, 12584–12585.

[34] Esteban-Martín, S., Strandberg, E., Fuertes, G., Ulrich, A. S., and Salgado, J. (2009) Influence of Whole-Body Dynamics on 15N PISEMA NMR Spectra of Membrane Proteins: A Theoretical Analysis. *Biophysical Journal 96*, 3233–3241.

[35] Esteban-Martín, S., Strandberg, E., Salgado, J., and Ulrich, A. S. (2010) Solid state NMR analysis of peptides in membranes: Influence of dynamics and labeling scheme. *Biochimica et Biophysica Acta (BBA) - Biomembranes 1798*, 252–257.

[36] Grage, S. L., Strandberg, E., Wadhwani, P., Esteban-Martín, S., Salgado, J., and Ulrich, A. S. (2012) Comparative analysis of the orientation of transmembrane peptides using solid-state 2H- and 15N-NMR: mobility matters. *European Biophysics Journal 41*, 475–482.

[37] Holt, A., Koehorst, R. B., Rutters-Meijneke, T., Gelb, M. H., Rijkers, D. T., Hemminga, M. A., and Killian, J. A. (2009) Tilt and Rotation Angles of a Transmembrane Model Peptide as Studied by Fluorescence Spectroscopy. *Biophysical Journal 97*, 2258–2266.

[38] Im, W., Lee, J., Kim, T., and Rui, H. (2009) Novel free energy calculations to explore mechanisms and energetics of membrane protein structure and function. *Journal of Computational Chemistry 30*, 1622–1633.

[39] Kim, T., and Im, W. (2010) Revisiting Hydrophobic Mismatch with Free Energy Simulation Studies of Transmembrane Helix Tilt and Rotation. *Biophysical Journal 99*, 175–183.

[40] Esteban-Martin, S., Str, E., berg„ Fuertes, G., Ulrich, A. S., and Salgado, J. (2009) Experiments Meet Hydrophobic Mismatch: A Re-evaluation Of The Orientation Of Model Transmembrane Peptides From Solid-State NMR. *Biophysical Journal 96*, 159a.

[41] Jo, S., and Im, W. (2011) Transmembrane Helix Orientation and Dynamics: Insights from Ensemble Dynamics with Solid-State NMR Observables. *Biophysical Journal 100*, 2913–2921.

[42] Im, W., Jo, S., and Kim, T. (2012) An ensemble dynamics approach to decipher solid-state NMR observables of membrane proteins. *Biochimica et Biophysica Acta (BBA) - Biomembranes 1818*, 252–262.

[43] Mcphee, J. B., and Hancock, R. E. W. (2005) Function and therapeutic potential of host defence peptides. *Journal of Peptide Science 11*, 677–687.

[44] Nizet, V. (2006) Antimicrobial peptide resistance mechanisms of human bacterial pathogens. *Current issues in molecular biology 8*, 11–26, PMID: 16450883.

[45] Csordás, A., and Michl, H. (1970) Isolierung und Strukturaufklärung eines hämolytisch wirkenden Polypeptides aus dem Abwehrsekret europäischer Unken. *Monatshefte für Chemie / Chemical Monthly 101*, 182–189.

[46] Soravia, E., Martini, G., and Zasloff, M. (1988) Antimicrobial properties of peptides from Xenopus granular gland secretions. *FEBS Letters 228*, 337–340.

[47] Zasloff, M., Martin, B., and Chen, H. C. (1988) Antimicrobial activity of synthetic magainin peptides and several analogues. *Proceedings of the National Academy of Sciences of the United States of America 85*, 910–913, 3.

[48] Cruciani, R. A., Barker, J. L., Zasloff, M., Chen, H. C., and Colamonici, O. (1991) Antibiotic magainins exert cytolytic activity against transformed cell lines through channel formation. *Proceedings of the National Academy of Sciences 88*, 3792–3796.

[49] Cruciani, R. A., Barker, J. L., Durell, S. R., Raghunathan, G., Robert Guy, H., Zasloff, M., and Stanley, E. F. (1992) Magainin 2, a natural antibiotic from frog skin, forms ion channels in lipid bilayer membranes. *European Journal of Pharmacology: Molecular Pharmacology 226*, 287–296.

[50] Matsuzaki, K., Mitani, Y., Akada, K.-y., Murase, O., Yoneyama, S., Zasloff, M., and Miyajima, K. (1998) Mechanism of Synergism between Antimicrobial Peptides Magainin 2 and PGLa. *Biochemistry 37*, 15144–15153.

[51] Selsted, M. E., and Ouellette, A. J. (2005) Mammalian defensins in the antimicrobial immune response. *Nature Immunology 6*, 551–557.

[52] Zanetti, M., Gennaro, R., and Romeo, D. (1997) The Cathelicidin Family of Antimicrobial Peptide Precursors: A Component of the Oxygen-Independent Defense Mechanisms of Neutrophilsa. *Annals of the New York Academy of Sciences 832*, 147–162.

[53] Wang, G., Li, X., and Wang, Z. (2009) APD2: the updated antimicrobial peptide database and its application in peptide design. *Nucleic Acids Research 37*, D933–D937.

[54] Miteva, M., Andersson, M., Karshikoff, A., and Otting, G. (1999) Molecular electroporation: a unifying concept for the description of membrane pore formation by antibacterial peptides, exemplified with NK-lysin. *FEBS Letters 462*, 155–158.

[55] Linde, C. M. A., Grundström, S., Nordling, E., Refai, E., Brennan, P. J., and Andersson, M. (2005) Conserved Structure and Function in the Granulysin and NK-Lysin Peptide Family. *Infection and Immunity 73*, 6332–6339, PMID: 16177304 PMCID: 1230960.

[56] Teixeira, V., Feio, M. J., and Bastos, M. (2012) Role of lipids in the interaction of antimicrobial peptides with membranes. *Progress in Lipid Research 51*, 149–177.

[57] Yang, S.-T., Yub Shin, S., Kim, Y.-C., Kim, Y., Hahm, K.-S., and Kim, J. I. (2002) Conformation-dependent antibiotic activity of tritrpticin, a cathelicidin-derived antimicrobial peptide. *Biochemical and Biophysical Research Communications 296*, 1044–1050.

[58] Park, C. B., Kim, H. S., and Kim, S. C. (1998) Mechanism of action of the antimicrobial peptide buforin II: buforin II kills microorganisms by penetrating the cell membrane and inhibiting cellular functions. *Biochem Biophys Res Commun 244*, 253–7, 1.

[59] Nicolas, P. (2009) Multifunctional host defense peptides: intracellular-targeting antimicrobial peptides. *FEBS Journal 276*, 6483–6496.

[60] Matsuzaki, K., Murase, O., Fujii, N., and Miyajima, K. (1995) Translocation of a Channel-Forming Antimicrobial Peptide, Magainin 2, across Lipid Bilayers by Forming a Pore. *Biochemistry 34*, 6521–6526.

[61] Matsuzaki, K., Murase, O., Fujii, N., and Miyajima, K. (1996) An Antimicrobial Peptide, Magainin 2, Induced Rapid Flip-Flop of Phospholipids Coupled with Pore Formation and Peptide Translocation. *Biochemistry 35*, 11361–11368.

[62] Matsuzaki, K., Yoneyama, S., and Miyajima, K. (1997) Pore formation and translocation of melittin. *Biophysical Journal 73*, 831–838.

[63] Pouny, Y., Rapaport, D., Mor, A., Nicolas, P., and Shai, Y. (1992) Interaction of antimicrobial dermaseptin and its fluorescently labeled analogs with phospholipid membranes. *Biochemistry 31*, 12416–12423.

[64] Strahilevitz, J., Mor, A., Nicolas, P., and Shai, Y. (1994) Spectrum of Antimicrobial Activity and Assembly of Dermaseptin-b and Its Precursor Form in Phospholipid Membranes. *Biochemistry 33*, 10951–10960.

[65] Ghosh, J. K., Shaool, D., Guillaud, P., Cicéron, L., Mazier, D., Kustanovich, I., Shai, Y., and Mor, A. (1997) Selective Cytotoxicity of Dermaseptin S3 toward IntraerythrocyticPlasmodium falciparum and the Underlying Molecular Basis. *Journal of Biological Chemistry 272*, 31609–31616.

[66] Gazit, E., Boman, A., Boman, H. G., and Shai, Y. (1995) Interaction of the Mammalian Antibacterial Peptide Cecropin P1 with Phospholipid Vesicles. *Biochemistry 34*, 11479–11488.

[67] Oren, Z., Lerman, J. C., Gudmundsson, G. H., Agerberth, B., and Shai, Y. (1999) Structure and organization of the human antimicrobial peptide LL-37 in phospholipid membranes: relevance to the molecular basis for its non-cell-selective activity. *Biochemical Journal 341*, 501.

[68] Wong, H., Bowie, J. H., and Carver, J. A. (1997) The Solution Structure and Activity of Caerin 1.1, an Antimicrobial Peptide from the Australian Green Tree Frog, Litoria Splendida. *European Journal of Biochemistry 247*, 545–557.

[69] Monaco, V., Formaggio, F., Crisma, M., Toniolo, C., Hanson, P., and Millhauser, G. L. (1999) Orientation and immersion depth of a helical lipopeptaibol in membranes using TOAC as an ESR probe. *Biopolymers 50*, 239–253.

[70] Oren, Z., and Shai, Y. (1997) Selective Lysis of Bacteria but Not Mammalian Cells by Diastereomers of Melittin: Structure−Function Study. *Biochemistry 36*, 1826–1835.

[71] Shai, Y., and Oren, Z. (1996) Diastereomers of Cytolysins, a Novel Class of Potent Antibacterial Peptides. *Journal of Biological Chemistry 271*, 7305–7308, 13.

[72] Matsuzaki, K., Fukui, M., Fujii, N., and Miyajima, K. (1993) Permeabilization and morphological changes in phosphatidylglycerol bilayers induced by an antimicrobial peptide, tachyplesin I. *Colloid and Polymer Science 271*, 901–908.

[73] Melo, M. N., and Castanho, M. A. (2007) Omiganan interaction with bacterial membranes and cell wall models. Assigning a biological role to saturation. *Biochimica et Biophysica Acta (BBA) - Biomembranes 1768*, 1277–1290.

[74] Andrushchenko, V. V., Aarabi, M. H., Nguyen, L. T., Prenner, E. J., and Vogel, H. J. (2008) Thermodynamics of the interactions of tryptophan-rich cathelicidin antimicrobial peptides with model and natural membranes. *Biochimica et Biophysica Acta (BBA) - Biomembranes 1778*, 1004–1014.

[75] Bastos, M. (2008) Energetics and Partition of Two Cecropin-Melittin Hybrid Peptides to Model Membranes of Different Composition . *Biophysical Journal 94*, 2128–2141.

[76] Steiner, H., Andreu, D., and Merrifield, R. (1988) Binding and action of cecropin and cecropin analogues: Antibacterial peptides from insects. *Biochimica et Biophysica Acta (BBA) - Biomembranes 939*, 260–266.

[77] Bechinger, B., and Lohner, K. (2006) Detergent-like actions of linear amphipathic cationic antimicrobial peptides. *Biochimica et Biophysica Acta (BBA) - Biomembranes 1758*, 1529–1539.

[78] Madden, T., and Cullis, P. (1982) Stabilization of bilayer structure for unsaturated phosphatidylethanolamines by detergents. *Biochimica et Biophysica Acta (BBA) - Biomembranes 684*, 149–153.

[79] Müller, K., Lipka, G., Lohner, K., and Laggner, P. (1985) The effect of the detergent cetyltrimethylammoniumchloride on the phase behaviour of dipalmitoylphosphatidylcholine: A high precision calorimetric study. *Thermochimica Acta 94*, 187–197.

[80] Posch, M., Rakusch, U., Mollay, C., and Laggner, P. (1983) Cooperative effects in the interaction between melittin and phosphatidylcholine model membranes. Studies by temperature scanning densitometry. *Journal of Biological Chemistry 258*, 1761–1766.

[81] Colotto, A., Lohner, K., and Laggner, P. In *Trends in Colloid and Interface Science VI*; Helm, C., Lösche, M., and Möhwald, H., Eds.; Progress in Colloid & Polymer Science 89; Steinkopff, 1992; pp 334–334.

[82] Dufourcq, J., Faucon, J.-F., Fourche, G., Dasseux, J.-L., Le Maire, M., and Gulik-Krzywicki, T. (1986) Morphological changes of phosphatidylcholine bilayers induced by melittin: vesicularization, fusion, discoidal particles. *Biochimica et Biophysica Acta (BBA) - Biomembranes 859*, 33–48.

[83] Monette, M., and Lafleur, M. (1995) Modulation of melittin-induced lysis by surface charge density of membranes. *Biophysical Journal 68*, 187–195.

[84] Dempsey, C. E., and Watts, A. (1987) A deuterium and phosphorus-31 nuclear magnetic resonance study of the interaction of melittin with dimyristoylphosphatidylcholine bilayers and the effects of contaminating phospholipase A2. *Biochemistry 26*, 5803–5811.

[85] Epand, R., and Epand, R. (1994) Relationship Between the Infectivity of Influenza Virus and the Ability of Its Fusion Peptide to Perturb Bilayers. *Biochemical and Biophysical Research Communications 202*, 1420–1425.

[86] Hallock, K. J., Lee, D.-K., and Ramamoorthy, A. (2003) MSI-78, an Analogue of the Magainin Antimicrobial Peptides, Disrupts Lipid Bilayer Structure via Positive Curvature Strain. *Biophysical Journal 84*, 3052–3060.

[87] Galanth, C., Abbassi, F., Lequin, O., Ayala-Sanmartin, J., Ladram, A., Nicolas, P., and Amiche, M. (2009) Mechanism of Antibacterial Action of Dermaseptin B2: Interplay between Helix−Hinge−Helix Structure and Membrane Curvature Strain. *Biochemistry 48*, 313–327.

[88] Haney, E. F., Nathoo, S., Vogel, H. J., and Prenner, E. J. (2010) Induction of non-lamellar lipid phases by antimicrobial peptides: a potential link to mode of action. *Chemistry and Physics of Lipids 163*, 82–93.

[89] Tönsing, K., Kakorin, S., Neumann, E., Liemann, S., and Huber, R. (1997) Annexin V and vesicle membrane electroporation. *European biophysics journal: EBJ 26*, 307–318, PMID: 9378099.

[90] Neumann, E. (1988) The electroporation hysteresis. *Ferroelectrics 86*, 325–333.

[91] Epand, R. F., Schmitt, M. A., Gellman, S. H., and Epand, R. M. (2006) Role of membrane lipids in the mechanism of bacterial species selective toxicity by two / -antimicrobial peptides. *Biochimica et Biophysica Acta (BBA) - Biomembranes 1758*, 1343–1350.

[92] Epand, R. M., Rotem, S., Mor, A., Berno, B., and Epand, R. F. (2008) Bacterial Membranes as Predictors of Antimicrobial Potency. *Journal of the American Chemical Society 130*, 14346–14352.

[93] Epand, R. F., Mowery, B. P., Lee, S. E., Stahl, S. S., Lehrer, R. I., Gellman, S. H., and Epand, R. M. (2008) Dual Mechanism of Bacterial Lethality for a Cationic Sequence-Random Copolymer that Mimics Host-Defense Antimicrobial Peptides. *Journal of Molecular Biology 379*, 38–50.

[94] Jean-Franc ois, F., Castano, S., Desbat, B., Odaert, B., Roux, M., Metz-Boutigue, M.-H., and Dufourc, E. J. (2008) Aggregation of Cateslytin -Sheets on Negatively Charged Lipids Promotes Rigid Membrane Domains. A New Mode of Action for Antimicrobial Peptides? *Biochemistry 47*, 6394–6402.

[95] Gandhavadi, M., Allende, D., Vidal, A., Simon, S. A., and McIntosh, T. J. (2002) Structure, composition, and peptide binding properties of detergent soluble bilayers and detergent resistant rafts. *Biophys J 82*, 1469–82, 3.

[96] Abraham, T., Lewis, R. N. A. H., Hodges, R. S., and McElhaney, R. N. (2005) Isothermal Titration Calorimetry Studies of the Binding of the Antimicrobial Peptide Gramicidin S to Phospholipid Bilayer Membranes. *Biochemistry 44*, 11279–11285.

[97] Allende, D., and McIntosh, T. J. (2003) Lipopolysaccharides in Bacterial Membranes Act like Cholesterol in Eukaryotic Plasma Membranes in Providing Protection against Melittin-Induced Bilayer Lysis. *Biochemistry 42*, 1101–1108.

[98] Hallock, K. J., Lee, D.-K., Omnaas, J., Mosberg, H. I., and Ramamoorthy, A. (2002) Membrane Composition Determines Pardaxin's Mechanism of Lipid Bilayer Disruption. *Biophysical Journal 83*, 1004–1013.

[99] Anisimova, E. V., Badyakina, A. O., Vasil'eva, N. V., and Nesmeyanova, M. A. (2005) Changes in the composition of anionic membrane phospholipids influence protein secretion and cell envelope biogenesis in Escherichia coli. *Microbiology 74*, 147–152.

[100] Lu, Y.-H., Guan, Z., Zhao, J., and Raetz, C. R. H. (2011) Three Phosphatidylglycerolphosphate Phosphatases in the Inner Membrane of Escherichia coli. *Journal of Biological Chemistry 286*, 5506–5518.

[101] Joyce, G. H., Hammond, R. K., and White, D. C. (1970) Changes in Membrane Lipid Composition in Exponentially Growing Staphylococcus aureus During the Shift from 37 to 25 C. *Journal of Bacteriology 104*, 323.

[102] Rest, M. E. v. d., Kamminga, A. H., Nakano, A., Anraku, Y., Poolman, B., and Konings, W. N. (1995) The plasma membrane of Saccharomyces cerevisiae: structure, function, and biogenesis. *Microbiological Reviews 59*, 304–322.

[103] Virtanen, J. A., Cheng, K. H., and Somerharju, P. (1998) Phospholipid composition of the mammalian red cell membrane can be rationalized by a superlattice model. *Proceedings of the National Academy of Sciences 95*, 4964–4969, 9.

[104] Aloia, R. C., Tian, H., and Jensen, F. C. (1993) Lipid composition and fluidity of the human immunodeficiency virus envelope and host cell plasma membranes. *Proceedings of the National Academy of Sciences 90*, 5181–5185.

[105] Utsugi, T., Schroit, A. J., Connor, J., Bucana, C. D., and Fidler, I. J. (1991) Elevated expression of phosphatidylserine in the outer membrane leaflet of human tumor cells and recognition by activated human blood monocytes. *Cancer research 51*, 3062–3066, PMID: 2032247.

[106] Dobrzyńska, I., Szachowicz-Petelska, B., Sulkowski, S., and Figaszewski, Z. (2005) Changes in electric charge and phospholipids composition in human colorectal cancer cells. *Molecular and Cellular Biochemistry 276*, 113–119.

[107] Yoon, W.-H., Park, H.-D., Lim, K., and Hwang, B.-D. (1996) Effect of O-Glycosylated Mucin on Invasion and Metastasis of HM7 Human Colon Cancer Cells. *Biochemical and Biophysical Research Communications 222*, 694–699.

[108] Burdick, M. D., Harris, A., Reid, C. J., Iwamura, T., and Hollingsworth, M. A. (1997) Oligosaccharides Expressed on MUC1 Produced by Pancreatic and Colon Tumor Cell Lines. *Journal of Biological Chemistry 272*, 24198–24202.

[109] Helmerhorst, E. J., Reijnders, I. M., van 't Hof, W., Veerman, E. C., and Nieuw Amerongen, A. V. (1999) A critical comparison of the hemolytic and fungicidal activities of cationic antimicrobial peptides. *FEBS Letters 449*, 105–110.

[110] Imura, Y., Choda, N., and Matsuzaki, K. (2008) Magainin 2 in Action: Distinct Modes of Membrane Permeabilization in Living Bacterial and Mammalian Cells . *Biophysical Journal 95*, 5757–5765.

[111] Bessalle, R., Haas, H., Goria, A., Shalit, I., and Fridkin, M. (1992) Augmentation of the antibacterial activity of magainin by positive-charge chain extension. *Antimicrob Agents Chemother 36*, 313–7, 2.

[112] Matsuzaki, K., Nakamura, A., Murase, O., Sugishita, K.-i., Fujii, N., and Miyajima, K. (1997) Modulation of Magainin 2−Lipid Bilayer Interactions by Peptide Charge. *Biochemistry 36*, 2104–2111.

[113] Dathe, M., Schümann, M., Wieprecht, T., Winkler, A., Beyermann, M., Krause, E., Matsuzaki, K., Murase, O., and Bienert, M. (1996) Peptide Helicity and Membrane Surface Charge Modulate the Balance of Electrostatic and Hydrophobic Interactions with Lipid Bilayers and Biological Membranes. *Biochemistry 35*, 12612–12622.

[114] Blondelle, S. E., and Houghten, R. A. (1992) Design of model amphipathic peptides having potent antimicrobial activities. *Biochemistry 31*, 12688–12694.

[115] Dathe, M., Nikolenko, H., Meyer, J., Beyermann, M., and Bienert, M. (2001) Optimization of the antimicrobial activity of magainin peptides by modification of charge. *FEBS Letters 501*, 146–150.

[116] Eisenberg, D., Weiss, R. M., Terwilliger, T. C., and Wilcox, W. (1982) Hydrophobic moments and protein structure. *Faraday Symposia of the Chemical Society 17*, 109.

[117] Brasseur, R. (1991) Differentiation of lipid-associating helices by use of three-dimensional molecular hydrophobicity potential calculations. *Journal of Biological Chemistry 266*, 16120–16127.

[118] Kondejewski, L. H., Jelokhani-Niaraki, M., Farmer, S. W., Lix, B., Kay, C. M., Sykes, B. D., Hancock, R. E. W., and Hodges, R. S. (1999) Dissociation of Antimicrobial and Hemolytic Activities in Cyclic Peptide Diastereomers by Systematic Alterations in Amphipathicity. *Journal of Biological Chemistry 274*, 13181–13192.

[119] Wieprecht, T., Dathe, M., Beyermann, M., Krause, E., Maloy, W. L., MacDonald, D. L., and Bienert, M. (1997) Peptide Hydrophobicity Controls the Activity and Selectivity of Magainin 2 Amide in Interaction with Membranes. *Biochemistry 36*, 6124–6132.

[120] Dathe, M., Wieprecht, T., Nikolenko, H., Handel, L., Maloy, W., MacDonald, D. L., Beyermann, M., and Bienert, M. (1997) Hydrophobicity, hydrophobic moment and angle subtended by charged residues modulate antibacterial and haemolytic activity of amphipathic helical peptides. *FEBS Letters 403*, 208–212.

[121] Uematsu, N., and Matsuzaki, K. (2000) Polar Angle as a Determinant of Amphipathic -Helix-Lipid Interactions: A Model Peptide Study. *Biophysical Journal 79*, 2075–2083.

[122] Liu, Z., Brady, A., Young, A., Rasimick, B., Chen, K., Zhou, C., and Kallenbach, N. R. (2007) Length Effects in Antimicrobial Peptides of the (RW)n Series. *Antimicrob. Agents Chemother. 51*, 597–603, 2.

[123] Liu, Z., Young, A. W., Hu, P., Rice, A. J., Zhou, C., Zhang, Y., and Kallenbach, N. R. (2007) Tuning the Membrane Selectivity of Antimicrobial Peptides by Using Multivalent Design. *ChemBioChem 8*, 2063–2065.

[124] Shai, Y., and Oren, Z. (2001) From "carpet" mechanism to de-novo designed diastereomeric cell-selective antimicrobial peptides. *Peptides 22*, 1629–1641.

[125] Ladokhin, A. S., and White, S. H. (1999) Folding of amphipathic -helices on membranes: energetics of helix formation by melittin. *Journal of Molecular Biology 285*, 1363–1369.

[126] Asthana, N., Yadav, S. P., and Ghosh, J. K. (2004) Dissection of Antibacterial and Toxic Activity of Melittin. *Journal of Biological Chemistry 279*, 55042 –55050.

[127] Pandey, B. K., Ahmad, A., Asthana, N., Azmi, S., Srivastava, R. M., Srivastava, S., Verma, R., Vishwakarma, A. L., and Ghosh, J. K. (2010) Cell-Selective Lysis by Novel Analogues of Melittin against Human Red Blood Cells and Escherichia coli. *Biochemistry 49*, 7920–7929.

[128] Johansson, J., Gudmundsson, G. H., Rottenberg, M. E., Berndt, K. D., and Agerberth, B. (1998) Conformation-dependent Antibacterial Activity of the Naturally Occurring Human Peptide LL-37. *Journal of Biological Chemistry 273*, 3718 –3724.

[129] La Rocca, P., Shai, Y., and Sansom, M. (1999) Peptide–bilayer interactions: simulations of dermaseptin B, an antimicrobial peptide. *Biophysical Chemistry 76*, 145–159.

[130] Wimley, W. C. (2010) Describing the Mechanism of Antimicrobial Peptide Action with the Interfacial Activity Model. *ACS Chemical Biology 5*, 905–917.

[131] Rathinakumar, R., Walkenhorst, W. F., and Wimley, W. C. (2011) Broad-Spectrum Antimicrobial Peptides by Rational Combinatorial Design and High-Throughput Screening: The Importance of Interfacial Activity. *J. Am. Chem. Soc. 131*, 7609–7617.

[132] Melo, M. N., Ferre, R., Feliu, L., Bardají, E., Planas, M., and Castanho, M. A. R. B. (2011) Prediction of Antibacterial Activity from Physicochemical Properties of Antimicrobial Peptides. *PLoS ONE 6*, 12.

[133] White, S. H., Wimley, W. C., Ladokhin, A. S., and Hristova, K. In *Methods in Enzymology*; Gary K. Ackers, M. L. J., Ed.; Academic Press, 1998; Vol. Volume 295; pp 62–87.

[134] Huang, H. W., Chen, F.-Y., and Lee, M.-T. (2004) Molecular Mechanism of Peptide-Induced Pores in Membranes. *Physical Review Letters 92*, 198304.

[135] Huey W., H. (2009) Free Energies of Molecular Bound States in Lipid Bilayers: Lethal Concentrations of Antimicrobial Peptides. *Biophysical Journal 96*, 3263–3272.

[136] Lee, M.-T., Chen, F.-Y., and Huang, H. W. (2004) Energetics of Pore Formation Induced by Membrane Active Peptides. *Biochemistry 43*, 3590–3599.

[137] Taboureau, O., Olsen, O. H., Nielsen, J. D., Raventos, D., Mygind, P. H., and Kristensen, H. (2006) Design of Novispirin Antimicrobial Peptides by Quantitative Structure–Activity Relationship. *Chemical Biology & Drug Design 68*, 48–57.

[138] Jenssen, H., Fjell, C. D., Cherkasov, A., and Hancock, R. E. W. (2008) QSAR modeling and computer-aided design of antimicrobial peptides. *Journal of Peptide Science 14*, 110–114, 1.

[139] Hilpert, K., Fjell, C. D., and Cherkasov, A. In *Peptide-Based Drug Design*; Otvos, L., Ed.; Methods In Molecular Biology™ 494; Humana Press, 2008; pp 127–159.

[140] Cherkasov, A., Hilpert, K., Jenssen, H., Fjell, C. D., Waldbrook, M., Mullaly, S. C., Volkmer, R., and Hancock, R. E. (2011) Use of Artificial Intelligence in the Design of Small Peptide Antibiotics Effective against a Broad Spectrum of Highly Antibiotic-Resistant Superbugs. *ACS Chem. Biol. 4*, 65–74.

[141] Fjell, C. D., Jenssen, H., Cheung, W. A., Hancock, R. E. W., and Cherkasov, A. (2011) Optimization of Antibacterial Peptides by Genetic Algorithms and Cheminformatics. *Chemical Biology & Drug Design 77*, 48–56.

[142] Pathak, N., Salas-Auvert, R., Ruche, G., Janna, M., McCarthy, D., and Harrison, R. G. (1995) Comparison of the effects of hydrophobicity, amphiphilicity, and -helicity on the activities of antimicrobial peptides. *Proteins: Structure, Function, and Bioinformatics 22*, 182–186.

[143] Frecer, V. (2006) QSAR analysis of antimicrobial and haemolytic effects of cyclic cationic antimicrobial peptides derived from protegrin-1. *Bioorganic & Medicinal Chemistry 14*, 6065–6074.

[144] Juretić, D., Vukičević, D., Ilić, N., Antcheva, N., and Tossi, A. (2009) Computational Design of Highly Selective Antimicrobial Peptides. *Journal of Chemical Information and Modeling 49*, 2873–2882.

[145] Torrent, M., Andreu, D., Nogués, V. M., and Boix, E. (2011) Connecting Peptide Physicochemical and Antimicrobial Properties by a Rational Prediction Model. *PLoS ONE 6*, e16968.

[146] Jenssen, H., Lejon, T., Hilpert, K., Fjell, C. D., Cherkasov, A., and Hancock, R. E. W. (2007) Evaluating Different Descriptors for Model Design of Antimicrobial Peptides with Enhanced Activity Toward P. aeruginosa. *Chemical Biology & Drug Design 70*, 134–142, 2.

[147] Karakoc, E., Sahinalp, S. C., and Cherkasov, A. (2011) Comparative QSAR- and Fragments Distribution Analysis of Drugs, Druglikes, Metabolic Substances, and Antimicrobial Compounds. *J. Chem. Inf. Model. 46*, 2167–2182.

[148] Langham, A. A., Khandelia, H., Schuster, B., Waring, A. J., Lehrer, R. I., and Kaznessis, Y. N. (2008) Correlation between simulated physicochemical properties and hemolycity of protegrin-like antimicrobial peptides: Predicting experimental toxicity. *Peptides 29*, 1085–1093.

[149] Hilpert, K., Elliott, M. R., Volkmer-Engert, R., Henklein, P., Donini, O., Zhou, Q., Winkler, D. F., and Hancock, R. E. (2006) Sequence Requirements and an Optimization Strategy for Short Antimicrobial Peptides. *Chemistry & Biology 13*, 1101–1107.

[150] Krauson, A. J., He, J., and Wimley, W. C. (2012) Gain-of-Function Analogues of the Pore-Forming Peptide Melittin Selected by Orthogonal High-Throughput Screening. *Journal of the American Chemical Society 134*, 12732–12741.

[151] Cevc, G. (2004) Lipid vesicles and other colloids as drug carriers on the skin. *Advanced Drug Delivery Reviews 56*, 675–711.

[152] Tieleman, D. P. (2006) Computer Simulations of Transport Through Membranes: Passive Diffusion, Pores, Channels and Transporters. *Clinical and Experimental Pharmacology and Physiology 33*, 893–903.

[153] Evans, E., Heinrich, V., Ludwig, F., and Rawicz, W. (2003) Dynamic Tension Spectroscopy and Strength of Biomembranes. *Biophysical Journal 85*, 2342–2350.

[154] Wang, Z.-J., and Frenkel, D. (2005) Pore nucleation in mechanically stretched bilayer membranes. *The Journal of Chemical Physics 123*, 154701–154701–5.

[155] Tieleman, D. P., Leontiadou, H., Mark, A. E., and Marrink, S.-J. (2003) Simulation of Pore Formation in Lipid Bilayers by Mechanical Stress and Electric Fields. *Journal of the American Chemical Society 125*, 6382–6383.

[156] Tolpekina, T. V., den Otter, W. K., and Briels, W. J. (2004) Nucleation free energy of pore formation in an amphiphilic bilayer studied by molecular dynamics simulations. *The Journal of Chemical Physics 121*, 12060–12066.

[157] Tolpekina, T. V., den Otter, W. K., and Briels, W. J. (2004) Simulations of stable pores in membranes: System size dependence and line tension. *The Journal of Chemical Physics 121*, 8014–8020.

[158] Loison, C., Mareschal, M., and Schmid, F. (2004) Pores in bilayer membranes of amphiphilic molecules: Coarse-grained molecular dynamics simulations compared with simple mesoscopic models. *The Journal of Chemical Physics 121*, 1890–1900.

[159] Farago, O., and Santangelo, C. D. (2005) Pore formation in fluctuating membranes. *The Journal of Chemical Physics 122*, 044901–044901–9.

[160] Wohlert, J., den Otter, W. K., Edholm, O., and Briels, W. J. (2006) Free energy of a transmembrane pore calculated from atomistic molecular dynamics simulations. *The Journal of Chemical Physics 124*, 154905–154905–9.

[161] Tsong, T. (1991) Electroporation of cell membranes. *Biophysical Journal 60*, 297–306.

[162] Weaver, J. C., and Chizmadzhev, Y. A. (1996) Theory of electroporation: A review. *Bioelectrochemistry and Bioenergetics 41*, 135–160, 2.

[163] Zhelev, D. V., and Needham, D. (1993) Tension-stabilized pores in giant vesicles: determination of pore size and pore line tension. *Biochimica et Biophysica Acta (BBA) - Biomembranes 1147*, 89–104.

[164] Akinlaja, J., and Sachs, F. (1998) The Breakdown of Cell Membranes by Electrical and Mechanical Stress. *Biophysical Journal 75*, 247–254, 1.

[165] Antonov, V. F., Petrov, V. V., Molnar, A. A., Predvoditelev, D. A., and Ivanov, A. S. (1980) The appearance of single-ion channels in unmodified lipid bilayer membranes at the phase transition temperature. *Nature 283*, 585–586, 5747.

[166] Blicher, A., Wodzinska, K., Fidorra, M., Winterhalter, M., and Heimburg, T. (2009) The Temperature Dependence of Lipid Membrane Permeability, its Quantized Nature, and the Influence of Anesthetics. *Biophysical Journal 96*, 4581–4591, 11.

[167] Glaser, R. W., Leikin, S. L., Chernomordik, L. V., Pastushenko, V. F., and Sokirko, A. I. (1988) Reversible electrical breakdown of lipid bilayers: formation and evolution of pores. *Biochimica et Biophysica Acta (BBA) - Biomembranes 940*, 275–287, 2.

[168] Israelachvili, J., and Pashley, R. (1984) Measurement of the hydrophobic interaction between two hydrophobic surfaces in aqueous electrolyte solutions. *Journal of Colloid and Interface Science 98*, 500–514.

[169] Notman, R., Anwar, J., Briels, W., Noro, M. G., and den Otter, W. K. (2008) Simulations of Skin Barrier Function: Free Energies of Hydrophobic and Hydrophilic Transmembrane Pores in Ceramide Bilayers. *Biophysical Journal 95*, 4763–4771.

[170] J.D., L. (1975) Stability of lipid bilayers and red blood cell membranes. *Physics Letters A 53*, 193–194.

[171] Karatekin, E., Sandre, O., Guitouni, H., Borghi, N., Puech, P.-H., and Brochard-Wyart, F. (2003) Cascades of Transient Pores in Giant Vesicles: Line Tension and Transport. *Biophysical Journal 84*, 1734–1749.

[172] Ting, C. L., Appelö, D., and Wang, Z.-G. (2011) Minimum Energy Path to Membrane Pore Formation and Rupture. *Physical Review Letters 106*, 168101.

[173] Tamba, Y., Ariyama, H., Levadny, V., and Yamazaki, M. (2010) Kinetic Pathway of Antimicrobial Peptide Magainin 2-Induced Pore Formation in Lipid Membranes. *The Journal of Physical Chemistry B 114*, 12018–12026, 37.

[174] Yang, L., Harroun, T. A., Heller, W. T., Weiss, T. M., and Huang, H. W. (1998) Neutron Off-Plane Scattering of Aligned Membranes. I. Method of Measurement. *Biophysical Journal 75*, 641–645.

[175] Yang, L., Weiss, T. M., Lehrer, R. I., and Huang, H. W. (2000) Crystallization of Antimicrobial Pores in Membranes: Magainin and Protegrin. *Biophysical Journal 79*, 2002–2009.

[176] Qian, S., Wang, W., Yang, L., and Huang, H. W. (2008) Structure of transmembrane pore induced by Bax-derived peptide: Evidence for lipidic pores. *Proceedings of the National Academy of Sciences 105*, 17379–17383.

[177] Lee, C. C., Sun, Y., Qian, S., and Huang, H. W. (2011) Transmembrane Pores Formed by Human Antimicrobial Peptide LL-37. *Biophysical Journal 100*, 1688–1696, 7.

[178] Sengupta, D., Leontiadou, H., Mark, A. E., and Marrink, S.-J. (2008) Toroidal pores formed by antimicrobial peptides show significant disorder. *Biochimica et Biophysica Acta (BBA) - Biomembranes 1778*, 2308–2317.

[179] García-Sáez, A. J., Chiantia, S., Salgado, J., and Schwille, P. (2007) Pore Formation by a Bax-Derived Peptide: Effect on the Line Tension of the Membrane Probed by AFM. *Biophysical Journal 93*, 103–112.

[180] Eisenberg, M., Hall, J. E., and Mead, C. A. (1973) The nature of the voltage-dependent conductance induced by alamethicin in black lipid membranes. *The Journal of Membrane Biology 14*, 143–176.

[181] Baumann, G., and Mueller, P. (1974) A molecular model of membrane excitability. *Journal of Supramolecular Structure 2*, 538–557, 5-6.

[182] Opsahl, L., and Webb, W. (1994) Transduction of membrane tension by the ion channel alamethicin. *Biophysical Journal 66*, 71–74.

[183] He, K., Ludtke, S., Worcester, D., and Huang, H. (1996) Neutron scattering in the plane of membranes: structure of alamethicin pores. *Biophysical Journal 70*, 2659–2666.

[184] Fox, J., R O, and Richards, F. M. (1982) A voltage-gated ion channel model inferred from the crystal structure of alamethicin at 1.5-A resolution. *Nature 300*, 325–330, PMID: 6292726.

[185] Qian, S., Wang, W., Yang, L., and Huang, H. W. (2008) Structure of the Alamethicin Pore Reconstructed by X-Ray Diffraction Analysis. *Biophysical Journal 94*, 3512–3522.

[186] Pieta, P., Mirza, J., and Lipkowski, J. (2012) Direct visualization of the alamethicin pore formed in a planar phospholipid matrix. *Proceedings of the National Academy of Sciences 109*, 21223–21227.

[187] Woolley, G. A., Starostin, A. V., Butan, R., James, D. A., Wenschuh, H., and Sansom, M. S. P. In *Novartis Foundation Symposium 225 - Gramicidin and Related Ion Channel-Forming Peptides*; organizers, D. J. C., and Cardew, G., Eds.; John Wiley & Sons, Ltd., 2007; p 62–73.

[188] Portlock, S. H., Clague, M. J., and Cherry, R. J. (1990) Leakage of internal markers from erythrocytes and lipid vesicles induced by melittin, gramicidin S and alamethicin: a comparative study. *Biochimica et Biophysica Acta (BBA) - Biomembranes 1030*, 1–10.

[189] Lehmann, J., Retz, M., Sidhu, S. S., Suttmann, H., Sell, M., Paulsen, F., Harder, J., Unteregger, G., and Stöckle, M. (2006) Antitumor Activity of the Antimicrobial Peptide Magainin II against Bladder Cancer Cell Lines. *European Urology 50*, 141–147.

[190] Hirsh, D. J., Hammer, J., Maloy, W. L., Blazyk, J., and Schaefer, J. (1996) Secondary Structure and Location of a Magainin Analogue in Synthetic Phospholipid Bilayers. *Biochemistry 35*, 12733–12741.

[191] Bechinger, B., Zasloff, M., and Opella, S. J. (1993) Structure and orientation of the antibiotic peptide magainin in membranes by solid-state nuclear magnetic resonance spectroscopy. *Protein Science : A Publication of the Protein Society 2*, 2077–2084, PMID: 8298457 PMCID: 2142334.

[192] Ludtke, S. J., He, K., Heller, W. T., Harroun, T. A., Yang, L., and Huang, H. W. (1996) Membrane Pores Induced by Magainin. *Biochemistry 35*, 13723–13728.

[193] Nguyen, K. T., Le Clair, S. V., Ye, S., and Chen, Z. (2009) Molecular Interactions between Magainin 2 and Model Membranes in Situ. *The Journal of Physical Chemistry B 113*, 12358–12363.

[194] Matsuzaki, K., Murase, O., Tokuda, H., Funakoshi, S., Fujii, N., and Miyajima, K. (1994) Orientational and Aggregational States of Magainin 2 in Phospholipid Bilayers. *Biochemistry 33*, 3342–3349.

[195] Matsuzaki, K., Murase, O., and Miyajima, K. (1995) Kinetics of Pore Formation by an Antimicrobial Peptide, Magainin 2, in Phospholipid Bilayers. *Biochemistry 34*, 12553–12559.

[196] Duclohier, H., Molle, G., and Spach, G. (1989) Antimicrobial peptide magainin I from Xenopus skin forms anion-permeable channels in planar lipid bilayers. *Biophysical Journal 56*, 1017–1021.

[197] He, K., Ludtke, S. J., Huang, H. W., and Worcester, D. L. (1995) Antimicrobial Peptide Pores in Membranes Detected by Neutron In-Plane Scattering. *Biochemistry 34*, 15614–15618.

[198] Münster, C., Spaar, A., Bechinger, B., and Salditt, T. (2002) Magainin 2 in phospholipid bilayers: peptide orientation and lipid chain ordering studied by X-ray diffraction. *Biochimica et Biophysica Acta (BBA) - Biomembranes 1562*, 37–44.

[199] Han, M., Mei, Y., Khant, H., and Ludtke, S. J. (2009) Characterization of Antibiotic Peptide Pores Using Cryo-EM and Comparison to Neutron Scattering. *Biophysical Journal 97*, 164–172.

[200] Ariyama, H., Tamba, Y., Levadny, V., and Yamazaki, M. The size of the pore in lipid membranes induced by antimicrobial peptide magainin 2. 2009.

[201] Bechinger, B. (2005) Detergent-like properties of magainin antibiotic peptides: A 31P solid-state NMR spectroscopy study. *Biochimica et Biophysica Acta (BBA) - Biomembranes 1712*, 101–108.

[202] Woo, H.-J., and Wallqvist, A. (2011) Spontaneous Buckling of Lipid Bilayer and Vesicle Budding Induced by Antimicrobial Peptide Magainin 2: A Coarse-Grained Simulation Study. *The Journal of Physical Chemistry B 115*, 8122–8129.

[203] Tamba, Y., and Yamazaki, M. (2009) Magainin 2-induced pore formation in the lipid membranes depends on its concentration in the membrane interface. *The Journal of Physical Chemistry. B 113*, 4846–4852, PMID: 19267489.

[204] Gregory, S. M., Pokorny, A., and Almeida, P. F. (2009) Magainin 2 Revisited: A Test of the Quantitative Model for the All-or-None Permeabilization of Phospholipid Vesicles. *Biophysical Journal 96*, 116–131, PMID: 19134472 PMCID: 2710023.

[205] Dempsey, C. E. (1990) The actions of melittin on membranes. *Biochimica et Biophysica Acta (BBA) - Reviews on Biomembranes 1031*, 143–161.

[206] Terwilliger, T. C., and Eisenberg, D. (1982) The Structure of Melittin .1. Structure Determination and Partial Refinement. *Journal of Biological Chemistry 257*, 6010–6015, 11.

[207] Terwilliger, T. C., and Eisenberg, D. (1982) The structure of melittin. II. Interpretation of the structure. *Journal of Biological Chemistry 257*, 6016–6022.

[208] Zhu, W. L., Nan, Y. H., Hahm, K.-S., and Shin, S. Y. (2007) Cell selectivity of an antimicrobial peptide melittin diastereomer with D-amino acid in the leucine zipper sequence. *Journal of Biochemistry and Molecular Biology 40*, 1090–1094, PMID: 18047808.

[209] Srivastava, R. M., Srivastava, S., Singh, M., Bajpai, V. K., and Ghosh, J. K. (2012) Consequences of Alteration in Leucine Zipper Sequence of Melittin in Its Neutralization of Lipopolysaccharide-induced Proinflammatory Response in Macrophage Cells and Interaction with Lipopolysaccharide. *Journal of Biological Chemistry 287*, 1980–1995.

[210] Tosteson, M., and Tosteson, D. (1981) The sting. Melittin forms channels in lipid bilayers. *Biophysical Journal 36*, 109–116.

[211] Kempf, C., Klausner, R. D., Weinstein, J. N., Van Renswoude, J., Pincus, M., and Blumenthal, R. (1982) Voltage-dependent trans-bilayer orientation of melittin. *The Journal of Biological Chemistry 257*, 2469–2476, PMID: 7061434.

[212] Irudayam, S. J., and Berkowitz, M. L. (2012) Binding and reorientation of melittin in a POPC bilayer: Computer simulations. *Biochimica et Biophysica Acta (BBA) - Biomembranes 1818*, 2975–2981.

[213] Parente, R. A., Nir, S., and Szoka, F. C. (1990) Mechanism of leakage of phospholipid vesicle contents induced by the peptide GALA. *Biochemistry 29*, 8720–8728.

[214] Hanke, W., and Boheim, G. (1980) The lowest conductance state of the alamethicin pore. *Biochimica et Biophysica Acta (BBA) - Biomembranes 596*, 456–462.

[215] Tosteson, M. T., Levy, J. J., Caporale, L. H., Rosenblatt, M., and Tosteson, D. C. (1987) Solid-phase synthesis of melittin: purification and functional characterization. *Biochemistry 26*, 6627–6631.

[216] Rex, S., and Schwarz, G. (1998) Quantitative Studies on the Melittin-Induced Leakage Mechanism of Lipid Vesicles. *Biochemistry 37*, 2336–2345.

[217] van den Bogaart, G., Guzmán, J. V., Mika, J. T., and Poolman, B. (2008) On the Mechanism of Pore Formation by Melittin. *Journal of Biological Chemistry 283*, 33854 –33857.

[218] Yang, L., Harroun, T. A., Weiss, T. M., Ding, L., and Huang, H. W. (2001) Barrel-Stave Model or Toroidal Model? A Case Study on Melittin Pores. *Biophysical Journal 81*, 1475–1485, 3.

[219] Park, S.-C., Kim, J.-Y., Shin, S.-O., Jeong, C.-Y., Kim, M.-H., Shin, S. Y., Cheong, G.-W., Park, Y., and Hahm, K.-S. (2006) Investigation of toroidal pore and oligomerization by melittin using transmission electron microscopy. *Biochemical and Biophysical Research Communications 343*, 222–228, PMID: 16540094.

[220] Ladokhin, A., Selsted, M., and White, S. (1997) Sizing membrane pores in lipid vesicles by leakage of co-encapsulated markers: pore formation by melittin. *Biophysical Journal 72*, 1762–1766.

[221] Allende, D., Simon, S., and McIntosh, T. J. (2005) Melittin-Induced Bilayer Leakage Depends on Lipid Material Properties: Evidence for Toroidal Pores. *Biophysical Journal 88*, 1828–1837.

[222] Hincha, D. K., and Crowe, J. H. (1996) The lytic activity of the bee venom peptide melittin is strongly reduced by the presence of negatively charged phospholipids or chloroplast galactolipids in the membranes of phosphatidylcholine large unilamellar vesicles. *Biochimica Et Biophysica Acta 1284*, 162–170, PMID: 8914580.

[223] Ghosh, A. K., Rukmini, R., and Chattopadhyay, A. (1997) Modulation of Tryptophan Environment in Membrane-Bound Melittin by Negatively Charged Phospholipids: Implications in Membrane Organization and Function. *Biochemistry 36*, 14291–14305.

[224] van den Bogaart, G., Mika, J. T., Krasnikov, V., and Poolman, B. (2007) The Lipid Dependence of Melittin Action Investigated by Dual-Color Fluorescence Burst Analysis. *Biophysical Journal 93*, 154–163.

[225] Aumelas, A., Mangoni, M., Roumestand, C., Chiche, L., Despaux, E., Grassy, G., Calas, B., and Chavanieu, A. (1996) Synthesis and Solution Structure of the Antimicrobial Peptide Protegrin-1. *European Journal of Biochemistry 237*, 575–583.

[226] Fahrner, R. L., Dieckmann, T., Harwig, S. S., Lehrer, R. I., Eisenberg, D., and Feigon, J. (1996) Solution structure of protegrin-1, a broad-spectrum antimicrobial peptide from porcine leukocytes. *Chemistry & Biology 3*, 543–550.

[227] Sokolov, Y., Mirzabekov, T., Martin, D. W., Lehrer, R. I., and Kagan, B. L. (1999) Membrane channel formation by antimicrobial protegrins. *Biochimica et Biophysica Acta (BBA) - Biomembranes 1420*, 23–29.

[228] Roumestand, C., Louis, V., Aumelas, A., Grassy, G., Calas, B., and Chavanieu, A. (1998) Oligomerization of protegrin-1 in the presence of DPC micelles. A proton high-resolution NMR study. *FEBS Letters 421*, 263–267.

[229] Mani, R., Tang, M., Wu, X., Buffy, J. J., Waring, A. J., Sherman, M. A., and Hong, M. (2006) Membrane-Bound Dimer Structure of a -Hairpin Antimicrobial Peptide from Rotational-Echo Double-Resonance Solid-State NMR. *Biochemistry 45*, 8341–8349.

[230] Jang, H., Ma, B., Lal, R., and Nussinov, R. (2008) Models of Toxic -Sheet Channels of Protegrin-1 Suggest a Common Subunit Organization Motif Shared with Toxic Alzheimer -Amyloid Ion Channels. *Biophysical Journal 95*, 4631–4642.

[231] Lazaridis, T., He, Y., and Prieto, L. (2013) Membrane Interactions and Pore Formation by the Antimicrobial Peptide Protegrin. *Biophysical Journal 104*, 633–642, 3.

[232] Capone, R., Mustata, M., Jang, H., Arce, F. T., Nussinov, R., and Lal, R. (2010) Antimicrobial Protegrin-1 Forms Ion Channels: Molecular Dynamic Simulation, Atomic Force Microscopy, and Electrical Conductance Studies. *Biophysical Journal 98*, 2644–2652.

[233] Ishitsuka, Y., Pham, D. S., Waring, A. J., Lehrer, R. I., and Lee, K. Y. C. (2006) Insertion selectivity of antimicrobial peptide protegrin-1 into lipid monolayers: Effect of head group electrostatics and tail group packing. *Biochimica et Biophysica Acta (BBA) - Biomembranes 1758*, 1450–1460.

[234] Wi, S., and Kim, C. (2008) Pore Structure, Thinning Effect, and Lateral Diffusive Dynamics of Oriented Lipid Membranes Interacting with Antimicrobial Peptide Protegrin-1: 31P and 2H Solid-State NMR Study. *The Journal of Physical Chemistry B 112*, 11402–11414.

[235] Langham, A. A., Ahmad, A. S., and Kaznessis, Y. N. (2008) On the nature of antimicrobial activity: a model for protegrin-1 pores. *Journal of the American Chemical Society 130*, 4338–4346.

[236] Lazaridis, T., and Karplus, M. (1999) Effective energy function for proteins in solution. *Proteins: Structure, Function, and Bioinformatics 35*, 133–152.

[237] Lazaridis, T. (2003) Effective energy function for proteins in lipid membranes. *Proteins: Structure, Function, and Bioinformatics 52*, 176–192, 2.

[238] Mazur, J., and Jernigan, R. L. (1991) Distance-dependent dielectric constants and their application to double-helical DNA. *Biopolymers 31*, 1615–1629.

[239] Lazaridis, T. (2005) Implicit solvent simulations of peptide interactions with anionic lipid membranes. *Proteins: Structure, Function, and Bioinformatics 58*, 518–527, 3.

[240] McLaughlin, S. In *Current Topics in Membranes and Transport*; Bronner, F., and Kleinzeller, A., Eds.; Academic Press, 1977; Vol. Volume 9; pp 71–144.

[241] Lazaridis, T. (2005) Structural Determinants of Transmembrane -Barrels. *Journal of Chemical Theory and Computation 1*, 716–722, 4.

[242] Mihajlovic, M., and Lazaridis, T. (2010) Antimicrobial peptides bind more strongly to membrane pores. *Biochimica et Biophysica Acta (BBA) - Biomembranes 1798*, 1494–1502, 8.

[243] Baker, N. A., Sept, D., Joseph, S., Holst, M. J., and McCammon, J. A. (2001) Electrostatics of nanosystems: Application to microtubules and the ribosome. *Proceedings of the National Academy of Sciences 98*, 10037–10041.

[244] Peitzsch, R., Eisenberg, M., Sharp, K., and McLaughlin, S. (1995) Calculations of the electrostatic potential adjacent to model phospholipid bilayers. *Biophysical Journal 68*, 729–738.

[245] Strandberg, E., Esteban-Martín, S., Salgado, J., and Ulrich, A. S. (2009) Orientation and Dynamics of Peptides in Membranes Calculated from 2H-NMR Data. *Biophysical Journal 96*, 3223–3232.

[246] Phillips, J. C., Braun, R., Wang, W., Gumbart, J., Tajkhorshid, E., Villa, E., Chipot, C., Skeel, R. D., Kalé, L., and Schulten, K. (2005) Scalable molecular dynamics with NAMD. *Journal of Computational Chemistry 26*, 1781–1802, 16.

[247] Jo, S., Lim, J. B., Klauda, J. B., and Im, W. (2009) CHARMM-GUI Membrane Builder for Mixed Bilayers and Its Application to Yeast Membranes. *Biophysical Journal 97*, 50–58, 1.

[248] Klauda, J. B., Venable, R. M., Freites, J. A., O'Connor, J. W., Tobias, D. J., Mondragon-Ramirez, C., Vorobyov, I., MacKerell, A. D., and Pastor, R. W. (2010) Update of the CHARMM All-Atom Additive Force Field for Lipids: Validation on Six Lipid Types. *J. Phys. Chem. B 114*, 7830–7843.

[249] Ashcroft, R. G., Coster, H. G. L., and Smith, J. R. (1981) The molecular organisation of bimolecular lipid membranes. The dielectric structure of the hydrophilic/hydrophobic interface. *Biochimica et Biophysica Acta (BBA) - Biomembranes 643*, 191–204, 1.

[250] Cevc, G., Watts, A., and Marsh, D. (1981) Titration of the phase transition of phosphatidylserine bilayer membranes. Effects of pH, surface electrostatics, ion binding, and head-group hydration. *Biochemistry 20*, 4955–4965, 17.

[251] Zhou, F., and Schulten, K. (1995) Molecular Dynamics Study of a Membrane-Water Interface. *The Journal of Physical Chemistry 99*, 2194–2207, 7.

[252] Stern, H. A., and Feller, S. E. (2003) Calculation of the dielectric permittivity profile for a nonuniform system: Application to a lipid bilayer simulation. *The Journal of Chemical Physics 118*, 3401.

[253] Cevc, G., Svetina, S., and Zeks, B. (1981) Electrostatic potential of bilayer lipid membranes with the structural surface charge smeared perpendicular to the membrane-solution interface. An extension of the Gouy-Chapman diffuse double layer theory. *The Journal of Physical Chemistry 85*, 1762–1767, 12.

[254] Yang, Y., Mayer, K. M., Wickremasinghe, N. S., and Hafner, J. H. (2008) Probing the Lipid Membrane Dipole Potential by Atomic Force Microscopy. *Biophysical Journal 95*, 5193–5199.

[255] Callenberg, K. M., Choudhary, O. P., de Forest, G. L., Gohara, D. W., Baker, N. A., and Grabe, M. (2010) APBSmem: A Graphical Interface for Electrostatic Calculations at the Membrane. *PLoS ONE 5*, e12722.

[256] Gesell, J., Zasloff, M., and Opella, S. J. (1997) Two-dimensional 1H NMR experiments show that the 23-residue magainin antibiotic peptide is an -helix in dodecylphosphocholine micelles, sodium dodecylsulfate micelles, and trifluoroethanol/water solution. *Journal of Biomolecular NMR 9*, 127–135, 2.

[257] Berman, H. M., Westbrook, J., Feng, Z., Gilliland, G., Bhat, T. N., Weissig, H., Shindyalov, I. N., and Bourne, P. E. (2000) The Protein Data Bank. *Nucleic acids research 28*, 235–42, 1.

[258] Flewelling, R. F., and Hubbell, W. L. (1986) The membrane dipole potential in a total membrane potential model. Applications to hydrophobic ion interactions with membranes. *Biophysical Journal 49*, 541–552, 2.

[259] Gawrisch, K., Ruston, D., Zimmerberg, J., Parsegian, V. A., Rand, R. P., and Fuller, N. (1992) Membrane dipole potentials, hydration forces, and the ordering of water at membrane surfaces. *Biophysical Journal 61*, 1213–1223, 5.

[260] Schamberger, J., and Clarke, R. J. (2002) Hydrophobic Ion Hydration and the Magnitude of the Dipole Potential. *Biophysical Journal 82*, 3081–3088, 6.

[261] Brockman, H. (1994) Dipole potential of lipid membranes. *Chemistry and Physics of Lipids 73*, 57–79, 1-2.

[262] Lairion, F., and Disalvo, E. A. (2004) Effect of Phloretin on the Dipole Potential of Phosphatidylcholine, Phosphatidylethanolamine, and Phosphatidylglycerol Monolayers. *Langmuir 20*, 9151–9155.

[263] Mashl, R. J., Scott, H. L., Subramaniam, S., and Jakobsson, E. (2001) Molecular Simulation of Dioleoylphosphatidylcholine Lipid Bilayers at Differing Levels of Hydration. *Biophysical Journal 81*, 3005–3015, 6.

[264] Sachs, J. N., Crozier, P. S., and Woolf, T. B. (2004) Atomistic simulations of biologically realistic transmembrane potential gradients. *The Journal of Chemical Physics 121*, 10847–10851, 22.

[265] Shinoda, K., Shinoda, W., Baba, T., and Mikami, M. (2004) Comparative molecular dynamics study of ether- and ester-linked phospholipid bilayers. *The Journal of Chemical Physics 121*, 9648.

[266] Villarreal, M. A., Díaz, S. B., Disalvo, E. A., and Montich, G. G. (2004) Molecular Dynamics Simulation Study of the Interaction of Trehalose with Lipid Membranes. *Langmuir 20*, 7844–7851, 18.

[267] Vorobyov, I., and Allen, T. W. (2010) The electrostatics of solvent and membrane interfaces and the role of electronic polarizability. *The Journal of Chemical Physics 132*, 185101.

[268] Becucci, L., Moncelli, M. R., Herrero, R., and Guidelli, R. (2000) Dipole Potentials of Monolayers of Phosphatidylcholine, Phosphatidylserine, and Phosphatidic Acid on Mercury. *Langmuir 16*, 7694–7700, 20.

[269] Ermakov, Y. A., Averbakh, A. Z., Yusipovich, A. I., and Sukharev, S. (2001) Dipole Potentials Indicate Restructuring of the Membrane Interface Induced by Gadolinium and Beryllium Ions. *Biophysical Journal 80*, 1851–1862, 4.

[270] Lewis, B. A., and Engelman, D. M. (1983) Lipid bilayer thickness varies linearly with acyl chain length in fluid phosphatidylcholine vesicles. *Journal of Molecular Biology 166*, 211–217.

[271] Wiener, M. C., King, G. I., and White, S. H. (1991) Structure of a fluid dioleoylphosphatidylcholine bilayer determined by joint refinement of x-ray and neutron diffraction data. I. Scaling of neutron data and the distributions of double bonds and water. *Biophysical Journal 60*, 568–576, 3.

[272] Mani, R., Buffy, J. J., Waring, A. J., Lehrer, R. I., and Hong, M. (2004) Solid-State NMR Investigation of the Selective Disruption of Lipid Membranes by Protegrin-1. *Biochemistry 43*, 13839–13848, 43.

[273] Srividya, N., and Muralidharan, S. (2008) Determination of the Line Tension of Giant Vesicles from Pore-Closing Dynamics. *J. Phys. Chem. B 112*, 7147–7152.

[274] Tang, M., Waring, A. J., and Hong, M. (2005) Intermolecular Packing and Alignment in an Ordered -Hairpin Antimicrobial Peptide Aggregate from 2D Solid-State NMR. *Journal of the American Chemical Society 127*, 13919–13927.

[275] Brooks, B. R. et al. (2009) CHARMM: The Biomolecular Simulation Program. *Journal of Computational Chemistry 30*, 1545–1614, 10.

[276] He, Y., Prieto, L., and Lazaridis, T. (2013) Modeling Peptide Binding To Anionic Membrane Pores. *Journal of Computational Chemistry In press.*

[277] Kabsch, W., and Sander, C. (1983) Dictionary of protein secondary structure: Pattern recognition of hydrogen-bonded and geometrical features. *Biopolymers 22*, 2577–2637.

[278] Lorian, V. *Antibiotics in laboratory medicine*; Lippincott Williams & Wilkins, 2005.

[279] Klocek, G., Schulthess, T., Shai, Y., and Seelig, J. (2009) Thermodynamics of Melittin Binding to Lipid Bilayers. Aggregation and Pore Formation. *Biochemistry 48*, 2586–2596, 12.

[280] Ben-Tal, N., Honig, B., Bagdassarian, C. K., and Ben-Shaul, A. (2000) Association Entropy in Adsorption Processes. *Biophysical Journal 79*, 1180–1187.

[281] Verly, R. M., Moraes, C. M. d., Resende, J. M., Aisenbrey, C., Bemquerer, M. P., Piló-Veloso, D., Valente, A. P., Almeida, F. C., and Bechinger, B. (2009) Structure and Membrane Interactions of the Antibiotic Peptide Dermadistinctin K by Multidimensional Solution and Oriented 15N and 31P Solid-State NMR Spectroscopy. *Biophysical Journal 96*, 2194–2203.

[282] Crandall, Y. M., and Bruch, M. D. (2008) Characterization of the structure and dynamics of mastoparan-X during folding in aqueous TFE by CD and NMR spectroscopy. *Biopolymers 89*, 197–209, 3.

[283] Lewis, J. R., and Cafiso, D. S. (1999) Correlation between the Free Energy of a Channel-Forming Voltage-Gated Peptide and the Spontaneous Curvature of Bilayer Lipids. *Biochemistry 38*, 5932–5938.

[284] Almeida, P. F., and Pokorny, A. (2009) Mechanisms of Antimicrobial, Cytolytic, and Cell-Penetrating Peptides: From Kinetics to Thermodynamics. *Biochemistry 48*, 8083–8093.

[285] Clark, K. S., Svetlovics, J., McKeown, A. N., Huskins, L., and Almeida, P. F. (2011) What Determines the Activity of Antimicrobial and Cytolytic Peptides in Model Membranes. *Biochemistry 50*, 7919–7932, 37.

[286] Verly, R. M., Rodrigues, M. A., Daghastanli, K. R. P., Denadai, A. M. L., Cuccovia, I. M., Bloch Jr, C., Frézard, F., Santoro, M. M., Piló-Veloso, D., and Bemquerer, M. P. (2008) Effect of cholesterol on the interaction of the amphibian antimicrobial peptide DD K with liposomes. *Peptides 29*, 15–24, 1.

[287] Sood, R., Domanov, Y., Pietiäinen, M., Kontinen, V. P., and Kinnunen, P. K. J. (2008) Binding of LL-37 to model biomembranes: Insight into target vs host cell recognition. *Biochimica et Biophysica Acta (BBA) - Biomembranes 1778*, 983–996, 4.

[288] Beschiaschvili, G., and Seelig, J. (1990) Melittin binding to mixed phosphatidylglycerol/phosphatidylcholine membranes. *Biochemistry 29*, 52–58.

[289] Rapaport, D., and Shai, Y. (1991) Interaction of fluorescently labeled pardaxin and its analogues with lipid bilayers. *Journal of Biological Chemistry 266*, 23769 –23775.

[290] Vivcharuk, V., Tolokh, I. S., and Gray, C. G. (2008) Prediction of binding free energy for adsorption of antimicrobial peptide lactoferricin B on a POPC membrane. *Physical Review E 77*.

[291] Jing, W., Svendsen, J. S., and Vogel, H. J. (2006) Comparison of NMR structures and model-membrane interactions of 15-residue antimicrobial peptides derived from bovine lactoferricinThis paper is one of a selection of papers published in this Special Issue, entitled 7th International Conference on Lactoferrin: Structure, Function, and Applications, and has undergone the Journal's usual peer review process. *Biochemistry and Cell Biology 84*, 312–326.

[292] Tolokh, I. S., Vivcharuk, V., Tomberli, B., and Gray, C. G. (2009) Binding free energy and counterion release for adsorption of the antimicrobial peptide lactoferricin B on a POPG membrane. *Physical Review E 80*, 031911.

[293] Lai, J. R., Epand, R. F., Weisblum, B., Epand, R. M., and Gellman, S. H. (2006) Roles of Salt and Conformation in the Biological and Physicochemical Behavior of Protegrin-1 and Designed Analogues: Correlation of Antimicrobial, Hemolytic, and Lipid Bilayer-Perturbing Activities. *Biochemistry 45*, 15718–15730.

[294] Vivcharuk, V., and Kaznessis, Y. (2010) Free Energy Profile of the Interaction between a Monomer or a Dimer of Protegrin-1 in a Specific Binding Orientation and a Model Lipid Bilayer. *The Journal of Physical Chemistry B 114*, 2790–2797.

[295] Yeh, I.-C., Ripoll, D. R., and Wallqvist, A. (2012) Free Energy Difference in Indolicidin Attraction to Eukaryotic and Prokaryotic Model Cell Membranes. *The Journal of Physical Chemistry B 116*, 3387–3396.

[296] Bulai, T., Bratosin, D., Pons, A., Montreuil, J., and Zanetta, J. P. (2003) Diversity of the human erythrocyte membrane sialic acids in relation with blood groups. *FEBS Lett 534*, 185–9, 1-3.

[297] Tziakas, D. N., Chalikias, G. K., Stakos, D., and Boudoulas, H. (2010) The role of red blood cells in the progression and instability of atherosclerotic plaque. *Int J Cardiol 142*, 2–7, 1.

[298] Mei, H., Liao, Z. H., Zhou, Y., and Li, S. Z. (2005) A new set of amino acid descriptors and its application in peptide QSARs. *Peptide Science 80*, 775–786.

[299] Bhonsle, J. B., Venugopal, D., Huddler, D. P., Magill, A. J., and Hicks, R. P. (2011) Application of 3D-QSAR for Identification of Descriptors Defining Bioactivity of Antimicrobial Peptides. *J. Med. Chem. 50*, 6545–6553.

[300] Liu, Z., Brady, A., Young, A., Rasimick, B., Chen, K., Zhou, C., and Kallenbach, N. R. (2006) Length Effects in Antimicrobial Peptides of the (RW)n Series. *Antimicrobial Agents and Chemotherapy 51*, 597–603.

[301] Fernández-Vidal, M., Jayasinghe, S., Ladokhin, A. S., and White, S. H. (2007) Folding Amphipathic Helices Into Membranes: Amphiphilicity Trumps Hydrophobicity. *Journal of Molecular Biology 370*, 459–470.

[302] Zhang, L., Benz, R., and Hancock, R. E. W. (2011) Influence of Proline Residues on the Antibacterial and Synergistic Activities of -Helical Peptides. *Biochemistry 38*, 8102–8111.

[303] Oren, Z., Hong, J., and Shai, Y. (1997) A Repertoire of Novel Antibacterial Diastereomeric Peptides with Selective Cytolytic Activity. *Journal of Biological Chemistry 272*, 14643–14649.

[304] Vermeer, L. S. et al. (2012) Conformational Flexibility Determines Selectivity and Antibacterial, Antiplasmodial, and Anticancer Potency of Cationic -Helical Peptides. *Journal of Biological Chemistry 287*, 34120–34133.

[305] Shai, Y. (1999) Mechanism of the binding, insertion and destabilization of phospholipid bilayer membranes by [alpha]-helical antimicrobial and cell non-selective membrane-lytic peptides. *Biochimica et Biophysica Acta (BBA) - Biomembranes 1462*, 55–70, 1-2.

[306] Oren, Z., and Shai, Y. (1996) A Class of Highly Potent Antibacterial Peptides Derived from Pardaxin, A Pore-Forming Peptide Isolated from Moses Sole Fish Pardachirus marmoratus. *European Journal of Biochemistry 237*, 303–310, 1.

[307] Ramamoorthy, A., Lee, D.-K., Narasimhaswamy, T., and Nanga, R. P. (2010) Cholesterol reduces pardaxin's dynamics–a barrel-stave mechanism of membrane disruption investigated by solid-state NMR. *Biochimica et Biophysica Acta (BBA) - Biomembranes 1798*, 223–227.

[308] Vad, B. S., Bertelsen, K., Johansen, C. H., Pedersen, J. M., Skrydstrup, T., Nielsen, N. C., and Otzen, D. E. (2010) Pardaxin Permeabilizes Vesicles More Efficiently by Pore Formation than by Disruption. *Biophysical Journal 98*, 576–585, 4.

[309] Wildman, K. A. H., Lee, D. K., and Ramamoorthy, A. (2003) Mechanism of lipid bilayer disruption by the human antimicrobial peptide, LL-37. *Biochemistry 42*, 6545–6558, 21.

[310] Porcelli, F., Verardi, R., Shi, L., Henzler-Wildman, K. A., Ramamoorthy, A., and Veglia, G. (2008) NMR structure of the cathelicidin-derived human antimicrobial peptide LL-37 in dodecylphosphocholine micelles. *Biochemistry 47*, 5565–5572, 20.

[311] Gable, J. E., Schlamadinger, D. E., Cogen, A. L., Gallo, R. L., and Kim, J. E. (2009) Fluorescence and UV Resonance Raman Study of Peptide-Vesicle Interactions of Human Cathelicidin LL-37 and Its F6W and F17W Mutants. *Biochemistry 48*, 11264–11272, 47.

[312] Rapaport, D., Peled, R., Nir, S., and Shai, Y. (1996) Reversible surface aggregation in pore formation by pardaxin. *Biophysical Journal 70*, 2502.

[313] Bolintineanu, D., Hazrati, E., Davis, H. T., Lehrer, R. I., and Kaznessis, Y. N. (2010) Antimicrobial mechanism of pore-forming protegrin peptides: 100 pores to kill E. coli. *Peptides 31*, 1–8.

[314] Bolintineanu, D. S., and Kaznessis, Y. N. (2011) Computational studies of protegrin antimicrobial peptides: A review. *Peptides 32*, 188–201.

[315] Huang, H. W. (2009) Free Energies of Molecular Bound States in Lipid Bilayers: Lethal Concentrations of Antimicrobial Peptides. *Biophysical Journal 96*, 3263–3272.

[316] White, S. H., and Wimley, W. C. (1999) MEMBRANE PROTEIN FOLDING AND STABILITY: Physical Principles. *Annual Review of Biophysics and Biomolecular Structure 28*, 319–365, PMID: 10410805.

[317] Chiu, S., Jakobsson, E., Subramaniam, S., and Scott, H. (1999) Combined Monte Carlo and Molecular Dynamics Simulation of Fully Hydrated Dioleyl and Palmitoyl-oleyl Phosphatidylcholine Lipid Bilayers. *Biophysical Journal 77*, 2462–2469.

[318] Silvestro, L., Gupta, K., Weiser, J. N., and Axelsen, P. H. (1997) The Concentration-Dependent Membrane Activity of Cecropin A. *Biochemistry 36*, 11452–11460.

[319] Yamamoto, N., and Tamura, A. (2010) Designed low amphipathic peptides with Î±-helical propensity exhibiting antimicrobial activity via a lipid domain formation mechanism. *Peptides 31*, 794–805.

[320] Gregory, S. M., Cavenaugh, A., Journigan, V., Pokorny, A., and Almeida, P. F. (2008) A Quantitative Model for the All-or-None Permeabilization of Phospholipid Vesicles by the Antimicrobial Peptide Cecropin A. *Biophysical Journal 94*, 1667–1680.

[321] Peitzsch, R. M., and McLaughlin, S. (1993) Binding of acylated peptides and fatty acids to phospholipid vesicles: Pertinence to myristoylated proteins. *Biochemistry 32*, 10436–10443.

[322] Wenk, M. R., and Seelig, J. (1998) Magainin 2 Amide Interaction with Lipid Membranes: Calorimetric Detection of Peptide Binding and Pore Formation. *Biochemistry 37*, 3909–3916.

[323] Wieprecht, T., Apostolov, O., and Seelig, J. (2000) Binding of the antibacterial peptide magainin 2 amide to small and large unilamellar vesicles. *Biophysical Chemistry 85*, 187–198.

[324] Wieprecht, T., Beyermann, M., and Seelig, J. (1999) Binding of Antibacterial Magainin Peptides to Electrically Neutral Membranes: Thermodynamics and Structure. *Biochemistry 38*, 10377–10387.

[325] Gaidukov, L., Fish, A., and Mor, A. (2003) Analysis of Membrane-Binding Properties of Dermaseptin Analogues: Relationships between Binding and Cytotoxicity. *Biochemistry 42*, 12866–12874.

[326] Allende, D., Vidal, A., Simon, S. A., and McIntosh, T. J. (2003) Bilayer interfacial properties modulate the binding of amphipathic peptides. *Chemistry and Physics of Lipids 122*, 65–76.

[327] Ladokhin, A. S., Selsted, M. E., and White, S. H. (1997) Bilayer interactions of indolicidin, a small antimicrobial peptide rich in tryptophan, proline, and basic amino acids. *Biophysical Journal 72*, 794–805, PMID: 9017204.

[328] Wimley, W. C., and White, S. H. (1996) Experimentally determined hydrophobicity scale for proteins at membrane interfaces. *Nature Structural & Molecular Biology 3*, 842–848.

[329] Ben-Tal, N., Honig, B., Peitzsch, R., Denisov, G., and McLaughlin, S. (1996) Binding of small basic peptides to membranes containing acidic lipids: theoretical models and experimental results. *Biophysical Journal 71*, 561–575.

[330] Mihajlovic, M., and Lazaridis, T. (2006) Calculations of pH-Dependent Binding of Proteins to Biological Membranes. *The Journal of Physical Chemistry B 110*, 3375–3384.

[331] Wieprecht, T., Dathe, M., Schumann, M., Krause, E., Beyermann, M., and Bienert, M. (1996) Conformational and Functional Study of Magainin 2 in Model Membrane Environments Using the New Approach of Systematic Double-d-Amino Acid Replacement. *Biochemistry 35*, 10844–10853.

[332] Wieprecht, T., Apostolov, O., Beyermann, M., and Seelig, J. (1999) Membrane Binding and Pore Formation of the Antibacterial Peptide PGLa: Thermodynamic and Mechanistic Aspects. *Biochemistry 39*, 442–452, 2.

[333] Schoch, P., and Sargent, D. F. (1980) Quantitative analysis of the binding of melittin to planar lipid bilayers allowing for the discrete-charge effect. *Biochimica et Biophysica Acta (BBA) - Biomembranes 602*, 234–247.

[334] Fernández-Vidal, M., White, S. H., and Ladokhin, A. S. (2011) Membrane Partitioning: "Classical" and "Nonclassical" Hydrophobic Effects. *The Journal of Membrane Biology 239*, 5–14, PMID: 21140141 PMCID: 3030945.

[335] Bhargava, K., and Feix, J. B. (2004) Membrane Binding, Structure, and Localization of Cecropin-Mellitin Hybrid Peptides: A Site-Directed Spin-Labeling Study. *Biophysical Journal 86*, 329–336.

[336] Dathe, M., Meyer, J., Beyermann, M., Maul, B., Hoischen, C., and Bienert, M. (2002) General aspects of peptide selectivity towards lipid bilayers and cell membranes studied by variation of the structural parameters of amphipathic helical model peptides. *Biochimica et Biophysica Acta (BBA) - Biomembranes 1558*, 171–186.

[337] Shin, S. Y., Kang, J. H., Jang, S. Y., Kim, Y., Kim, K. L., and Hahm, K.-S. (2000) Effects of the hinge region of cecropin A(1-8)-magainin 2(1-12), a synthetic antimicrobial peptide, on liposomes, bacterial and tumor cells. *Biochimica et Biophysica Acta (BBA) - Biomembranes 1463*, 209–218.

[338] Sato, H., and Feix, J. B. (2006) Peptide–membrane interactions and mechanisms of membrane destruction by amphipathic -helical antimicrobial peptides. *Biochimica et Biophysica Acta (BBA) - Biomembranes 1758*, 1245–1256.

[339] Sato, H., and Feix, J. B. (2008) Lysine-Enriched Cecropin-Mellitin Antimicrobial Peptides with Enhanced Selectivity. *Antimicrobial Agents and Chemotherapy 52*, 4463–4465, PMID: 18852279 PMCID: 2592880.

[340] Andreu, D., Merrifield, R. B., Steiner, H., and Boman, H. G. (1985) N-Terminal analogs of cecropin A: synthesis, antibacterial activity, and conformational properties. *Biochemistry 24*, 1683–1688.

[341] Lee, K., Shin, S. Y., Kim, K., Lim, S. S., Hahm, K.-S., and Kim, Y. (2004) Antibiotic activity and structural analysis of the scorpion-derived antimicrobial peptide IsCT and its analogs. *Biochemical and Biophysical Research Communications 323*, 712–719.

[342] Kozlov, S. A., Vassilevski, A. A., Feofanov, A. V., Surovoy, A. Y., Karpunin, D. V., and Grishin, E. V. (2006) Latarcins, Antimicrobial and Cytolytic Peptides from the Venom of the Spider Lachesana tarabaevi (Zodariidae) That Exemplify Biomolecular Diversity. *Journal of Biological Chemistry 281*, 20983 –20992.

[343] Vasilevskiĭ, A. A., Kozlov, S. A., Zhmak, M. N., Kudelina, I. A., Dubovskiĭ, P. V., Shaturskiĭ, O. I., Arsen'ev, A. S., and Grishin, E. V. (2007) Synthetic analogues of antimicrobial peptides from the venom of the Central Asian spider Lachesana tarabaevi. *Bioorganicheskaia Khimiia 33*, 405–412, PMID: 17886431.

[344] Shlyapnikov, Y. M., Andreev, Y. A., Kozlov, S. A., Vassilevski, A. A., and Grishin, E. V. (2008) Bacterial production of latarcin 2a, a potent antimicrobial peptide from spider venom. *Protein Expression and Purification 60*, 89–95, PMID: 18455432.

[345] Grishin, E. V., Polyansky, A. A., Vassilevski, A. A., Volynsky, P. E., Vorontsova, O. V., Samsonova, O. V., Egorova, N. S., Krylov, N. A., Feofanov, A. V., and Arseniev, A. S. (2009) N-terminal amphipathic helix as a trigger of hemolytic activity in antimicrobial peptides: A case study in latarcins. *FEBS Letters 583*, 2425–2428.

[346] Lee, K. H., Shin, S. Y., Hong, J. E., Yang, S.-T., Kim, J. I., Hahm, K.-S., and Kim, Y. (2003) Solution structure of termite-derived antimicrobial peptide, spinigerin, as determined in SDS micelle by NMR spectroscopy. *Biochemical and Biophysical Research Communications 309*, 591–597.

[347] Boulanger, N., Munks, R. J. L., Hamilton, J. V., Vovelle, F., Brun, R., Lehane, M. J., and Bulet, P. (2002) Epithelial Innate Immunity: A NOVEL ANTIMICROBIAL PEPTIDE WITH ANTIPARASITIC ACTIVITY IN THE BLOOD-SUCKING INSECT STOMOXYS CALCITRANS. *Journal of Biological Chemistry 277*, 49921 –49926.

[348] Dubovskii, P. V., Vassilevski, A. A., Samsonova, O. V., Egorova, N. S., Kozlov, S. A., Feofanov, A. V., Arseniev, A. S., and Grishin, E. V. (2011) Novel lynx spider toxin shares common molecular architecture with defense peptides from frog skin. *FEBS Journal 278*, 4382–4393.

[349] Satoe, K., Ai, A., Mitsuhiro, M., Jun, I., and Minoru, Y. (2005) Interactions of an Antimicrobial Peptide Moricin with Lipid Bilayers. *Pept Sci 2004*, 251–254.

[350] Dai, H., Rayaprolu, S., Gong, Y., Huang, R., Prakash, O., and Jiang, H. (2008) Solution structure, antibacterial activity, and expression profile of Manduca sexta moricin. *Journal of Peptide Science 14*, 855–863.

[351] Kuhn-Nentwig, L., Müller, J., Schaller, J., Walz, A., Dathe, M., and Nentwig, W. (2002) Cupiennin 1, a New Family of Highly Basic Antimicrobial Peptides in the Venom of the Spider Cupiennius salei(Ctenidae). *Journal of Biological Chemistry 277*, 11208 –11216.

[352] Li, M.-L., Liao, R.-W., Qiu, J.-W., Wang, Z.-J., and Wu, T.-M. (2000) Antimicrobial activity of synthetic all- mastoparan M. *International Journal of Antimicrobial Agents 13*, 203–208.

[353] Murata, K., Shinada, T., Ohfune, Y., Hisada, M., Yasuda, A., Naoki, H., and Nakajima, T. (2008) Novel mastoparan and protonectin analogs isolated from a solitary wasp, Orancistrocerus drewseni drewseni. *Amino Acids 37*, 389–394.

[354] Hirai, Y., Kuwada, M., Yasuhara, T., Yoshida, H., and Nakajima, T. (1979) A new mast cell degranulating peptide homologous to mastoparan in the venom of Japanese hornet (Vespa xanthoptera). *Chemical & Pharmaceutical Bulletin 27*, 1945–1946, PMID: 540363.

[355] Wang, G., Li, Y., and Li, X. (2005) Correlation of Three-dimensional Structures with the Antibacterial Activity of a Group of Peptides Designed Based on a Nontoxic Bacterial Membrane Anchor. *Journal of Biological Chemistry 280*, 5803 –5811.

[356] Li, X., Li, Y., Han, H., Miller, D. W., and Wang, G. (2006) Solution Structures of Human LL-37 Fragments and NMR-Based Identification of a Minimal Membrane-Targeting Antimicrobial and Anticancer Region. *Journal of the American Chemical Society 128*, 5776–5785.

[357] Bloch, J., Leite, J. R. S., Silva, L. P., Rodrigues, M. I. S., Prates, M. V., Brand, G. D., Lacava, B. M., Azevedo, R. B., Bocca, A. L., and Albuquerque, S. (2005) Phylloseptins: a novel class of anti-bacterial and anti-protozoan peptides from the Phyllomedusa genus. *Peptides 26*, 565–573.

[358] Bechinger, B., Resende, J. M., Moraes, C. M., Prates, M. V., Cesar, A., Almeida, F. C. L., Mundim, N. C. C. R., Valente, A. P., Bemquerer, M. P., and Piló-Veloso, D. (2008) Solution NMR structures of the antimicrobial peptides phylloseptin-1, -2, and -3 and biological activity: the role of charges and hydrogen bonding interactions in stabilizing helix conformations. *Peptides 29*, 1633–1644, PMID: 18656510.

[359] Park, J., Jung, J., and Lee, B. (1994) Antimicrobial Peptides from the Skin of a Korean Frog, Rana rugosa. *Biochemical and Biophysical Research Communications 205*, 948–954.

[360] Won, H., Park, S., Kim, H. E., Hyun, B., Kim, M., Lee, B. J., and Lee, B. (2002) Effects of a tryptophanyl substitution on the structure and antimicrobial activity of C-terminally truncated gaegurin 4. *European Journal of Biochemistry 269*, 4367–4374.

[361] Chi, S.-W., Kim, J.-S., Kim, D.-H., Lee, S.-H., Park, Y.-H., and Han, K.-H. (2007) Solution structure and membrane interaction mode of an antimicrobial peptide gaegurin 4. *Biochemical and Biophysical Research Communications 352*, 592–597.

[362] Conlon, J. M., al Dhaheri, A., al Mutawa, E., al Kharrge, R., Ahmed, E., Kolodziejek, J., Nowotny, N., Nielsen, P. F., and Davidson, C. (2007) Peptide defenses of the Cascades frog Rana cascadae: implications for the evolutionary history of frogs of the Amerana species group. *Peptides 28*, 1268–1274.

[363] Subasinghage, A. P., Conlon, J. M., and Hewage, C. M. (2008) Conformational analysis of the broad-spectrum antibacterial peptide, ranatuerin-2CSa: Identification of a full length helix-turn-helix motif. *Biochimica et Biophysica Acta (BBA) - Proteins & Proteomics 1784*, 924–929.

[364] Brand, G. D., Leite, J. R. S. A., Silva, L. P., Albuquerque, S., Prates, M. V., Azevedo, R. B., Carregaro, V., Silva, J. S., Sá, V. C. L., Brandão, R. A., and Bloch, C. (2002) Dermaseptins from Phyllomedusa oreades andPhyllomedusa distincta. *Journal of Biological Chemistry 277*, 49332 –49340.

[365] Savoia, D., Guerrini, R., Marzola, E., and Salvadori, S. (2008) Synthesis and antimicrobial activity of dermaseptin S1 analogues. *Bioorganic & Medicinal Chemistry 16*, 8205–8209, PMID: 18676150.

[366] Batista, C. V., Scaloni, A., Rigden, D. J., Silva, L. R., Rodrigues Romero, A., Dukor, R., Sebben, A., Talamo, F., and Bloch, C. (2001) A novel heterodimeric antimicrobial peptide from the tree-frog Phyllomedusa distincta. *FEBS Letters 494*, 85–89.

[367] Raimondo, D., Andreotti, G., Saint, N., Amodeo, P., Renzone, G., Sanseverino, M., Zocchi, I., Molle, G., Motta, A., and Scaloni, A. (2005) A folding-dependent mechanism of antimicrobial peptide resistance to degradation unveiled by solution structure of distinctin. *Proceedings of the National Academy of Sciences of the United States of America 102*, 6309–6314.

[368] Skerlavaj, B., Benincasa, M., Risso, A., Zanetti, M., and Gennaro, R. (1999) SMAP-29: a potent antibacterial and antifungal peptide from sheep leukocytes. *FEBS Letters 463*, 58–62.

[369] Sawai, M. V., Waring, A. J., Kearney, W. R., McCray, P. B., Forsyth, W. R., Lehrer, R. I., and Tack, B. F. (2002) Impact of single-residue mutations on the structure and function of ovispirin/novispirin antimicrobial peptides. *Protein Eng. 15*, 225–232.

[370] Steinstraesser, L., Tack, B. F., Waring, A. J., Hong, T., Boo, L. M., Fan, M.-H., Remick, D. I., Su, G. L., Lehrer, R. I., and Wang, S. C. (2002) Activity of Novispirin G10 against Pseudomonas aeruginosa In Vitro and in Infected Burns. *Antimicrobial Agents and Chemotherapy 46*, 1837–1844.

[371] Eckert, R., Qi, F., Yarbrough, D. K., He, J., Anderson, M. H., and Shi, W. (2006) Adding Selectivity to Antimicrobial Peptides: Rational Design of a Multidomain Peptide against Pseudomonas spp. *Antimicrobial Agents and Chemotherapy 50*, 1480–1488.

[372] Jacobsen, F., Mohammadi-Tabrisi, A., Hirsch, T., Mittler, D., Mygind, P. H., Sonksen, C. P., Raventos, D., Kristensen, H. H., Gatermann, S., Lehnhardt, M., Daigeler, A., Steinau, H. U., and Steinstraesser, L. (2007) Antimicrobial activity of the recombinant designer host defence peptide P-novispirin G10 in infected full-thickness wounds of porcine skin. *Journal of Antimicrobial Chemotherapy 59*, 493–498.

[373] Bals, R., Wang, X., Zasloff, M., and Wilson, J. M. (1998) The peptide antibiotic LL-37/hCAP-18 is expressed in epithelia of the human lung where it has broad antimicrobial activity at the airway surface. *Proceedings of the National Academy of Sciences of the United States of America 95*, 9541 –9546.

[374] Wang, G., Elliott, M., Cogen, A. L., Ezell, E. L., Gallo, R. L., and Hancock, R. E. W. (2012) Structure, Dynamics, and Antimicrobial and Immune Modulatory Activities of Human LL-23 and Its Single-Residue Variants Mutated on the Basis of Homologous Primate Cathelicidins. *Biochemistry 51*, 653–664.

[375] Li, X., Li, Y., Peterkofsky, A., and Wang, G. (2006) NMR studies of aurein 1.2 analogs. *Biochimica Et Biophysica Acta 1758*, 1203–1214, PMID: 16716252.

[376] Larrick, J. W., Hirata, M., Shimomoura, Y., Yoshida, M., Zheng, H., Zhong, J., and Wright, S. C. (1993) Antimicrobial activity of rabbit CAP18-derived peptides. *Antimicrobial agents and chemotherapy 37*, 2534–2539, PMID: 8109914.

[377] Travis, S. M., Anderson, N. N., Forsyth, W. R., Espiritu, C., Conway, B. D., Greenberg, E. P., McCray, P. B., Lehrer, R. I., Welsh, M. J., and Tack, B. F. (2000) Bactericidal Activity of Mammalian Cathelicidin-Derived Peptides. *Infection and Immunity 68*, 2748–2755.

[378] Xiao, Y., Dai, H., Bommineni, Y. R., Soulages, J. L., Gong, Y.-X., Prakash, O., and Zhang, G. (2006) Structure-activity relationships of fowlicidin-1, a cathelicidin antimicrobial peptide in chicken. *FEBS Journal 273*, 2581–2593.

[379] Xiao, Y., Herrera, A. I., Bommineni, Y. R., Soulages, J. L., Prakash, O., and Zhang, G. (2009) The Central Kink Region of Fowlicidin-2, an α-Helical Host Defense Peptide, Is Critically Involved in Bacterial Killing and Endotoxin Neutralization. *Journal of Innate Immunity 1*, 268–280.

[380] Cole, A. M., Weis, P., and Diamond, G. (1997) Isolation and Characterization of Pleurocidin, an Antimicrobial Peptide in the Skin Secretions of Winter Flounder. *Journal of Biological Chemistry 272*, 12008 –12013.

[381] Yoshida, K., Mukai, Y., Niidome, T., Takashi, C., Tokunaga, Y., Hatakeyama, T., and Aoyagi, H. (2001) Interaction of pleurocidin and its analogs with phospholipid membrane and their antibacterial activity. *Journal of Peptide Research 57*, 119.

[382] Lee, J., and Lee, D. G. (2008) Structure-antimicrobial activity relationship between pleurocidin and its enantiomer. *Experimental & Molecular Medicine 40*, 370–376, PMID: 18779649 PMCID: 2679270.

[383] Silphaduang, U., and Noga, E. J. (2001) Antimicrobials: Peptide antibiotics in mast cells of fish. *Nature 414*, 268–269.

[384] Chekmenev, E. Y. et al. (2006) Investigating molecular recognition and biological function at interfaces using piscidins, antimicrobial peptides from fish. *Biochimica Et Biophysica Acta 1758*, 1359–1372, PMID: 16815244.

[385] Verdon, J., Berjeaud, J.-M., Lacombe, C., and Héchard, Y. (2008) Characterization of anti-Legionella activity of warnericin RK and delta-lysin I from Staphylococcus warneri. *Peptides 29*, 978–984.

[386] Dhople, V. M., and Nagaraj, R. (2005) Conformation and activity of -lysin and its analogs. *Peptides 26*, 217–225.

[387] Ribeiro, P. D., and Medina-Acosta, E. (2003) Prevention of lethal murine candidiasis using HP (2–20), an antimicrobial peptide derived from the N-terminus of Helicobacter pylori ribosomal protein L1. *Peptides 24*, 1807–1814.

[388] Lee, K., Lee, D., Park, Y., Kang, D.-I., Shin, S., Hahm, K.-S., and Kim, Y. (2006) Interactions between the plasma membrane and the antimicrobial peptide HP (2-20) and its analogues derived from Helicobacter pylori. *Biochemical Journal 394*, 105.

[389] Wenschuh, H., Beyermann, M., Haber, H., Seydel, J. K., Krause, E., Bienert, M., Carpino, L. A., El-Faham, A., and Albericio, F. (1995) Stepwise Automated Solid Phase Synthesis of Naturally Occurring Peptaibols Using FMOC Amino Acid Fluorides. *J. Org. Chem. 60*, 405–410.

[390] Dathe, M., Kaduk, C., Tachikawa, E., Melzig, M. F., Wenschuh, H., and Bienert, M. (1998) Proline at position 14 of alamethicin is essential for hemolytic activity, catecholamine secretion from chromaffin cells and enhanced metabolic activity in endothelial cells. *Biochimica et Biophysica Acta (BBA) - Biomembranes 1370*, 175–183.

[391] Oh, D., Shin, S. Y., Lee, S., Kang, J. H., Kim, S. D., Ryu, P. D., Hahm, K.-S., and Kim, Y. (2000) Role of the Hinge Region and the Tryptophan Residue in the Synthetic Antimicrobial Peptides, Cecropin A(1−8)−Magainin 2(1−12) and Its Analogues, on Their Antibiotic Activities and Structures. *Biochemistry 39*, 11855–11864.

[392] Yang, L. (2001) Barrel-Stave Model or Toroidal Model? A Case Study on Melittin Pores. *Biophysical Journal 81*, 1475–1485.

[393] Strömstedt, A. A., Wessman, P., Ringstad, L., Edwards, K., and Malmsten, M. (2007) Effect of lipid headgroup composition on the interaction between melittin and lipid bilayers. *Journal of Colloid and Interface Science 311*, 59–69.

[394] Christensen, B., Fink, J., Merrifield, R. B., and Mauzerall, D. (1988) Channel-forming properties of cecropins and related model compounds incorporated into planar lipid membranes. *Proceedings of the National Academy of Sciences of the United States of America 85*, 5072–5076, PMID: 2455891 PMCID: 281690.

[395] Dubovskii, P. V., Volynsky, P. E., Polyansky, A. A., Chupin, V. V., Efremov, R. G., and Arseniev, A. S. (2006) Spatial Structure and Activity Mechanism of a Novel Spider Antimicrobial Peptide. *Biochemistry 45*, 10759–10767.

[396] Vorontsova, O. V., Egorova, N. S., Arseniev, A. S., and Feofanov, A. V. (2011) Haemolytic and cytotoxic action of latarcin Ltc2a. *Biochimie 93*, 227–241.

[397] Corzo, G., Villegas, E., Gómez-Lagunas, F., Possani, L. D., Belokoneva, O. S., and Nakajima, T. (2002) Oxyopinins, Large Amphipathic Peptides Isolated from the Venom of the Wolf Spider Oxyopes kitabensis with Cytolytic Properties and Positive Insecticidal Cooperativity with Spider Neurotoxins. *Journal of Biological Chemistry 277*, 23627–23637.

[398] Pukala, T. L., Boland, M. P., Gehman, J. D., Kuhn-Nentwig, L., Separovic, F., and Bowie, J. H. (2007) Solution Structure and Interaction of Cupiennin 1a, a Spider Venom Peptide, with Phospholipid Bilayers. *Biochemistry 46*, 3576–3585.

[399] Pukala, T. L., Doyle, J. R., Llewellyn, L. E., Kuhn-Nentwig, L., Apponyi, M. A., Separovic, F., and Bowie, J. H. (2007) Cupiennin 1a, an antimicrobial peptide from the venom of the neotropical wandering spider Cupiennius salei, also inhibits the formation of nitric oxide by neuronal nitric oxide synthase. *FEBS Journal 274*, 1778–1784.

[400] Arbuzova, A., and Schwarz, G. (1999) Pore-forming action of mastoparan peptides on liposomes: a quantitative analysis. *Biochimica et Biophysica Acta (BBA) - Biomembranes 1420*, 139–152.

[401] Gehman, J. D., Luc, F., Hall, K., Lee, T.-H., Boland, M. P., Pukala, T. L., Bowie, J. H., Aguilar, M.-I., and Separovic, F. (2008) Effect of Antimicrobial Peptides from Australian Tree Frogs on Anionic Phospholipid Membranes. *Biochemistry 47*, 8557–8565.

[402] Kim, H. J., Kim, S. S., Lee, M. H., Lee, B. J., and Ryu, P. D. (2004) Role of C-terminal heptapeptide in pore-forming activity of antimicrobial agent, gaegurin 4. *The Journal of Peptide Research 64*, 151–158.

[403] Lee, D. G., Kim, P. I., Park, Y., Park, S.-C., Woo, E.-R., and Hahm, K.-S. (2002) Antifungal mechanism of SMAP-29 (1–18) isolated from sheep myeloid mRNA against Trichosporon beigelii. *Biochemical & Biophysical Research Communications 295*, 591.

[404] Yamaguchi, S., Huster, D., Waring, A., Lehrer, R. I., Kearney, W., Tack, B. F., and Hong, M. (2001) Orientation and dynamics of an antimicrobial peptide in the lipid bilayer by solid-state NMR spectroscopy. *Biophysical Journal 81*, 2203.

[405] Gutsmann, T., Hagge, S. O., Larrick, J. W., Seydel, U., and Wiese, A. (2001) Interaction of CAP18-Derived Peptides with Membranes Made from Endotoxins or Phospholipids. *Biophysical Journal 80*, 2935–2945.

[406] Saravanan, R., and Bhattacharjya, S. (2011) Oligomeric structure of a cathelicidin antimicrobial peptide in dodecylphosphocholine micelle determined by NMR spectroscopy. *Biochimica et Biophysica Acta (BBA) - Biomembranes 1808*, 369–381.

[407] Subbalakshmi, C., Krishnakumari, V., Sitaram, N., and Nagaraj, R. (1998) Interaction of indolicidin, a 13-residue peptide rich in tryptophan and proline and its analogues with model membranes. *Journal of Biosciences 23*, 9–13.

[408] Zhao, H., Mattila, J.-P., Holopainen, J. M., and Kinnunen, P. K. (2001) Comparison of the Membrane Association of Two Antimicrobial Peptides, Magainin 2 and Indolicidin. *Biophysical Journal 81*, 2979–2991.

[409] Gamen, S., Hanson, D. A., Kaspar, A., Naval, J., Krensky, A. M., and Anel, A. (1998) Granulysin-Induced Apoptosis. I. Involvement of at Least Two Distinct Pathways. *The Journal of Immunology 161*, 1758–1764.

[410] Campagna, S., Saint, N., Molle, G., and Aumelas, A. (2007) Structure and Mechanism of Action of the Antimicrobial Peptide Piscidin. *Biochemistry 46*, 1771–1778.

[411] Verdon, J., Falge, M., Maier, E., Bruhn, H., Steinert, M., Faber, C., Benz, R., and Héchard, Y. (2009) Detergent-Like Activity and [alpha]-Helical Structure of Warnericin RK, an Anti-Legionella Peptide. *Biophysical Journal 97*, 1933–1940.

[412] Raghunathan, G., Seetharamulu, P., Brooks, B. R., and Guy, H. R. (1990) Models of -hemolysin membrane channels and crystal structures. *Proteins: Structure, Function, and Bioinformatics 8*, 213–225.

[413] Park, S.-C., Kim, M.-H., Hossain, M. A., Shin, S. Y., Kim, Y., Stella, L., Wade, J. D., Park, Y., and Hahm, K.-S. (2008) Amphipathic -helical peptide, HP (2–20), and its analogues derived from Helicobacter pylori: Pore formation mechanism in various lipid compositions. *Biochimica et Biophysica Acta (BBA) - Biomembranes 1778*, 229–241.

[414] Yang, L., Weiss, T. M., Harroun, T. A., Heller, W. T., and Huang, H. W. (1999) Supramolecular Structures of Peptide Assemblies in Membranes by Neutron Off-Plane Scattering: Method of Analysis. *Biophysical Journal 77*, 2648–2656, 5.

[415] Shai, Y., Bach, D., and Yanovsky, A. (1990) Channel formation properties of synthetic pardaxin and analogues. *Journal of Biological Chemistry 265*, 20202–20209.